Soil Water Extremes and Streambank Erosion: A Comprehensive Study of Erosion Dynamics and Predictive Modeling

A Dissertation Presented for the

Doctor of Philosophy

Degree

The University of Tennessee, Knoxville

Probal Saha

August 2025

ACKNOWLEDGMENTS

I would like to express my deepest gratitude to Dr. John S. Schwartz and Dr. Jon M. Hathaway, my Ph.D. advisors and mentors, whose guidance, expertise, and constant encouragement shaped my research and academic development in water resources engineering. Their commitment to scientific rigor and real-world relevance instilled in me the values necessary for impactful and independent research. I am equally thankful to my committee members, Dr. Chris Cox, and Dr. Daniel Yoder, for their insightful feedback and critical evaluations that significantly improved the depth and clarity of my dissertation.

I would also like to acknowledge the early mentorship and opportunity from Dr. A. N. Thanos Papanicolaou and Dr. Christopher G. Wilson, who played formative roles in cultivating my research interests during the initial stages of my PhD journey.

I am profoundly thankful to my wife, Binata, for her unwavering love, sacrifice, and patience throughout this demanding journey. Her persistent support has been my greatest source of strength. To our beloved daughter, Bornika, your presence brought joy and purpose to this journey in ways words cannot express.

ABSTRACT

Streambank erosion processes are influenced by complex interactions between soil moisture dynamics, erosion resistance, and hydraulic forces. This dissertation investigates these interrelationships through three interlinked studies that advance both the understanding and modeling of erosion under temporally and spatially variable hydrologic conditions. The first study explores the spatiotemporal variability of soil moisture extremes across geophysically distinct watersheds in Tennessee. Using projected soil moisture, it identifies how physiographic factors and hydroclimatic variability jointly influence the occurrence of hydrologic extremes. The second study quantifies the effect of soil moisture on key erosion resistance parameters—critical shear stress (τ_c) and erodibility coefficient (K_d), through extensive Jet Erosion Tests (JET) under varying seasonal moisture conditions. Quadratic relationships are established, revealing how low to high soil moisture transitions impact bank resistance and erosion susceptibility. The third study integrates these dynamic soil moisture relationships into the Bank Stability and Toe Erosion Model (BSTEM), creating a modified framework where τ_c and K_d evolve over time in response to observed moisture conditions. This dynamic BSTEM model is evaluated across three natural streambanks and compared with traditional static configurations. Statistical comparisons demonstrate that the dynamic model captures the timing and magnitude of observed lateral retreat accurately, particularly at sites where suitable Manning's n values align with field conditions. While the dynamic model does not universally outperform static configurations, its ability to respond to temporal transitions in erosion behavior offers clear advantages, especially during rapid erosion transitions. Together, these studies demonstrate that integrating time-varying hydrologic drivers with erosion resistance improves both conceptual understanding and predictive accuracy in streambank erosion modeling.

Keywords: Streambank erosion, Soil moisture dynamics, BSTEM, Critical shear stress, Erodibility coefficient, Hydrologic variability.

TABLE OF CONTENTS

CHAPTER-1 INTRODUCTION 1

REFERENCES 5

CHAPTER-2 BACKGROUND 8

2.1 SPATIO-TEMPORAL SOIL WATER EXTREMES 10

2.1.1 Projected Climatic Extremes and Soil Water Balance 10

2.1.2 Spatio-temporal Extremes 10

2.2 SOIL MOISTURE AND STREAMBANK EROSION 11

2.2.1 Fundamentals of Streambank Erosion 11

2.2.2 Hydrologic Extremes on Streambank Erosion 12

2.2.3 Critical Shear Strength and Erodibility 12

2.2.4 Techniques for Measuring τ_c and K_d 13

2.3 DYNAMIC SOIL MOISTURE AND EROSION MODELING 13

2.3.1 Fluvial Erosion Estimations in Models 13

2.3.2 Mass Failure and Geotechnical Stability 14

2.3.3 Erosion Models and Factor of Safety Approaches 14

2.3.4 Shear Stress Estimation in Meandering Channels 14

2.3.5 Manning's n and Boundary Shear Stress 15

2.4 Knowledge Gaps and Contributions 15

REFERENCES 18

CHAPTER-3 CLIMATE CHANGE IMPACTS ON SPATIO-TEMPORAL SOIL WATER EXTREMES IN GEOPHYSICALLY DIVERSE WATERSHEDS: A COMPARISON BETWEEN EAST AND WEST TENNESSEE WATERSHEDS 25

3.1 INTRODUCTION 27

3.2 STUDY SITE CHARACTERISTICS 29

3.3 MATERIALS AND METHODS 32

3.3.1 Summary of Approach 32

3.3.2 Data Descriptions ... 33

3.3.3 Hydrological modeling using VIC ... 36

3.4 RESULT AND DISCUSSION ... 38

3.4.1 Calibration and Validation of the VIC Model ... 38

3.4.2 Water Budget Trends & Temporal Extremes ... 39

3.4.3 Temporal and Spatial Extremes ... 43

3.4.4 Spatial Extremes' Impacting Factors ... 47

3.5 CONCLUSION ... 51

REFERENCES ... 53

CHAPTER-4 FIELD-BASED INVESTIGATION OF SOIL MOISTURE DYNAMICS AND THEIR INFLUENCE ON SHEAR STRESS AND ERODIBILITY COEFFICIENTS FOR ENHANCED BANK EROSION PREDICTION ... 60

4.1 INTRODUCTION ... 62

4.2 MATERIALS AND METHODS ... 65

4.2.1 Study Site Characteristics ... 65

4.2.2 Study Design ... 67

4.2.3 Data Collection ... 69

4.2.4 Statistical Analysis ... 70

4.3 RESULTS AND DISCUSSIONS ... 71

4.3.1 Relationship Between SM with τ_c and K_d ... 71

4.3.2 Statistical Relationship & Correlations ... 73

4.3.3 Relationship Between K_d and τ_c ... 74

4.4 CONCLUSIONS ... 76

REFERENCES ... 78

CHAPTER-5 DYNAMIC EROSION MODELING OF STREAMBANKS: INTEGRATING SOIL MOISTURE–BASED PREDICTIONS OF CRITICAL SHEAR STRESS AND ERODIBILITY COEFFICIENTS INTO BSTEM ... 85

5.1 INTRODUCTION ... 87

5.2 MATERIALS AND METHODS ... 90
5.2.1 Study Site Characteristics ... 90
5.2.2 Study Design ... 92
5.2.3 Data Descriptions ... 94
5.2.4 Erosion Model BSTEM ... 96
5.2.5 Hydrological Model SWMM ... 101
5.2.6 Statistical Assessment of the Modified Model ... 101
5.3 RESULTS ... 103
5.3.1 SWMM Model Outputs ... 103
5.3.2 Impact of Roughness in Erosion Retreat ... 105
5.3.3 Impact of Soil Moisture on Temporal Erosion Prediction ... 107
5.3.4 Performance Assessment of Modified Model ... 112
5.4 DISCUSSIONS ... 114
5.5 CONCLUSIONS ... 117
REFERENCES ... 119
CHAPTER-6 SUMMARY AND CONCLUSIONS ... 122
APPENDIX ... 125
VITA ... 134

LIST OF TABLES

Table 3-1 Geo-climatic characteristics of the study area watersheds 30

Table 3-2 Description of the Input Data Sources for the Hydrological Simulation 33

Table 3-3 Summary on the climatic trends & extremes Overview 35

Table 3-4 Allowable ranges and selected values of the calibration parameters 37

Table 3-5 NSE Coefficient and MAE for the Nolichucky Watershed at each SDA 39

Table 3-6 Summary of the water budget trends and extremes for climate change impacts 41

Table 3-7 Plant available water (PAW) and percentage of the days below average wilting point within growing season (180 days) 44

Table 3-8 Standardized regression estimates of Hydrological processes, Soil textures, and Watershed processes with Soil moisture. 50

Table 4-1 Description of the input data sources 69

Table 5-1 Description of Input Data Sources for Dynamic Erosion Modeling 94

Table 5-2 Description of the Bank sites 96

Table 5-3 Statistical comparison between observed and modeled lateral retreat rates across different Manning’s n scenarios and modeling approaches. 108

Table 5-4 Performance metrics of static and dynamic erosion models based on observed lateral retreat events 114

Table A-1 Comparison of field-derived and function generated critical shear stress and erodibility coefficients in relation to real-time soil moisture 129

Table A-2 Erosion rate estimated from the field-derived critical shear stress, erodibility coefficients and boundary shear stress 130

Table A-3 Sieve test for site-1 streambank soil 131

Table A-4 Experimental Parameters for Organic Sediment (OS) Sample 132

Table A-5 Hydrometer test for site-1 streambank soil texture 133

LIST OF FIGURES

Figure 3-1 a. Selected Study Sites at the East and West of Tennessee State in the US and Study Site Comparison between Obion and Nolichucky River Watersheds for b. Elevation, c. Land Cover, and d. Soil Coverage. 31

Figure 3-2 Methodology Flow Chart of the Study 32

Figure 3-3 Monthly Flow Calibration of Nolichucky watershed with USGS data 40

Figure 3-4 Soil Moisture and Evapotranspiration Validations of Nolichucky watershed with NRCS-SCAN and MODIS data 40

Figure 3-5 Hot Moments of Soil Moisture for RCP4.5 & RCP8.5 Scenarios 43

Figure 3-6 Soil Moisture Hotspots Extremes during 2046-55 for RCP4.5 & RCP8.5 Scenarios 46

Figure 3-7 a. Correlations of Hydrological processes, b. Soil textures and c. Watershed Attributes with Soil Moisture for Obion & Nolichucky Watersheds 48

Figure 4-1 Location of bank erosions at the selected study site in Knoxville, Tennessee a. Elevation, and b. Land Cover. 66

Figure 4-2 The JET Device installed at the bank of Conner Creek, Knox County, TN 67

Figure 4-3 Methodology Flow Chart of the study. 68

Figure 4-4 The variability of (a) critical shear stress (τ_c), (b) erodibility coefficients (K_d), and (c) erosion rate with dynamic soil water content 71

Figure 4-5 The relationship between critical shear stress (τ_c) and erodibility coefficients (K_d) for soil moisture ranges of (a) less than 20%, (b) 20-30%, and (c) greater than 30% 75

Figure 5-1 Location of bank erosions at the selected study site in Knoxville, Tennessee a. Elevation, and b. Land Cover. 91

Figure 5-2 Bank and cross-section profiles for the selected sites. 92

Figure 5-3 Methodology Flow Chart of the study. 93

Figure 5-4 Soil water content of streambank sites at Connor Creek 95

Figure 5-5 Temporal Trends of Streambank Lateral Retreat at Three Monitoring Sites 97

Figure 5-6 Dynamic BSTEM Erosion Model Schematics 98

Figure 5-7 Calibration of flow downstream of Connor Creek watershed 103

Figure 5-8 SWMM Model derived flow depths at each bank erosion sites 104

Figure 5-9 Modeled lateral retreat sensitivity to manning's n under dynamic and static soil moisture conditions at three streambank erosion sites 106

Figure 5-10 Comparison of modeled and observed cumulative lateral retreat at Site-1 under dynamic, Static A, and Static B scenarios at Manning's n = 0.045, 0.050, and 0.055. 109

Figure 5-11 Comparison of modeled and observed cumulative lateral retreat at Site-2 under dynamic, Static A, and Static B scenarios at Manning's n = 0.045, 0.050, and 0.055. 110

Figure 5-12 Comparison of modeled and observed cumulative lateral retreat at Site-3 under dynamic, Static A, and Static B scenarios at Manning's n = 0.045, 0.050, and 0.055. 111

Figure 5-13 Time-series comparison of modeled and observed lateral retreat under dynamic, wet static, and dry static τ_c–K_d conditions 113

Figure A-1 Annual and monthly temperature trends and frequency percentiles of Obion 125

Figure A-2 Annual and monthly temperature trends and frequency percentiles of Nolichucky 126

Figure A-3 Annual and monthly precipitation trends and Frequency percentiles of Obion 127

Figure A-4 Annual and monthly precipitation trends and Frequency percentiles of Nolichucky 128

CHAPTER-1

INTRODUCTION

Climate change is anticipated to intensify the hydrological cycle, leading to increased magnitude and high-intensity rainfall events. These changes will have significant impacts on the soil water budget—the balance of precipitation, runoff, evapotranspiration, and baseflow—that governs ecosystem functioning and water resource dynamics. Prior research has shown that regional geoclimatic characteristics strongly influence how watersheds respond to climatic shifts, particularly in terms of soil moisture and runoff dynamics (He et al., 2019; Zheng et al., 2018). In the United States, observed increases in rainfall amounts and intensities over the 20th century are projected to continue into the 21st century (Nearing et al., 2004), potentially leading to more frequent extremes such as flash floods and prolonged dry spells. These shifts are expected to result in more frequent extreme precipitation events coupled with extended dry periods, exacerbating soil water scarcity (Berg & Sheffield, 2018).

Although previous studies have examined climate-driven extremes like drought and erratic precipitation in the context of agricultural yield loss (Reyes & Elias, 2019; Schauberger et al., 2017), channel degradation (Aktar, 2013; Brannigan et al., 2022), and socio-economic outcomes (Wheeler & von Braun, 2013), there has been limited focus on soil moisture extremes. Understanding how climate-induced hydrologic variability influences soil moisture is essential, not only for ecosystem sustainability and agricultural productivity but also for fluvial processes such as streambank erosion. The first study of this dissertation addresses this gap by investigating the drivers and patterns of spatio-temporal soil moisture extremes across geophysically diverse watersheds. By comprehensively assessing these dynamics, the study aims to inform water resource management strategies under future scenarios how soil moisture variability contributes to broader geomorphic and hydrologic changes.

In recent decades, extreme events have increasingly caused riverbank erosion and flood disasters in vulnerable regions (Aktar, 2013; Rahman et al., 2015). Streambank erosion is a fundamental geomorphic process in fluvial dynamics, influencing the physical, ecological, and socio-economic aspects of the environment (Duró et al., 2020; T. Wynn & Mostaghimi, 2006). The impact of hydrological extreme events on erosion is multifaceted, involving alterations in rainfall intensity and timing, evapotranspiration patterns, and soil moisture alterations. Events such as high-intensity storms following dry periods can trigger amplified bank erosion by enhancing discharge and runoff (Brown et al., 2020). Among these variables, soil moisture plays a pivotal role by influencing both the erosion resistance of streambank materials and their susceptibility to hydraulic forces (Moragoda et al., 2022). Evaluating how soil moisture interacts with soil shear forces to influence erosion susceptibility is vital to comprehend the dynamic characteristics of streambank failure (Li et al., 2022; Singh & Thompson, 2016a; Wang et al., 2024).

Seasonal fluctuations in soil moisture, combined with high-intensity storm events, are likely to influence key streambank erosion resistance parameters such as hydraulic shear stress (τ_c) and soil erodibility coefficient (K_d) (Schnauder & Sukhodolov, 2012; T. M. Wynn et al., 2008a). Despite their significance, these variables have received limited attention in dynamic field settings, highlighting a critical gap in current erosion research. Understanding how soil moisture variations alter τ_c and K_d is essential for improving predictions of bank erodibility under variable flow conditions. Accordingly, the second study of this dissertation focuses on evaluating the effects of temporally varying soil moisture on erosion resistance parameters τ_c and K_d across a range of hydrologic conditions—from dry to high-flow events.

Traditional erosion modeling approaches, including the widely used Bank Stability and Toe Erosion Model (BSTEM), often rely on fixed input values for critical shear stress (τ_c) and erodibility coefficient (K_d), derived from point-in-time measurements (Daly et al., 2015; Simon et al., 2000). However, multiple laboratory studies have shown that τ_c and K_d are not static but vary significantly with changes in soil moisture, which affects pore-water pressure, matric suction, and ultimately, soil strength (Li et al., 2022; Simon & Collison, 2001). As streambank conditions evolve across seasons—from dry to saturated states—models that assume constant erosion resistance parameters risk misrepresenting erosion potential. Integrating dynamic soil moisture relationships into erosion models can provide a more realistic simulation of seasonal erosion processes and improve predictive accuracy.

This final chapter aims to develop and evaluate a dynamic erosion modeling approach by incorporating soil moisture–dependent τ_c and K_d into BSTEM. Field-based Jet Erosion Test (JET) data from a range of soil moisture conditions serves as the foundation for establishing functional relationships between SM, τ_c, and K_d. These relationships are embedded into BSTEM through custom modifications that allow real-time updating of erosion resistance parameters. In doing so, this study addresses a key gap in current streambank modeling practices—namely, the omission of temporal variability in erosion resistance—and evaluates whether soil moisture–responsive modeling improves BSTEM's ability to capture observed seasonal patterns of lateral retreat. By coupling hydrologic variability with empirical parameterization, this work contributes to the growing body of research emphasizing the role of soil moisture in driving erosion dynamics (Klavon et al., 2017a; Moragoda et al., 2022).

This project aims to assess the spatio-temporal variability of soil water extremes and their influence on channel morphology and erosion processes. The chapters of this dissertation address the following key research questions:

1. How will climate change impact soil moisture spatio-temporally in geophysically diverse watersheds, and what are the driving factors behind soil moisture extremes?
2. How do temporal variations in naturally occurring soil moisture influence critical shear stress (τ_c) and the erodibility coefficient (K_d) of cohesive streambank soils?
3. Can erosion models better capture seasonal streambank erosion variability by integrating critical shear stress (τ_c) and erodibility coefficient (K_d) as functions of dynamic soil moisture?

REFERENCES

Aktar, N. (2013). Impact of Climate Change on Riverbank Erosion. IJSBAR) International Journal of Sciences: Basic and Applied Research (IJSBAR, 7(1), 36–42. http://gssrr.org/index.php?journal=JournalOfBasicAndApplied

Aktar, N., & Nazneen Aktar, M. (2013). Impact of Climate Change on Riverbank Erosion. International Journal of Sciences: Basic and Applied Research (IJSBAR) International Journal of Sciences: Basic and Applied Research, 7(1), 36–42. http://gssrr.org/index.php?journal=JournalOfBasicAndApplied

Berg, A., & Sheffield, J. (2018). Climate Change and Drought: the Soil Moisture Perspective. Current Climate Change Reports, 4(2), 180–191. https://doi.org/10.1007/S40641-018-0095-0/FIGURES/1

Brannigan, N., Mullan, D., Vandaele, K., Graham, C., McKinley, J., & Meneely, J. (2022). Modelling soil erosion by water under future climate change: Addressing methodological gaps. CATENA, 216, 106403. https://doi.org/https://doi.org/10.1016/j.catena.2022.106403

Brown, D. R. N., Brinkman, T. J., Bolton, W. R., Brown, C. L., Cold, H. S., Hollingsworth, T. N., & Verbyla, D. L. (2020). Implications of climate variability and changing seasonal hydrology for subarctic riverbank erosion. Climatic Change, 162(2), 1–20. https://doi.org/10.1007/S10584-020-02748-9/FIGURES/9

Daly, E. R., Miller, R. B., & Fox, G. A. (2015). Modeling streambank erosion and failure along protected and unprotected composite streambanks. Advances in Water Resources, 81, 114–127. https://doi.org/10.1016/J.ADVWATRES.2015.01.004

Duró, G., Crosato, A., Kleinhans, M. G., Roelvink, D., & Uijttewaal, W. S. J. (2020). Bank Erosion Processes in Regulated Navigable Rivers. Journal of Geophysical Research: Earth Surface, 125(7). https://doi.org/10.1029/2019JF005441

He, M., Anderson, M., Schwarz, A., Das, T., Lynn, E., Anderson, J., Munévar, A., Vasquez, J., & Arnold, W. (2019). Potential Changes in Runoff of California's Major Water Supply Watersheds in the 21st Century. Water, 11(1651). https://doi.org/10.3390/w11081651

Klavon, K., Fox, G., Guertault, L., Langendoen, E., Enlow, H., Miller, R., & Khanal, A. (2017). Evaluating a process-based model for use in streambank stabilization: insights on the Bank Stability and Toe Erosion Model (BSTEM). Earth Surface Processes and Landforms, 42(1), 191–213. https://doi.org/10.1002/ESP.4073

Li, M., Liu, Q., Zhang, H., Wells, R. R., Wang, L., & Geng, J. (2022). Effects of antecedent soil moisture on rill erodibility and critical shear stress. CATENA, 216, 106356. https://doi.org/10.1016/J.CATENA.2022.106356

Moragoda, N., Kumar, M., & Cohen, S. (2022). Representing the role of soil moisture on erosion resistance in sediment models: Challenges and opportunities. Earth-Science Reviews, 229, 104032. https://doi.org/10.1016/j.earscirev.2022.104032

Nearing, M., Pruski, F. F., & O'Neal, M. R. (2004). Expected climate change impacts on soil erosion rates: A review. Journal of Soil and Water Conservation, 59(1), 43–50. https://www.jswconline.org/content/59/1/43

Rahman, M. A. T. M. T., Islam, S., & Rahman, S. H. (2015). Coping with flood and riverbank erosion caused by climate change using livelihood resources: a case study of Bangladesh. Climate and Development, 7(2), 185–191. https://doi.org/10.1080/17565529.2014.910163

Reyes, J. J., & Elias, E. (2019). Spatio-temporal variation of crop loss in the United States from 2001 to 2016. Environmental Research Letters, 14(7), 074017. https://doi.org/10.1088/1748-9326/ab1ac9

Schauberger, B., Archontoulis, S., Arneth, A., Balkovic, J., Ciais, P., Deryng, D., Elliott, J., Folberth, C., Khabarov, N., Müller, C., Pugh, T. A. M., Rolinski, S., Schaphoff, S., Schmid, E., Wang, X., Schlenker, W., & Frieler, K. (2017). Consistent negative response of US crops to high temperatures in observations and crop models. Nature Communications, 8, 13931. https://doi.org/10.1038/ncomms13931

Schnauder, I., & Sukhodolov, A. N. (2012). Flow in a tightly curving meander bend: effects of seasonal changes in aquatic macrophyte cover. Earth Surface Processes and Landforms, 37(11), 1142–1157. https://doi.org/10.1002/ESP.3234

Simon, A., & Collison, A. J. C. (2001). Pore-water pressure effects on the detachment of cohesive streambeds: seepage forces and matric suction. Earth Surface Processes and Landforms, 26(13), 1421–1442. https://doi.org/10.1002/ESP.287

Simon, A., Curini, A., Darby, S. E., & Langendoen, E. J. (2000). Bank and near-bank processes in an incised channel. Geomorphology, 35(3–4), 193–217. https://doi.org/10.1016/S0169-555X(00)00036-2

Singh, H. V., & Thompson, A. M. (2016). Effect of antecedent soil moisture content on soil critical shear stress in agricultural watersheds. Geoderma, 262, 165–173. https://doi.org/10.1016/J.GEODERMA.2015.08.011

Wang, X., Qin, X., Tan, J., Yang, L., Ou, L., Duan, X., & Deng, Y. (2024). Effect of the moisture content and dry density on the shear strength parameters of collapsing wall in hilly granite areas of South China. International Soil and Water Conservation Research, 12(3), 697–713. https://doi.org/10.1016/J.ISWCR.2023.09.006

Wheeler, T., & von Braun, J. (2013). Climate Change Impacts on Global Food Security. Science, 341(6145), 508–513. https://doi.org/10.1126/science.1239402

Wynn, T. M., Henderson, M. B., & Vaughan, D. H. (2008). Changes in streambank erodibility and critical shear stress due to subaerial processes along a headwater stream, southwestern Virginia, USA. Geomorphology, 97(3–4), 260–273. https://doi.org/10.1016/j.geomorph.2007.08.010

Wynn, T., & Mostaghimi, S. (2006). The effects of vegetation and soil type on streambank erosion, Southwestern Virginia, USA. Journal of the American Water Resources Association, 42(1), 69–82. https://doi.org/10.1111/j.1752-1688.2006.tb03824.x

Zheng, H., Chiew, F. H. S., Charles, S., & Podger, G. (2018). Future climate and runoff projections across South Asia from CMIP5 global climate models and hydrological modelling. Journal of Hydrology: Regional Studies, 18, 92–109. https://doi.org/10.1016/J.EJRH.2018.06.004

CHAPTER-2

BACKGROUND

This chapter aims to provide a comprehensive understanding of the interplay between spatio-temporal soil moisture variability, streambank erosion dynamics, and erosion modeling approaches, with a particular focus on how these processes vary across different geophysical settings and hydrologic conditions. The chapter is organized as follows:

I. The first section reviews previous studies on climate-driven hydrologic shifts and their impacts on the spatio-temporal variability of soil moisture. It highlights how changes in precipitation intensity, consecutive dry days, and temperature extremes contribute to soil water balance fluctuations, and emphasizes the need for region-specific analysis across geophysically diverse watersheds.

II. The following section explores the link between soil moisture variability and streambank erosion, focusing on how moisture dynamics influence erosion mechanisms such as fluvial detachment and mass failure. Special attention is given to the role of seasonally varying soil moisture in altering critical shear stress (τc) and erodibility coefficient (Kd), both of which are key to understanding bank retreat processes.

III. The final section reviews existing streambank erosion models, such as BSTEM, and discusses how erosion prediction is influenced by parameters including τc, Kd, and boundary shear stress derived from Manning's n. It identifies limitations in current modeling practices—particularly the use of static parameters—and introduces the need for integrating dynamic, soil moisture-responsive formulations into erosion modeling frameworks.

Significant contributions from this research include advancing the understanding of soil moisture extremes and improving the predictive capability of erosion models under dynamic hydrologic conditions.

2.1 SPATIO-TEMPORAL SOIL WATER EXTREMES

2.1.1 Projected Climatic Extremes and Soil Water Balance

The sixth assessment report (AR6 WGIII) by the Intergovernmental Panel on Climate Change (IPCC) assesses that global average temperatures are projected to rise by 1.1°-4.9°C by 2100 (Kikstra et al., 2022). As these increases exceed the critical 2°C threshold, they are expected to generate substantial and potentially irreversible consequences for water resources, biodiversity, agriculture, and land cover (Blanc & Reilly, 2017; Hitz & Smith, 2004). Failure to adapt to these spatio-temporal changes could severely affect infrastructure and natural systems, especially in water-stressed and ecologically vulnerable regions (Fischer et al., 2005; Malikov et al., 2020).

Adaptation strategies are becoming increasingly essential, as projections show significant socio-economic and environmental losses in their absence (Burke & Emerick, 2016). Model-based assessments suggest that practical adaptation could yield positive global welfare benefits, with estimated costs ranging from $32.7 billion to $54.5 billion between 2015 and 2100 (Beach et al., 2015). In contrast, effective mitigation strategies could reduce the overall economic impact of climatic extremes by up to 75–100% (Tubiello & Fischer, 2007). Achieving long-term sustainability under these changing conditions will require not only global mitigation but also regionally tailored investments in technology and water management efficiency (Müller et al., 2010). Therefore, many future planning and policy decisions demand region-specific assessments, especially regarding water scarcity and the factors driving hydrologic variability (Hunt & Watkiss, 2010; Ziervogel et al., 2014). Understanding hydrologic impacts is crucial as it enables informed decisions and targeted adaptations to mitigate risks, enhance resilience, and sustain ecosystem services. This study contributes to this effort by investigating the spatio-temporal variability of projected extremes and their effects on soil moisture and water balance dynamics, thereby identifying key factors that shape soil water extremes across contrasting geophysical regions.

2.1.2 Spatio-temporal Extremes

Future climate projections indicate an increased frequency of both consecutive dry days and high-intensity precipitation events, thereby amplifying the risks of droughts and floods (Aliyar et al., 2021;

Khan et al., 2020; Zhang et al., 2012). Studies examining the spatio-temporal variability of daily precipitation across the U.S. and other countries project irregular and extreme precipitation intensities (Dhakal & Tharu, 2018; McLeod et al., 2017; Steinschneider & Lall, 2015, 2016). Further, temporal analysis of temperature trends reveals a notable rise in minimum temperatures across various regions worldwide, indicating a general warming trend (Kostopoulou et al., 2014). This escalation in the frequency and severity of extreme temperature events will lead to recurrent climate hazards, profoundly impacting socio-economic development and exacerbating over time (Mallick et al., 2021). Long-term studies of annual and seasonal temperature patterns in the eastern U.S. support this warming trend, suggesting critical implications on future water resources availability (Sayemuzzaman et al., 2014). However, the spatio-temporal alterations of these hydrological extremes remain insufficiently understood, particularly across geophysically diverse landscapes (Kloog et al., 2014). Current studies often lack the resolution or scope to capture how climate variability manifests differently across regions, despite the importance of these patterns for local hydrology and water management. Understanding these patterns of hydrologic extremes is essential for assessing soil moisture variability, runoff, and flood risk across watersheds (Joshi et al., 2019; Rao et al., 2020). There is a critical need to investigate how such extremes evolve over time and across diversified geophysical characteristics. Such an investigation can provide valuable insights into the regional sensitivity of water resources and inform more targeted, adaptive water management strategies.

2.2 SOIL MOISTURE AND STREAMBANK EROSION

2.2.1 Fundamentals of Streambank Erosion

Streambank erosion is a complex and dynamic process that significantly influences river channel morphology, aquatic habitat development, sediment transport, and the structural stability of nearby infrastructure—posing serious ecological and socio-economic risks (Duró et al., 2020; Florsheim et al., 2008; T. Wynn & Mostaghimi, 2006). It generally occurs through three interrelated mechanisms: fluvial erosion, subaerial processes and geotechnical mass failure. Fluvial erosion, particularly at the bank toe, results from hydraulic shear forces exerted by flowing water, which detach and transport soil or rock particles from the bank surface (Sutarto, 2018). Subaerial processes are crucial in preconditioning streambanks for fluvial erosion, which includes weakening and weathering events affecting the soil matrix's moisture conditions (Thorne & Tovey, 1981). These preconditioning mechanisms involve the detachment of soil particles due to high porewater pressures, and loss of matric suction from extensive water exposure (Simon & Rinaldi, 2000). Mass failure involves the gravitational collapse of large sections of the streambank when destabilizing forces exceed material's shear strength (Thorne & Tovey, 1981). This failure mode is governed by internal slope stability and is heavily influenced by pore-water pressure, matric suction, and changes in soil weight due to moisture variations (Simon & Rinaldi, 2000). Factors such as bank height, slope angle, soil cohesion, root reinforcement, and vegetation cover all influence the likelihood of failure (Klavon et al., 2017b).

2.2.2 Hydrologic Extremes on Streambank Erosion

Soil erosion is strongly influenced by hydrologic extremes, which involve complex interactions among rainfall intensity, precipitation patterns, evapotranspiration rates, and soil water content. These extremes—such as intense storms, flash floods, or rapid wetting after prolonged dry periods—can cause rapid changes in soil moisture and flow dynamics, leading to elevated erosion risks (Nearing et al., 2004). For example, initial storm events after prolonged dry spells can saturate the upper soil layers, reducing matric suction that weakens soil cohesion, leading to elevated erosion risks (Brown et al., 2020). Over the past few decades, field observations have documented more frequent and severe streambank erosion events in vulnerable regions, particularly during flashy storm events (Aktar, 2013; Rahman et al., 2015). In response to increasing runoff volumes and storm intensities, effective strategies and accurate prediction tools become increasingly critical for mitigating streambank retreat and managing erosion hazards (Ahmad et al., 2023). Collectively, these studies emphasize the need to investigate how dynamic shifts in hydrologic conditions influence streambank erosion processes and quantify erosion potential under real-world dynamic characteristics at the local scale.

2.2.3 Critical Shear Strength and Erodibility

Accurate estimation of erosion resistance parameters as critical shear stress (τc) and erodibility coefficient (Kd) is essential for modeling streambank erosion, particularly under variable hydrologic conditions. Shear strength acting on streambanks is further shaped by three-dimensional flow fields, channel morphology, roughness distribution, and secondary currents (Klavon et al., 2017b). These parameters are influenced by a combination of factors including soil texture, moisture content, temperature, vegetation cover, and exposure to subaerial processes (Daly et al., 2015; T. M. Wynn et al., 2008a; T. Wynn & Mostaghimi, 2006). This raises the question of whether shear stress and erodibility coefficient can be significantly impacted by dynamic seasonal changes.

2.2.4 Techniques for Measuring τ_c and K_d

Various techniques to estimate fluvial shear strength parameters include flumes, rotating cylinder apparatus (Moore & Masch, 1962), hole erosion tests (HET) (Wan & Fell, 2004), cohesive strength meters (CSM) (Tolhurst et al., 1999), and jet erosion tests (JETs). The original JET (Hanson & Cook, 2004) and the mini-JET (Simon et al., 2010) are commonly used, with data analyzed through the Blaisdell, Scour Depth, and Iterative methods (Blaisdell et al., 1981; Daly et al., 2013). JET variability in erodibility parameters can span 3-4 orders of magnitude at the site and watershed scales due to soil property heterogeneity and extrinsic erosion factors (Hanson & Simon, 2001; Wynn et al., 2008), necessitating estimation by averaging multiple data points to achieve more reliable and representative values. However, laboratory conditions show much less variability across post-processing techniques (Akinola et al., 2019; Khanal et al., 2016). Given the inherent variability in erosion resistance parameters, particularly under changing seasonal soil moisture conditions, understanding and accurately quantifying τc and Kd remains critical for advancing streambank erosion prediction and model performance.

2.3 DYNAMIC SOIL MOISTURE AND EROSION MODELING

2.3.1 Fluvial Erosion Estimations in Models

The erosion rate (ER) in a model is estimated using the erodibility coefficient (K_d), boundary shear stress (τ) and critical shear stress (τ_c) as: $ER = K_d * (\tau - \tau_c)$. For fluvial erosion, the boundary shear stress (τ) is calculated by dividing the bank cross-section into segments influenced by roughness. The hydraulic radius (R) for each segment is estimated by the ratio of cross-sectional area (A) and wetted perimeter (P_n). The shear stress (τ) on each node of the streambank is then calculated using: $\tau_o = \gamma_w$

$R\ S$, where γ_w = unit weight of water (9.807 kN/m^3), and S = channel slope (m/m) (Klavon et al., 2017b).

2.3.2 Mass Failure and Geotechnical Stability

The bank mass failure can be explained using two limit equilibrium methods: horizontal layers (Simon & Rinaldi, 2000) and cantilever failures (Thorne & Tovey, 1981). For streambank stability, the shear strength of saturated soil is estimated by the Mohr-Coulomb criterion as: $\tau_f = c' + (\sigma - \mu_w) \tan \phi'$, where c' is the effective cohesion, σ is the normal stress, ϕ' is the internal friction angle, and μ_w is the pore-water pressure. In unsaturated zones, where streambanks often lie above the water table, the concept of apparent cohesion (ca) becomes important. It includes both electro-chemical bonding in the soil texture and cohesion from surface tension at the air-water interface: $c_a = c' + (\mu_a - \mu_w) \tan\phi^b = c' + \psi \tan \phi^b$, where c_a is the apparent cohesion (kPa), μ_a is the pore-air pressure (kPa), and ψ is the matric suction (kPa). The parameter ϕ^b is the rate of shear strength increase with suction, typically ranging from 10º for unsaturated to 20º for saturated conditions (Fredlund & Rahardjo, 1993). Given that τ_c and K_d are sensitive to soil water dynamics, and seasonal variability, accurate representation of these parameters is critical for improving streambank erosion prediction in modeling frameworks.

2.3.3 Erosion Models and Factor of Safety Approaches

Erosion estimation models such as CONCEPTS, BSTEM, CCHE2D, Delft3D, and HEC-RAS are widely used to simulate channel morphodynamics and assess bank stability (Abdul-Kadir & Ariffin, 2012; Klavon et al., 2017b; Langendoen et al., 2001). These models calculate bank stability by computing the factor of safety (FoS), the ratio of driving to resisting forces for a failure plane, using methods such as horizontal layers, vertical slices, and cantilever shear failures (Klavon et al., 2017b).

2.3.4 Shear Stress Estimation in Meandering Channels

The general shear stress equation, while applicable to straight channels, does not account for the curvature-induced secondary circulation and variations, which can significantly impact flow dynamics and erosion patterns in natural meandering streams (Dietrich & Richards, 1987). To account for these effects, the erosion model modifies the equation using a perturbation method (Crosato, 2009). Considering the water depth downstream gradients and flow velocity as small, shear stress is given by: $\tau_0 = \gamma_w n^2 (u + U)^2 / R^{1/3}$. Such modifications in the model enable it to better assess the impacts of increased near-bank velocity.

2.3.5 Manning's n and Boundary Shear Stress

Flow resistance in vegetated open channels arises from both viscous and pressure drag, which can be decomposed into grain, form, and vegetal roughness components (Temple et al., 1987), the total shear stress is modified with these three components: $\tau_o = \tau_g + \tau_f + \tau_v$, where the subscripts g, f, and v represent grain, form, and vegetal components, respectively. Manning's roughness (n) for each component is applied to estimate the individual contributions to the total boundary shear stress (Temple, 1980): $n^2 = n_g^2 + n_f^2 + n_v^2$. Further, the grain roughness for the nodes of the bank profile is estimated by Strickler's equation (Chow, 1959): $n_g = 0.0417\ (d_{50}^{1/6})$. In modeling applications where a total Manning's n is provided, the model estimates the grain roughness component (ng) using Strickler's equation and then applies the correction by equation: $\tau_g = \tau_o\ (n_g^2 / n^2)$, to isolate the effective boundary shear stress attributable to grain resistance, excluding form and vegetal roughness effects. These roughness-based corrections to boundary shear stress are critical for improving model accuracy, particularly in channels with complex boundary conditions such as variable sediment sizes, and irregular bank geometry across different layers. In cases where the total roughness, Manning's n is unknown, applying a range of plausible total roughness values could identify the most realistic estimate of boundary shear stress.

2.4 Knowledge Gaps and Contributions

IPCC reports and previous studies have projected rising global temperatures and erratic precipitation, which can obstruct water use, resulting in critical water scarcity and significant financial losses. The current understanding largely emphasizes broad-scale impacts on agriculture, infrastructure, and water resources, but fails to provide adequate insight into localized spatio-temporal variability of these changes, particularly in relation to soil moisture. Furthermore, existing literature highlights a growing trend in consecutive dry days, intensified precipitation, and temperature anomalies, yet the spatial and seasonal manifestation of these hydraulic extremes remains underexplored, especially across varying physiographic regions. This creates uncertainty in understanding the hydrologic consequences of climate-induced changes at the watershed scale.

Gap 1: Lack of localized understanding of climate-induced soil moisture variability

This study addresses this first gap by evaluating the spatio-temporal variability of climate-induced soil moisture extremes and identifying the dominant factors responsible for these changes across geophysically diverse watersheds. These findings are intended to support adaptive water management planning under climate uncertainty.

The mechanisms of streambank erosion, namely fluvial erosion, subaerial weakening, and mass failure—are well documented, but their sensitivity to changing soil moisture remains insufficiently understood. Existing models and studies frequently treat erosion resistance parameters such as critical shear stress (τc) and erodibility coefficient (Kd) as fixed values. This static assumption fails to capture the dynamic nature of soil strength as influenced by seasonal or episodic changes in soil water content. While field-based Jet Erosion Tests (JETs) are commonly used to quantify τc and Kd, their results are often interpreted without considering the real-time soil moisture conditions at the time of testing. This omission limits the ability to establish predictive relationships between soil water variability and erosion resistance in a wider range. Moreover, despite evidence of large variability in erodibility parameters at the site and watershed scales, only a few lab studies evaluated how this variability correlates with shifts in soil moisture.

Gap 2: Lack of field-based understanding of soil moisture's impact on τc and Kd

This study bridges this second gap by pairing JET-derived τc and Kd values with time-resolved soil moisture data across seasons. The objective is to evaluate how erosion resistance evolves in response to wet and dry seasons and to generate more accurate, field-based parameterizations for use in erosion prediction.

Although process-based erosion models such as BSTEM, HEC-RAS, and CONCEPTS incorporate established hydraulic and geotechnical frameworks for estimating fluvial erosion and mass failure, they predominantly use static values for key parameters—namely, critical shear stress (τc), erodibility coefficient (Kd), and Manning's roughness (n). Specifically, the erosion rate (ER) is directly influenced by these parameters. This simplification limits their ability to predict seasonal erosion dynamically as these parameters vary significantly across space and time in natural streambanks. Soil strength parameters (τc and Kd) vary not only between sites but also over time within a site, especially under fluctuating soil moisture. Similarly, manning's n is often applied as a single value across the bank profile, known to affect τ dominantly by altering flow resistance.

Gap 3: Static modeling frameworks that ignore time-varying erosion resistance

This study addresses this third gap by developing a modified version of BSTEM that incorporates field-derived equations linking soil moisture with τc and Kd, thereby enabling dynamic updates of erosion resistance in real-time. It also tests a range of Manning's n values to evaluate how model sensitivity shifts under different roughness assumptions. Together, these enhancements enable more accurate and responsive erosion modeling, especially under temporally varying hydrologic conditions, and represent a significant step toward integrating physically meaningful, time-varying inputs into bank erosion prediction frameworks.

Together, these gaps led to the formulation of three central research objectives. First, to evaluate the spatio-temporal variability of soil moisture extremes and identify their climatic and physiographic drivers. Second, to assess how temporal variation of soil moisture influences τ_c and K_d through field-based erosion resistance measurements. Third, to enhance the predictive capabilities of the BSTEM model by integrating dynamic, soil moisture-driven equations for τc and Kd and testing its performance across a range of Manning's n values. By addressing these objectives, this study contributes novel insights into climate–soil–erosion interactions and improves the predictive capacity of erosion modeling frameworks.

REFERENCES

Abdul-Kadir, M. A., & Ariffin, J. (2012). Advances on Bank Erosion Studies: A Review. ASM Sci. J., 6(2), 128–137.

Ahmad, D., Kanwal, M., & Afzal, M. (2023). Climate change effects on riverbank erosion Bait community flood-prone area of Punjab, Pakistan: an application of livelihood vulnerability index. Environment, Development and Sustainability, 25(9), 9387–9415. https://doi.org/10.1007/S10668-022-02440-1/FIGURES/6

Aktar, N. (2013). Impact of Climate Change on Riverbank Erosion. IJSBAR) International Journal of Sciences: Basic and Applied Research (IJSBAR, 7(1), 36–42. http://gssrr.org/index.php?journal=JournalOfBasicAndApplied

Aliyar, Q., Dhungana, S., & Shrestha, S. (2021). Spatio-temporal trend mapping of precipitation and its extremes across Afghanistan (1951–2010). Theoretical and Applied Climatology, 147(1–2), 605–626. https://doi.org/10.1007/s00704-021-03851-2

Beach, R. H., Cai, Y., Thomson, A., Zhang, X., Jones, R., McCarl, B. A., Crimmins, A., Martinich, J., Cole, J., Ohrel, S., DeAngelo, B., McFarland, J., Strzepek, K., & Boehlert, B. (2015). Climate change impacts on US agriculture and forestry: benefits of global climate stabilization. Environmental Research Letters, 10(9), 95004. https://doi.org/10.1088/1748-9326/10/9/095004

Blaisdell, F. W., Hebaus, G. G., & Anderson, C. L. (1981). Ultimate Dimensions of Local Scour. Journal of the Hydraulics Division, 107(3), 327–337. https://doi.org/10.1061/JYCEAJ.0005630

Blanc, E., & Reilly, J. (2017). Approaches to Assessing Climate Change Impacts on Agriculture: An Overview of the Debate. Review of Environmental Economics and Policy, 11(2), 247–257. https://doi.org/10.1093/reep/rex011

Brown, D. R. N., Brinkman, T. J., Bolton, W. R., Brown, C. L., Cold, H. S., Hollingsworth, T. N., & Verbyla, D. L. (2020). Implications of climate variability and changing seasonal hydrology for subarctic riverbank erosion. Climatic Change, 162(2), 1–20. https://doi.org/10.1007/S10584-020-02748-9/FIGURES/9

Burke, M., & Emerick, K. (2016). Adaptation to Climate Change: Evidence from US Agriculture. American Economic Journal: Economic Policy, 8(3), 106–140. https://doi.org/10.1257/pol.20130025

Chow, V. T. (1959). Open-channel hydraulics. McGraw-Hill Book Co., New York, N.Y.

Crosato, A. (2009). Physical explanations of variations in river meander migration rates from model comparison. Earth Surface Processes and Landforms, 34(15), 2078–2086. https://doi.org/10.1002/ESP.1898

Daly, E. R., Fox, G. A., Al-Madhhachi, A. T., & Miller, R. B. (2013). A Scour Depth Approach for Deriving Erodibility Parameters from Jet Erosion Tests. Transactions of the ASABE, 56(6), 1343–1351. https://doi.org/10.13031/TRANS.56.10350

Daly, E. R., Miller, R. B., & Fox, G. A. (2015). Modeling streambank erosion and failure along protected and unprotected composite streambanks. Advances in Water Resources, 81, 114–127. https://doi.org/10.1016/J.ADVWATRES.2015.01.004

Dhakal, N., & Tharu, B. (2018). Spatio-temporal trends in daily precipitation extremes and their connection with North Atlantic tropical cyclones for the southeastern United States. International Journal of Climatology, 38(10), 3822–3831. https://doi.org/10.1002/joc.5535

Dietrich, W. E., & Richards, K. S. (1987). River Channels: Environment and Process.

Duró, G., Crosato, A., Kleinhans, M. G., Roelvink, D., & Uijttewaal, W. S. J. (2020). Bank Erosion Processes in Regulated Navigable Rivers. Journal of Geophysical Research: Earth Surface, 125(7). https://doi.org/10.1029/2019JF005441

Fischer, G., Shah, M., N. Tubiello, F., & van Velhuizen, H. (2005). Socio-economic and climate change impacts on agriculture: an integrated assessment, 1990–2080. Philosophical Transactions of the Royal Society B: Biological Sciences, 360(1463), 2067–2083. https://doi.org/10.1098/rstb.2005.1744

Florsheim, J. L., Mount, J. F., & Chin, A. (2008). Bank Erosion as a Desirable Attribute of Rivers. BioScience, 58(6), 519–529. https://doi.org/10.1641/B580608

Fredlund, D. G., & Rahardjo, H. (1993). Soil Mechanics for Unsaturated Soils. Soil Mechanics for Unsaturated Soils. https://doi.org/10.1002/9780470172759

Hanson, G. J., & Cook, K. R. (2004). APPARATUS, TEST PROCEDURES, AND ANALYTICAL METHODS TO MEASURE SOIL ERODIBILITY IN SITU. Applied Engineering in Agriculture, 20(4), 455–462. https://doi.org/10.13031/2013.16492

Hanson, G. J., & Simon, A. (2001). Erodibility of cohesive streambeds in the loess area of the Midwestern USA. Hydrological Processes, 15(1), 23–38. https://doi.org/10.1002/HYP.149

Hitz, S., & Smith, J. (2004). Estimating global impacts from climate change. Global Environmental Change, 14(3), 201–218. https://doi.org/10.1016/j.gloenvcha.2004.04.010

Hunt, A., & Watkiss, P. (2010). Climate change impacts and adaptation in cities: a review of the literature. Climatic Change, 104(1), 13–49. https://doi.org/10.1007/s10584-010-9975-6

Joshi, S., Garbrecht, J., & Brown, D. (2019). Observed Spatiotemporal Trends in Intense Precipitation Events across United States: Applications for Stochastic Weather Generation. Climate, 7(3), 36. https://doi.org/10.3390/cli7030036

Khan, N., Shahid, S., Chung, E.-S., Behlil, F., & Darwish, M. S. J. (2020). Spatiotemporal changes in precipitation extremes in the arid province of Pakistan with removal of the influence of natural climate variability. Theoretical and Applied Climatology, 142(3–4), 1447–1462. https://doi.org/10.1007/s00704-020-03389-9

Kikstra, J. S., Nicholls, Z. R. J., Smith, C. J., Lewis, J., Lamboll, R. D., Byers, E., Sandstad, M., Meinshausen, M., Gidden, M. J., Rogelj, J., Kriegler, E., Peters, G. P., Fuglestvedt, J. S., Skeie, R. B., Samset, B. H., Wienpahl, L., Van Vuuren, D. P., Van Der Wijst, K. I., Al Khourdajie, A., … Riahi, K. (2022). The IPCC Sixth Assessment Report WGIII climate assessment of mitigation pathways: from emissions to global temperatures. Geoscientific Model Development, 15(24), 9075–9109. https://doi.org/10.5194/GMD-15-9075-2022

Klavon, K., Fox, G., Guertault, L., Langendoen, E., Enlow, H., Miller, R., & Khanal, A. (2017). Evaluating a process-based model for use in streambank stabilization: insights on the Bank Stability and Toe Erosion Model (BSTEM). Earth Surface Processes and Landforms, 42(1), 191–213. https://doi.org/10.1002/esp.4073

Kloog, I., Nordio, F., Coull, B. A., & Schwartz, J. (2014). Predicting spatiotemporal mean air temperature using MODIS satellite surface temperature measurements across the Northeastern USA. Remote Sensing of Environment, 150, 132–139. https://doi.org/10.1016/j.rse.2014.04.024

Kostopoulou, E., Giannakopoulos, C., Hatzaki, M., Karali, A., Hadjinicolaou, P., Lelieveld, J., & Lange, M. A. (2014). Spatio-temporal patterns of recent and future climate extremes in the eastern Mediterranean and Middle East region. Natural Hazards and Earth System Sciences, 14(6), 1565–1577. https://doi.org/10.5194/nhess-14-1565-2014

Langendoen, E. J., Simon, A., & Thomas, R. E. (2001). CONCEPTS - A Process-Based Modeling Tool to Evaluate Stream-Corridor Restoration Designs. Proceedings of the 2001 Wetlands Engineering and River Restoration Conference, 1–11. https://doi.org/10.1061/40581(2001)109

Malikov, E., Miao, R., & Zhang, J. (2020). Distributional and temporal heterogeneity in the climate change effects on U.S. agriculture. Journal of Environmental Economics and Management, 104, 102386. https://doi.org/10.1016/j.jeem.2020.102386

Mallick, J., Islam, A. R. Md. T., Ghose, B., Islam, H. M. T., Rana, Y., Hu, Z., Bhat, S. A., Pal, S. C., & Ismail, Z. Bin. (2021). Spatiotemporal trends of temperature extremes in Bangladesh under changing climate using multi-statistical techniques. Theoretical and Applied Climatology, 147(1–2), 307–324. https://doi.org/10.1007/s00704-021-03828-1

McLeod, J., Shepherd, M., & Konrad, C. E. (2017). Spatio-temporal rainfall patterns around Atlanta, Georgia and possible relationships to urban land cover. Urban Climate, 21, 27–42. https://doi.org/10.1016/j.uclim.2017.03.004

Moore, W. L., & Masch, F. D. (1962). Experiments on the scour resistance of cohesive sediments. Journal of Geophysical Research, 67(4), 1437–1446. https://doi.org/10.1029/JZ067I004P01437

Müller, C., Bondeau, A., Popp, A., Waha, K., & Fader, M. (2010). Development and Climate Change CLIMATE CHANGE IMPACTS ON AGRICULTURAL YIELDS. http://faostat.fao.org/default.aspx

Nearing, M., Pruski, F. F., & O'Neal, M. R. (2004). Expected climate change impacts on soil erosion rates: A review. Journal of Soil and Water Conservation, 59(1), 43–50. https://www.jswconline.org/content/59/1/43

Rahman, M. A. T. M. T., Islam, S., & Rahman, S. H. (2015). Coping with flood and riverbank erosion caused by climate change using livelihood resources: a case study of Bangladesh. Climate and Development, 7(2), 185–191. https://doi.org/10.1080/17565529.2014.910163

Sayemuzzaman, M., Jha, M. K., & Mekonnen, A. (2014). Spatio-temporal long-term (1950–2009) temperature trend analysis in North Carolina, United States. Theoretical and Applied Climatology, 120(1–2), 159–171. https://doi.org/10.1007/s00704-014-1147-6

Simon, A., & Rinaldi, M. (2000). Channel instability in the loess area of the midwestern United States. Journal of the American Water Resources Association, 36(1), 133−150. https://doi.org/10.1111/j.1752-1688.2000.tb04255.x

Simon, A., Thomas, R. E., & Klimetz, L. (2010). COMPARISON AND EXPERIENCES WITH FIELD TECHNIQUES TO MEASURE CRITICAL SHEAR STRESS AND ERODIBILITY OF COHESIVE DEPOSITS.

Steinschneider, S., & Lall, U. (2015). Daily Precipitation and Tropical Moisture Exports across the Eastern United States: An Application of Archetypal Analysis to Identify Spatiotemporal Structure. Journal of Climate, 28(21), 8585–8602. https://doi.org/10.1175/jcli-d-15-0340.1

Steinschneider, S., & Lall, U. (2016). Spatiotemporal Structure of Precipitation Related to Tropical Moisture Exports over the Eastern United States and Its Relation to Climate Teleconnections. Journal of Hydrometeorology, 17(3), 897–913. https://doi.org/10.1175/jhm-d-15-0120.1

Sutarto, T. E. (2018). A Short Review on Various Techniques for Measuring Stream Bank Soil Erosion Strength. Proceedings - 2018 International Conference on Applied Science and Technology, ICAST 2018, 252–258. https://doi.org/10.1109/iCAST1.2018.8751560

Temple, D. M. (1980). Tractive Force Design of Vegetated Channels. Transactions of the ASAE, 23(4), 884–0890. https://doi.org/10.13031/2013.34681

Temple, D. M., Robinson, K., Ahring, R., & Davis, A. (1987). Stability Design of Grass-lined Open Channels - Google Books. US Department of Agriculture, Agriculture Handbook 667. https://www.google.com/books/edition/Stability_Design_of_Grass_lined_Open_Cha/G3B7JmODtxwC?hl=en&gbpv=0

Thorne, C. R., & Tovey, N. K. (1981). Stability of composite river banks. Earth Surface Processes and Landforms, 6(5), 469–484. https://doi.org/10.1002/ESP.3290060507

Tolhurst, T. J., Black, K. S., Shayler, S. A., Mather, S., Black, I., Baker, K., & Paterson, D. M. (1999). Measuring the in situ Erosion Shear Stress of Intertidal Sediments with the Cohesive Strength Meter (CSM). Estuarine, Coastal and Shelf Science, 49, 281–294. http://www.idealibrary.comon

Tubiello, F. N., & Fischer, G. (2007). Reducing climate change impacts on agriculture: Global and regional effects of mitigation, 2000–2080. Technological Forecasting and Social Change, 74(7), 1030–1056. https://doi.org/10.1016/j.techfore.2006.05.027

Venkata Rao, G., Venkata Reddy, K., Srinivasan, R., Sridhar, V., Umamahesh, N. V, & Pratap, D. (2020). Spatio-temporal analysis of rainfall extremes in the flood-prone Nagavali and Vamsadhara Basins in eastern India. Weather and Climate Extremes, 29, 100265. https://doi.org/10.1016/j.wace.2020.100265

Wan, C. F., & Fell, R. (2004). Investigation of Rate of Erosion of Soils in Embankment Dams. Journal of Geotechnical and Geoenvironmental Engineering, 130(4), 373–380. https://doi.org/10.1061/(ASCE)1090-0241(2004)130:4(373)

Wynn, T. M., Henderson, M. B., & Vaughan, D. H. (2008a). Changes in streambank erodibility and critical shear stress due to subaerial processes along a headwater stream, southwestern Virginia, USA. Geomorphology, 97(3–4), 260–273. https://doi.org/10.1016/j.geomorph.2007.08.010

Wynn, T. M., Henderson, M. B., & Vaughan, D. H. (2008b). Changes in streambank erodibility and critical shear stress due to subaerial processes along a headwater stream, southwestern Virginia, USA. Geomorphology, 97(3–4), 260–273. https://doi.org/10.1016/j.geomorph.2007.08.010

Wynn, T., & Mostaghimi, S. (2006). The effects of vegetation and soil type on streambank erosion, Southwestern Virginia, USA. Journal of the American Water Resources Association, 42(1), 69–82. https://doi.org/10.1111/j.1752-1688.2006.tb03824.x

Zhang, Q., Singh, V. P., Li, J., Jiang, F., & Bai, Y. (2012). Spatio-temporal variations of precipitation extremes in Xinjiang, China. Journal of Hydrology, 434–435, 7–18. https://doi.org/10.1016/j.jhydrol.2012.02.038

Ziervogel, G., New, M., van Garderen, E., Midgley, G., Taylor, A., Hamann, R., Stuart-Hill, S., Myers, J., & Warburton, M. (2014). Climate change impacts and adaptation in South Africa. WIREs Climate Change, 5(5), 605–620. https://doi.org/10.1002/wcc.295

CHAPTER-3

CLIMATE CHANGE IMPACTS ON SPATIO-TEMPORAL SOIL WATER EXTREMES IN GEOPHYSICALLY DIVERSE WATERSHEDS: A COMPARISON BETWEEN EAST AND WEST TENNESSEE WATERSHEDS

PUBLICATION STATEMENT

Saha, P., Hathaway, J., Schwartz, J. S. et al. (2024). Climate change impacts on spatiotemporal soil water extremes in geophysically diverse watersheds: A comparison between East and West Tennessee watersheds. JOHE, 29(3), 05024003. https://doi.org/10.1061/JHYEFF.HEENG-6117

The first author led research design, data processing, modeling, analysis, and manuscript writing. Co-authors contributed to methodological feedback and manuscript editing.

RESEARCH QUESTION

How will climate change impact soil moisture spatio-temporally in geophysically diverse watersheds, and what are the driving factors behind soil moisture extremes?

ABSTRACT

Climate change impacts hydrologic processes, compelling more regional water budget studies to understand spatio-temporal hydrological extremes. This study investigates the effects of climate change on water budgets, with a focus on soil moisture, in two Tennessee watersheds with different geo-climatic characteristics, Obion and Nolichucky Rivers. Using the hydrological model VIC, the study projects water budgets for these watersheds until 2099, analyzing annual and seasonal runoff, recharge, and soil moisture to identify trends and extremes. Results show that an increase in temperature of 2.7-6.4°C and a change of precipitation by 1-4% is predicted for Tennessee, which will impact seasonal patterns, water balances, and soil moisture regimes. The overlapping of such impacts can lower soil moisture below the wilting point during 40-50% of the growing season, impacting crop yields. The study identifies field capacity, clay soil percentage, and organic matter as key factors impacting the spatial extremes of croplands' irrigation requirements. These findings underscore the need to understand soil moisture variability and extreme soil water conditions to optimize soil-water management scenarios and mitigate future water shortage risks.

3.1 INTRODUCTION

Regional trends from the CMIP5 (Coupled Model Inter-comparison Project Phase 5) indicate that soil water deficits will likely increase due to infrequent extreme precipitation and enhanced evaporation (Trudel, et al., 2016). Multiple studies have projected a rise in the severity of hydrological drought by 2100 and soil water extremes exceeding 40% under high-end climate scenarios (Spinoni, 2019; Hejazi et al., 2015; Khatri, et al., 2018). Previous studies suggest that future systems must be more open, collaborative, and diverse to work with systemic issues (Fazey, et al., 2020). Hence, while all these general patterns are valuable, actionable regional descriptions of climate change effects are critically needed.

Understanding the impact of climate change on different geo-climatic watersheds is crucial for the sustainable management of soil water deficits in the short and long term (Earman & Dettinger, 2011; Meixner, et al., 2016; Anand, et al., 2018; Rahman, et al., 2019; Saha et al., 2020). Previous studies have demonstrated that geo-climatic characteristics significantly influence runoff and soil moisture responses to climate change, with multiple watersheds showing variable results. (He et al., 2019; Zheng, et al., 2018; Sanchez-Gomez, et al., 2009; Roy et al., 2021). Moreover, studies examining the impact of climate change on hydrology globally indicate that changes in runoff are not uniform and will vary depending on regional precipitation distribution. (Arora & Boer, 2001). Therefore, understanding the impact of climate change on different watersheds is critical for developing effective soil-water management strategies to mitigate water shortages in the future.

Urbanization and agricultural expansion in the Southeast United States under a changing climate threaten crop yields, infrastructural sustainability, and river ecosystems, making the region vulnerable to future soil water deficits (Schilling, et al., 2015; Acharya, et al., 2012; Gao, et al., 2010; Hayhoe et al., 2008). In Tennessee, a comparison of the spatial and temporal patterns of soil water extreme conditions would provide valuable insight into the role of watershed-scale characteristics in regulating climate change effects due to the large variability in land cover, topography, and geology from east to west. This study aims to understand the co-evolution of shifts in the regional climate with land use changes for representative concentration pathways (RCPs) based on greenhouse gas concentrations and the implications of this co-play on water budget trajectories. The novelty of this work lies in its exploration of the interplay between climate change and land use changes in regulating soil water deficits, providing actionable information for sustainable management in Tennessee and other regions facing similar challenges.

Previous research on the impact of climate change on water budgets has not adequately addressed soil moisture, which is critical for intensively managed agricultural watersheds (Ghaneeizad, et al., 2018; Lobanova, 2018). The soil water budget, which is the balance of precipitation, runoff, evapotranspiration, and baseflow fluxes, plays a significant role in the function and structure of agroecosystems and crop yield dynamics. Based on soil moisture metrics, future projections suggest an increase in drought occurrences, primarily attributed to increases in evaporative demand (Berg & Sheffield, 2018). However, the complex nature of the soil environment poses challenges in accurately predicting the effects of climate change on the quality and functionality necessary for agricultural yield (Furtak & Wolińska, 2023). While existing models and observations qualitatively support this relationship, uncertainties persist regarding quantitative aspects. Addressing these uncertainties through observations is crucial for precisely representing this critical relationship (Seneviratne, et al., 2010). The lack of understanding of how geo-spatial heterogeneity and management decision making offset climate impacts has made it difficult to predict water budgets for agriculture and beyond. Existing studies have mainly focused on precipitation, evapotranspiration, and runoff, neglecting soil moisture, which is essential for predicting the effects of climate change on water budgets in these agricultural watersheds.

Previous studies conducted in Tennessee have highlighted the declining groundwater flow resulting from excessive withdrawals over the past three decades. This decline indicates potential future soil water deficits that may have severe consequences on the region's hydrology (Haugh, 2012; Razmara, et al., 2016; Meixner, et al., 2016). Moreover, a warming climate and erratic precipitation patterns are the primary drivers of soil moisture depletion and extreme drought in the state (McLaughlin, et al., 2007; Liu, et al., 2014). A study conducted on the Obion River in Tennessee found that the changing climate could lead to a decrease in the utilization of available water, which would have significant implications for the region's water management strategies (Wilson, et al., 2018). However, the factors driving the observed spatial extremes are not yet fully understood, making this study interesting specifically for soil moisture.

Projected increases in soil water extremes and soil moisture conditions that do not meet crop physiology thresholds have the potential to severely impact crop yields in Tennessee. Despite a few existing studies, there is a lack of research that can capture the effects of spatial heterogeneity and climate feedbacks on crop production using mesoscale models (Chu, et al., 2019; Raje, et al., 2013), whereas this study aims to address this research gap. This study on the projected impact of climate changes on soil moisture across eastern and western Tennessee will help understand future soil water extreme conditions and guide actionable future climate strategies. Besides, the topographical, pedological, and land cover differences across the state provide a rich dataset of hydrological responses and water budget extremes that can apply to other watersheds facing similar challenges.

The objectives of this study aim to address the current limitations in literature and provide insight into the impacts of climate change on the soil water budget in Tennessee. Specifically, the study aims to (1) develop a future dynamic water budget using a mesoscale hydrological model based on four climate models in two geophysically diverse watersheds in Tennessee, representative of the Mississippi Loess and Blue Ridge regions in the SE, until 2099; (2) identify short and long-term trends and extremes (i.e., hot moments) of hydrologic responses to future climate scenarios; (3) compare the locations of soil water extremes (i.e., hotspots) in diverse geophysical watersheds in East and West Tennessee; and (4) statistically identify the factors impacting soil moisture for locations with a cropland cover using structural equation models. By achieving these objectives, the study can provide valuable insights into the impacts of climate change on the soil water budget in Tennessee and help guide future adaptation strategies for agricultural production.

3.2 STUDY SITE CHARACTERISTICS

The study chose the Obion and Nolichucky River watersheds **(Figure 3-1)** due to their different geo-climatic characteristics, shown in **Table 3-1**. The Obion watershed is in Ecoregions 65 and 74 (Southwestern Plains and Mississippi Valley Loess Plains), while the Nolichucky watershed is in Ecoregions 66 and 67 (Blue Ridge and Ridge & Valley). These two watersheds were chosen because they represent distinct geophysical regions within the state of Tennessee, allowing for the examination of how hydrological processes and responses may vary across different terrain types. Furthermore, the inclusion of both watersheds enables the study to capture a wide range of soil moisture conditions and water budget extremes that may be encountered across the state.

The Obion watershed exhibits an elevation range of 42 m to 204 m, while the Nolichucky watershed ranges from 275 m to 2037 m **(Figure 3-1b)**. The Obion watershed is relatively flat and topographically symmetrical compared to Nolichucky. The west of Obion is flat (0-2% slope), while the east is hilly (2-9% slope) with a few scattered steep slopes (9-15%). In the Nolichucky, the eastern portion is occupied by the Appalachian Mountains (9-15% slope), while the western part features a steeper topography (2-9% slope). The Obion watershed has more extensive cropland coverage than the Nolichucky, with a significant amount of forest cover in the eastern region **(Figure 3-1c)**. Important cash crops such as soybeans, corn, cotton, and wheat are grown in the area, which plays a vital role in the economic strength of Tennessee. In terms of soils **(Figure 3-1d)**, the Obion watershed has a considerable portion of loess-derived silty loam soils (MrB) with a broad fragipan coverage in the central region. On the other hand, the Nolichucky watershed features a mountainous bedrock system in eastern Tennessee with shallower soil profiles and a much smaller area of fragipan soils.

Table 3-1 Geo-climatic characteristics of the study area watersheds

Characteristics	Parameters	Obion	Nolichucky
Topography Slope	Flat (0-2%)	45.5%	7.1%
	Gentle (2-9%)	40.1%	19.6%
	Moderate (9-15%)	9.5%	14.5%
	Strong (15-25%)	3.9%	16.6%
	Steep (>25%)	1.1%	42.2%
Climate	Baseline Annual Rainfall	1347 mm	1253 mm
	Baseline Avg. Temperature	15.5°C	12.9°C
	Growing Seasons	Long (6-8 Months)	Short (4-6 Months)
Land use cover	Forest & Woodlands	35.6%	68.0%
	Pasture	25.4%	10.1%
	Cropland	37.8%	21.5%
	Urban	0.7%	0.5%
Soils	Dominant Texture	Sand	Clay
	Fragipan/ Bedrock	Fragipan	Bedrock
	Glacial Presence	Yes	No

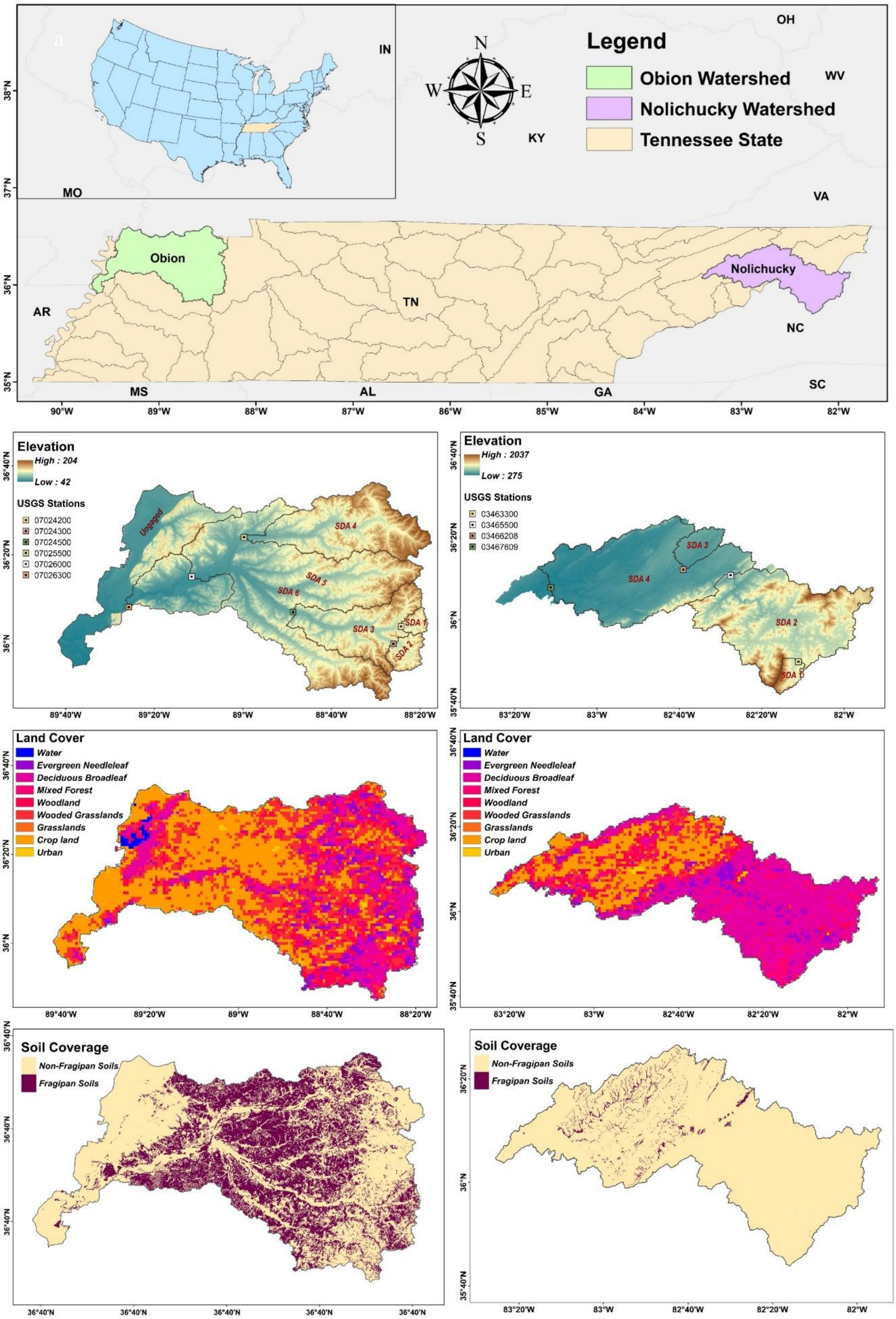

Figure 3-1 a. Selected Study Sites at the East and West of Tennessee State in the US and Study Site Comparison between Obion and Nolichucky River Watersheds for b. Elevation, c. Land Cover, and d. Soil Coverage.

3.3 MATERIALS AND METHODS

3.3.1 Summary of Approach

The study employed the Variable Infiltration Capacity (VIC) model to project future water budgets within the Obion and Nolichucky River watersheds, as illustrated in **Figure 3-2**. The study identified trends in runoff, recharge, and soil moisture due to climate change and occurrences of extreme conditions using both annual and monthly analyses. Previous studies showed that the acceptable baseline period for climate projections is 10 years, and the climate intensity extremes are accepted as 95^{th} and 99^{th} percentiles for different water balance parameters (such as precipitation, temperature and runoff) (Wrzesien & Pavelsky, 2020; Yin, et al., 2018; Dunkerley, 2019). Based on that, the extreme conditions were defined operationally as the 1^{st} and 99^{th} frequency percentiles (low and high) for this study, representing the worst-case scenarios for runoff and recharge. In terms of soil moisture, the average wilting point and field capacity were applied as the thresholds for identifying extreme conditions. Field capacity (FC) is the maximum amount of water held in soil after excess water has drained away, and wilting point (WP) is the point when there is no water available to the plant (depends on plant variety, but usually around 15 bars for sunflower, wheat, and corn). (Rai, et al., 2017; Briggs & Shantz, 1912) The VIC model estimates field capacity and wilting point as a fractional water content at 1/3 bar tension and 15 bar tension, respectively, based on the predefined USDA class and soil types (Liang, et al., 1994; Schaake, 2000).

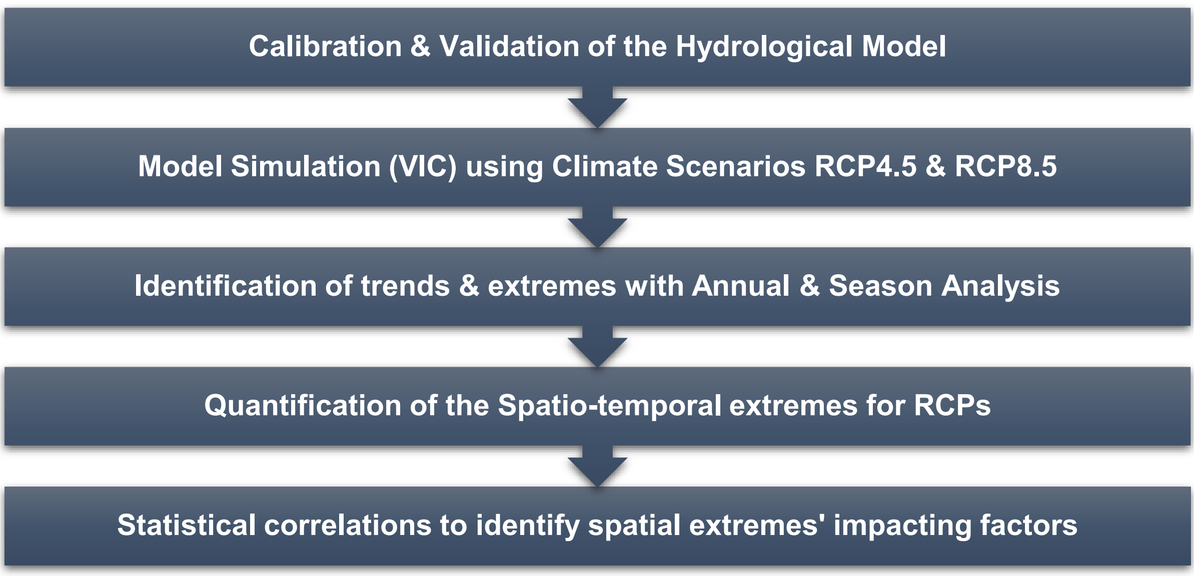

Figure 3-2 Methodology Flow Chart of the Study

For this study, the average wilting point was computed as the spatial mean of croplands at 1 km resolution within each watershed for comparison purposes (the vegetation data defines croplands). The conditions were examined in detail during three distinct decadal periods, with the period from 2006 to 2015 considered the baseline period. The conditions during the periods of 2046 to 2055 (short term) and 2090 to 2099 (long term) were compared to the baseline period. The study identified the hottest and driest locations (i.e., hot spots) and time periods (i.e., hot moments) during the three extreme months, using the 1st and 99th percentiles for temperature and rainfall in each of these three periods (Supplementary A). Finally, a statistical correlation analysis of soil moisture was performed on croplands to assess the impacts of spatial water extremes on hydrological processes, soil textures, and watershed attributes.

3.3.2 Data Descriptions

To construct the regional hydrologic VIC model, the watersheds were divided into sub-drainage areas using the available United States Geological Survey (USGS) monitoring stations as "outlets." The Obion watershed was divided into six sub-drainage areas, while the Nolichucky watershed was divided into four. The VIC model was then incorporated with climate, soil, vegetation, and elevation data, whose sources are presented in **Table 3-2**. To ensure accuracy, the model was calibrated using existing streamflow data (1996-2013) from USGS stations and validated with evaporation data (2000-2013) from MODIS (Moderate Resolution Imaging Spectroradiometer) and soil moisture data (2003-2013) from NRCS-SCAN (Natural Resources Conservation Service- Soil Climate Analysis Network).

Table 3-2 Description of the Input Data Sources for the Hydrological Simulation

Data Type	Description	Source
Climate	1 km Resolution	Multivariate Adaptive Constructed Analogs (MACA) Data portal
Soil	1 Km Resolution	Soil Information for Environmental Modeling and Ecosystem Management (Soil Info)
		USDA Web Soil Survey (WSS)
Vegetation	1 km Resolution	AVHRR- Global Land Cover Facility (GLCF), University of Maryland
Elevation	30 m DEM	Tennessee GIS data server
Streamflow	Monthly	United States Geological Survey (USGS)
Evapotranspiration	Monthly	MODIS- USGS Geo Data Portal

Climate Models and Scenarios

Four climate models were selected from the Coupled Model Inter-comparison Project Phase 5 (CMIP5) that best captures the scenarios of Tennessee and exhibit less than 10% bias deviation (Sheffield et al., 2013). The moderate scenario RCP4.5 and the extreme scenario RCP8.5 were used, and the four models were averaged for analysis.

- Geophysical Fluid Dynamics Laboratory model (GFDL-ESM2M) (Dunne et al., 2006)
- Met Office Hadley Centre Global Environment Model (HadGEM2-CC) (Collins, 2008)
- Institut Pierre-Simon Laplace model (IPSL-CM5A-MR) (Sepulchre, et al., 2019)
- Model for Interdisciplinary Research on Climate (MIROC-ESM-CHEM) (JAMSTEC, 2014)

Climate Data Overview

The temperature in the Obion and Nolichucky watersheds is expected to increase under the RCP4.5 and RCP8.5 climate scenarios, with the latter projecting a greater increase. Specifically, the projected temperature increases for the Obion and Nolichucky under RCP4.5 are 2.7°C (17.5%) and 2.5°C (19.6%), respectively, compared to 6.4°C (41.4%) and 5.9°C (45.7%) under RCP8.5 during 2015-99. Precipitation projections are more variable, with the Obion projected to experience an 11mm (0.8%) increase under RCP4.5 and an 18 mm (1.3%) decrease under RCP8.5, while Nolichucky is expected to see a 47 mm (3.8%) increase under RCP4.5 and a 24 mm (1.9%) increase under RCP8.5. However, these changes in annual precipitation may mask seasonal shifts and alterations in rainfall distribution. To determine climate extremes, frequency histograms were constructed for both watersheds under both climate scenarios, identifying the 1st and 99th percentiles as the extreme months. A monthly scatter plot was generated to pinpoint the three consecutive months meeting the extreme criteria over the next century. Seasonal analyses were carried out by comparing the baseline and projected scenarios' extreme limits to detect early or late seasonal shifts, and **Table 3-3** summarizes the annual and seasonal trend analyses with the frequency percentiles.

Table 3-3 Summary on the climatic trends & extremes Overview

Category			Projection Trends	Baseline Scenario (2006-15)	Projection Alterations	Climate Extremes	Hottest & Driest Months
Obion River Watershed	Temperature	RCP4.5	Increase	15.5°C	+2.7°C (17.7%)	Above 41°C & Below -8°C	June, July, August
		RCP8.5	Increase	15.5°C	+6.4°C (41.4%)	Above 45°C & Below -8°C	June, July, August
	Precipitation	RCP4.5	Increase	1347mm	+11mm (0.8%)	Above 350mm & Below 4mm	August, September, October
		RCP8.5	Decrease	1347mm	-18 mm (1.3%)	Above 375mm & below 3mm	July, August, September
Nolichucky River Watershed	Temperature	RCP4.5	Increase	12.9°C	+2.5°C (19.4%)	Above 36°C & Below -9°C	June, July, August
		RCP8.5	Increase	12.9°C	+5.9°C (45.7%)	Above 45°C & Below -9°C	June, July, August
	Precipitation	RCP4.5	Increase	1253mm	+47 mm (3.8%)	Above 295mm & below 10mm	September, October, November
		RCP8.5	Increase	1253mm	+24 mm (1.9%)	Above 315mm & below 10mm	September, October, November

3.3.3 Hydrological modeling using VIC

Model Overview

There are various hydrologic models available, such as SWMM, HEC-HMS, SWAT, and HSPF. However, for studies on land-atmosphere interactions involving climate change, the variable infiltration capacity (VIC) model is particularly suitable (Gao, et al., 2010; Saha, et al., 2019). VIC version 5.1.0 has been extensively used from the basin to the global scale to conduct hydrologic studies and analyze the impacts of climate change (Hamman, et al., 2018). The model operates on a grid cell basis (supplementary B) and considers three soil layers with varying infiltration capacities. The model also includes vegetation tiles that characterize the grid cell surface, such as Leaf Area Index, roughness root depth, resistance, and albedo. The model simulates the interaction among the soil layers based on their relative wetness and estimates evapotranspiration utilizing the Penman-Monteith method. The model computes evapotranspiration as the area-weighted sum of soil evaporation and transpiration for the current vegetation, using the current architectural resistance and Leaf Area Index to compute canopy resistance in the absence of limitations from soil moisture, temperature, vapor pressure deficit, or insolation (UW, 2021). The Brooks-Corey relationship is used to regulate soil moisture from the second layer, which then infiltrates the third layer via gravity drainage. Finally, the Arno model is used to estimate baseflow from the third layer (Liang, et al., 1994; Ghaneeizad, et al., 2018). Although the study does not use any specific crop variables, it specifically focuses on the water availability of different soil textures. The model estimates the soil water content at specific pressures (wilting point and field capacity) using sand, clay, and water percentage along with other coefficients (methodology and equations applied are shared in Supplementary G) (UW, 2021).

VIC Model Setup, Calibration, and Simulation

To downscale the projected climate raster data set consisting of maximum temperature, minimum temperature, precipitation, and wind speed into 1 km resolution shapefiles for each parameter, Python scripts were used with Inverse Distance Weighted (IDW) interpolation. The input data was supplemented with Advanced Very High-Resolution Radiometer (AVHRR) land cover data to ensure geophysical diversity, and the soil and land cover data were processed through ArcGIS Zonal Statistics to generate inputs for the model. The simulation period was from 2006-2099, and the model ran in water balance mode at a daily time step with outputs at daily, monthly, and annual scales. The VIC flow output was calibrated using a Shuffled Complex Evolution Algorithm (SCE-UA) with seven critical parameters, including baseflow (D_s, D_{smax}), soil moisture (W_s), infiltration (b), exponent (n), and the depth of the 2nd and 3rd layers. The SCE Algorithm analysis was conducted following the guidelines from Troy (Troy, et al., 2008). The calibration parameters were selected to match the monthly streamflow at the USGS gages within set limits. In estimating the calibration parameters, heterogeneity within each sub-drainage area was considered to represent the basin better. The allowable ranges and selected values of the calibration parameters for the watersheds are summarized in **Table 3-4**.

In the next section, we summarize the results of the model calibration. Following calibration, we utilized data from four selected CMIP5 climate models and two scenarios of RCP4.5 and RCP8.5 up to the year 2099 to simulate hydrologic responses in the Obion and Nolichucky watersheds. These responses encompassed water balance parameters, including runoff, soil moisture, and net recharge, for each grid and time step.

Table 3-4 Allowable ranges and selected values of the calibration parameters

Parameter		**Acceptable Range**	**Unit**	**Approach**	**Accepted values**
Infiltration	b	0.001-1.00	-	Horton Model	0.2
Baseflow	D_s	0.001-1.00	-	Calibration	0.1-0.9
	D_{smax}	0.100-50.00	mm/d	k_{sat} x slope	Variable
Soil Moisture	W_s	0.200-1.00	-	Calibration	0.5-0.9
Layer 2 Depth	2^{nd} Layer	0.1-3.0	m	Constant	Variable
	3^{rd} Layer	0.1-3.0	m	Sensitivity Analysis	Variable
Exponent	n	0.1-30.00	-	$3 + 2b_1$	Variable

Spatial Correlation Analysis

To identify the factors that impact soil water extremes and their effects on crop production and irrigation water use, we conducted a spatial correlation analysis of soil moisture using IBM SPSS (Statistical Package for the Social Sciences) for the RCP8.5 high-end climate scenario. This analysis uses advanced statistical methods, including structural equation modeling (SEM), hypothesis testing, correlation analysis, multiple regression, and analysis of variance (Hoyle, 1995), to identify patterns and models in the data. We used the Pearson correlation coefficient to determine the strength and direction of the relationship between continuous variables (Block, et al., 2009). The analysis was focused on soil moisture and included hydrological processes, soil textures, and watershed attributes, which are all known to influence spatial soil moisture variations and irrigation requirements for croplands (Kim, 2013). By conducting a spatial correlation analysis on cropland cover with these attributes, we were able to identify the factors that impact soil water extremes.

3.4 RESULT AND DISCUSSION

3.4.1 Calibration and Validation of the VIC Model

For Obion Watershed, VIC model simulations were conducted using the methodology of Ghaneeizad et al. (2018), which involved calibrating and validating the model with observed streamflow (USGS), evapotranspiration (MODIS), and soil moisture (NRCS-SCAN) data. The resulting Nash-Sutcliffe coefficients for multiple sub-drainage areas within the Obion River watershed were found to be within the acceptable range of 0.67-0.75, indicating a suitable model performance (Ghaneeizad, et al., 2018). Similarly, for the Nolichucky watershed, the model was calibrated using observed streamflow data for the sub-drainage areas (SDA). The simulated monthly streamflow curves matched well with the observed data from 1996 to 2013, particularly for the whole Nolichucky (SDA 4) **(Figure 3-3)**. The Nash-Sutcliffe coefficients for streamflow **(Table 3-5)** ranged from 0.60-0.93 for SDA 1, 2, and 4, with the lower coefficient for SDA 3 due to the presence of the Nolichucky Dam at the outlet, which restricts the natural flow regime. Additionally, the mean absolute error (MAE) value for the whole Nolichucky (SDA 4) was found to be within the acceptable range.

Table 3-5 NSE Coefficient and MAE for the Nolichucky Watershed at each SDA

Watershed	SDA	Ds	Ws	NSE Coef.	MAE	USGS Station
Nolichucky	1	0.9	0.9	0.60	0.30	3463300
	2	0.9	0.9	0.80	0.21	3465500
	3	0.1	0.5	0.24	0.57	3466208
		0.9	0.9			
	4 (Whole)	0.1	0.5	0.93	0.11	3466500
		0.9	0.9			

The model validations were performed using available observed monthly MODIS evapotranspiration (2000-2013) and annual NRCS-SCAN soil moisture data (2003-2013) for the Nolichucky watershed **(Figure 3-4)**. The model evapotranspiration and soil moisture showed great correspondence with the MODIS and NRCS validation datasets, having a correlation of 0.95 and 0.66. Further, the mean absolute errors (MAE) of model evapotranspiration (mm) and soil moisture (%) data are 14.1 and 2.8, which shows that the results are within the acceptable range.

3.4.2 Water Budget Trends & Temporal Extremes

The projected water budget trends and extremes were compared in the Obion and Nolichucky watersheds for the RCP4.5 and RCP8.5 scenarios. The baseline scenarios are the estimated temporal mean of the water budget parameters during 2006-2015. As noted above, the extreme scenarios for runoff and net recharge are estimated using the 1st and 99th percentiles, whereas the soil moisture extremes are identified using field capacity and wilting point focusing on crops. The trend and extremes comparison from 2006-99 are summarized in **Table 3-6**.

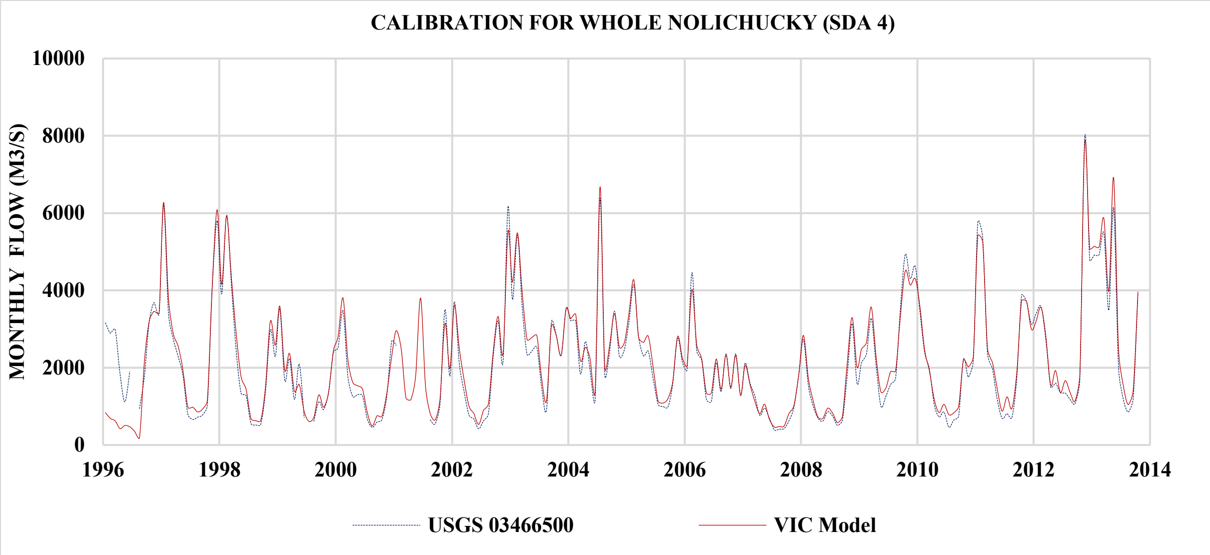

Figure 3-3 Monthly Flow Calibration of Nolichucky watershed with USGS data

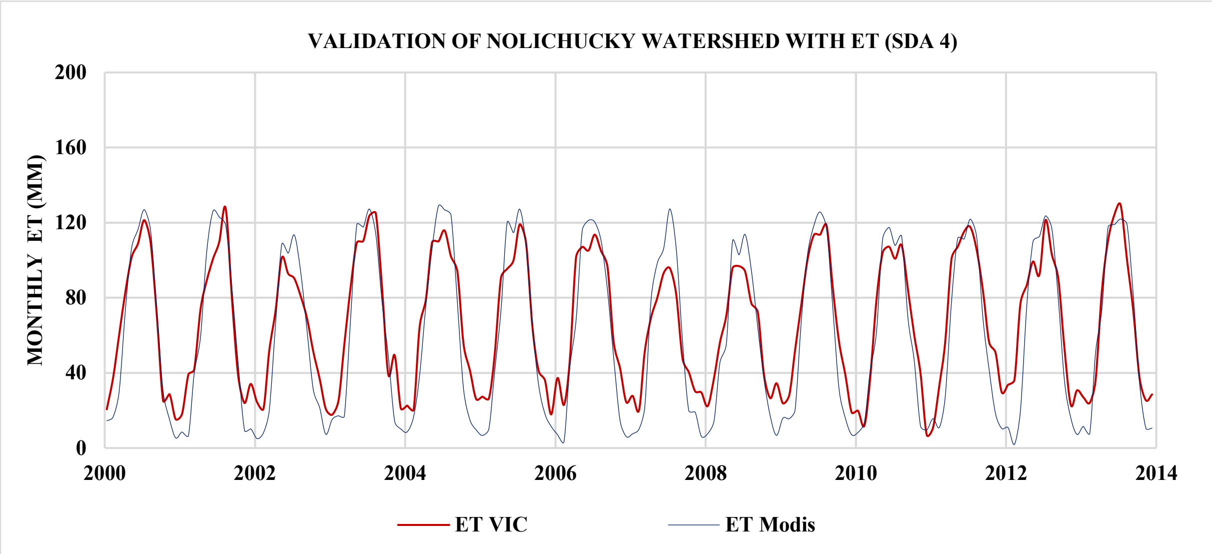

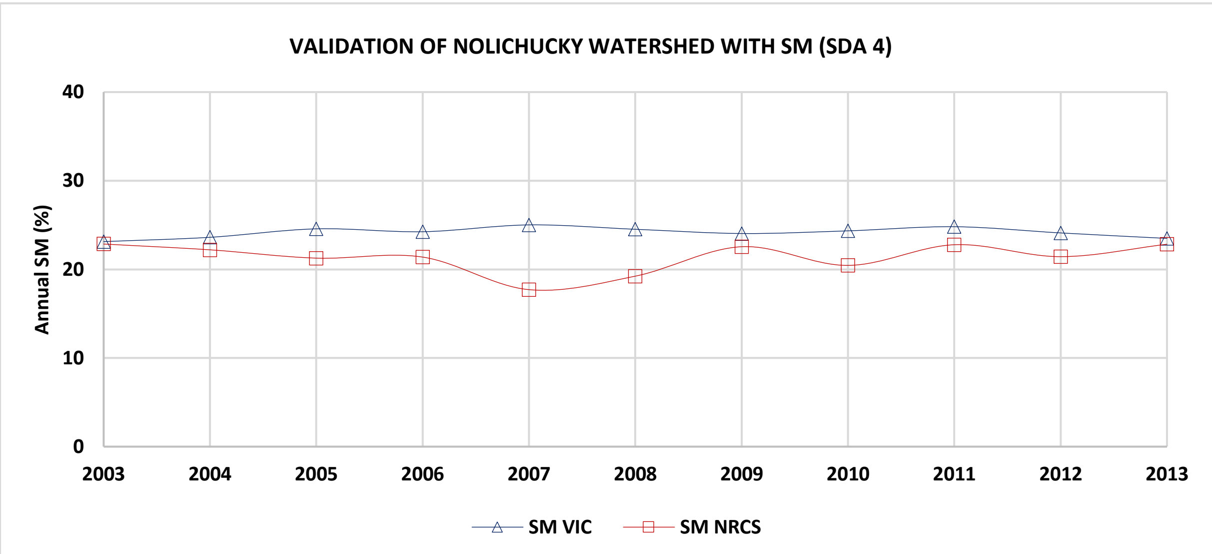

Figure 3-4 Soil Moisture and Evapotranspiration Validations of Nolichucky watershed with NRCS-SCAN and MODIS data

Table 3-6 Summary of the water budget trends and extremes for climate change impacts

Category			Projection Trends	Baseline Scenario	Projection Alterations	Extreme Scenarios	Extreme Months
Obion River Watershed	Runoff	RCP4.5	Increase	194mm	+11mm (5.7%)	Above 700mm & Below 1mm	August, September, October
		RCP8.5	Increase	194mm	+2.4mm (1.2%)	Above 800mm & Below 1mm	July, August, September
	Soil Moisture	RCP4.5	Decrease	27%	-0.2% (0.7%)	FC- 31.3%, CR-15.7%, WP- 9.8%	August, September, October
		RCP8.5	Decrease	27%	- 1.6% (5.9%)		August, September, October
	Recharge	RCP4.5	Increase	314mm	18.4mm (5.9%)	Above 160mm & below 26mm	May, June, July
		RCP8.5	Decrease	314mm	-29.3mm (9.3%)	Above 165mm & below 25mm	May, June, July
Nolichucky River Watershed	Runoff	RCP4.5	Increase	88mm	+2.6 mm (2.9%)	Above 160mm & below 2mm	September, October, November
		RCP8.5	Decrease	88mm	-2.3 mm (2.6%)	Above 45°C & Below -9°C	August, September, October
	Soil Moisture	RCP4.5	Decrease	24%	-0.3% (1.3%)	FC- 31.3%, CR-15.7%, WP- 11%	August, September, October
		RCP8.5	Decrease	24%	-1.1% (4.6%)		August, September, October
	Recharge	RCP4.5	Decrease	238mm	-6mm (2.5%)	Above 110mm & below 10mm	May, June, July
		RCP8.5	Decrease	238mm	- 44mm (18.4%)	Above 120mm & below 10mm	May, June, July

Runoff

The simulated runoff showed mild increasing trends for RCP4.5 and RCP8.5 climate scenarios in the Obion watershed from 2006-99, but only RCP4.5 exhibited mild increases in Nolichucky. RCP8.5 showed a slight negative trend in Nolichucky, with all changes being within ±5.7%. Previous studies indicate that runoff increase ranges from 14 to 22 mm during 1915-2005 in diverse North-Central US watersheds (Ryberg, et al., 2014) and a potential change of 10-26 mm during 2025-34 in Tennessee (McCabe, 1999). While the assessment aligns with previous studies for RCP4.5 (as usual scenario), it significantly reduces for RCP8.5 (extreme scenario). Low runoff extreme months in the Obion watershed for RCP4.5 were August, September, and October, whereas, for RCP8.5, they were July, August, and September, indicating a seasonal shift of dry days towards the summer. The Nolichucky watershed's extreme months for RCP4.5 were September, October, and November, but for RCP8.5, they were August, September, and October, suggesting an earlier shift. Previous research agrees that geo-climatic characteristics impact the seasonal runoff responses to climate change and differ based on precipitation distribution (He et al., 2019; Arora & Boer, 2001). Such a shift of the dry days by a month earlier could cause water scarcity despite similar precipitation patterns in the future (Coffel, et al., 2019).

Net Recharge

Annual net recharge decreased under all scenarios, except the RCP4.5 scenario in the Obion watershed only. A study on the South-central high plains of the US reported an annual net recharge of 8-18 mm over the next century (Meixner, et al., 2016), which is comparable to our findings of -6 to 18 mm within TN, USA. In the Obion watershed, the months with extremely limited recharge remain the same for both RCP scenarios. In contrast, the Nolichucky watershed showed a shift of low recharge months from May, June, and July for RCP4.5 towards June, July, and August for RCP8.5. Over the past three decades, prior groundwater flow analyses in Tennessee indicated a potential decline due to withdrawals, leading to low recharge (Haugh, 2012; Razmara, et al., 2016). On top of that, a month shifting of annual net recharge in the future could potentially expedite the lowering trend of groundwater.

Soil Moisture

The soil moisture average from the climate models decreased in both watersheds for both RCP4.5 and RCP8.5 scenarios. A previous study on soil moisture trends in Tennessee indicated a potential change of 1.5-2.5% (Georgakakos & Smith, 2001), which aligns with our findings. However, concerning results showed a few extreme values below the wilting point in the top two soil layers (60 cm) during the extreme months of August, September, and October for the Obion watershed. To address these concerns, the changes in soil moisture with climate change patterns were further explored by looking for temporal (hot moments) and spatial (hotspots) extremes.

3.4.3 Temporal and Spatial Extremes

Soil Moisture Hot moments

The study examined hot moments during three periods: the baseline (2006-15), short-term (2046-55), and long-term (2090-99) for extreme months. The results showed that in both climate scenarios, soil moisture drops below the average wilting point of 9.8% in the Obion watershed during the 2046-55 and 2090-99 periods **(Figure 3-5)**, indicating a need for irrigation as 40-50% of the growing season falls below the wilting point. The low soil moisture in the short and long term is directly influenced by precipitation patterns. However, in the Nolichucky watershed, soil moisture levels during the extreme months period for both scenarios remain well above the average wilting point of 11%.

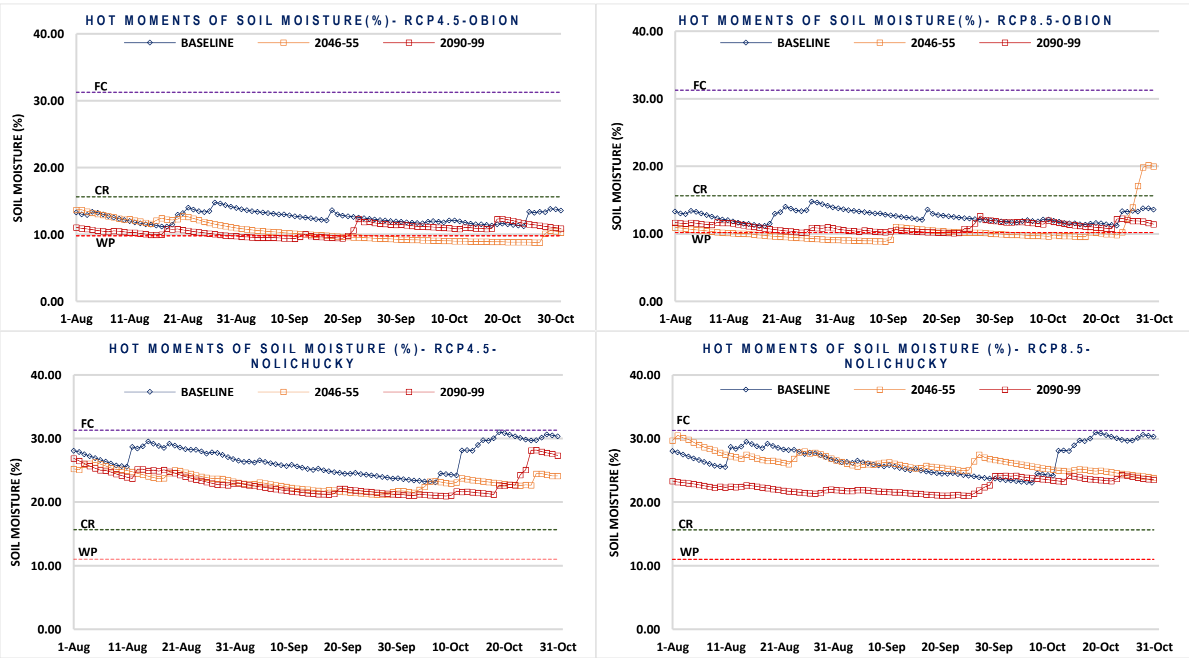

Figure 3-5 Hot Moments of Soil Moisture for RCP4.5 & RCP8.5 Scenarios

On further observation over the hot moments, it is evident that the combined high temperatures and low precipitation at Obion are causing low soil moisture. In the Obion watershed, the temperature reaches as high as 36-43°C during July-August, and the precipitation approaches zero during August-October (Supplementary B). The growing season of the major crops within the region is from April to October (approximately 180 days). The overlapping impacts of increasing temperature and less rainfall lower soil moisture below the wilting point from August to October, potentially impacting the crop yield. Water-efficient crops or water management like drip irrigation may be needed for future water efficiency (Rouzi, et al., 2018; Ibragimov, et al., 2007). The percentage of the growing season under the wilting point for the short- and long-term forecasts is also summarized in **Table 3-7**.

The estimation of plant available water (PAW) for the growing season is a crucial factor in assessing the water resources available for crops (Morgan, et al., 2003). PAW is defined as the amount of water that the soil can retain and make accessible to plants during their growth period (PAW = FC-WP). The maximum plant available water for Obion is 21.71% (5.13 in), whereas for Nolichucky, it is 21.62% (5.11 in). Further assessment reveals that average soil available water without irrigation (AW= SM-WP) during the growing season decreases from 0.39 inches to a range of 0.5-0.11 inches under short-term and long-term scenarios in the Obion watershed. This reduction in soil available water implies that there might be a significant increase in the demand for irrigation water (such as a 60% for an application rate of 0.5 inches) for crops like corn, soybean, and cotton in Tennessee.

Table 3-7 Plant available water (PAW) and percentage of the days below average wilting point within growing season (180 days)

Watersheds	**Scenarios**	**Baseline**		**Short-term**		**Long-term**	
		Available Water (mm)	Below WP	Available Water (mm)	Below WP	Available Water (mm)	Below WP
Obion	RCP4.5	9.91	0%	2.79	33.90%	1.27	32.20%
	RCP8.5	9.91	0%	2.54	46.10%	2.29	23.30%
Nolichucky	RCP4.5	80.52	0%	59.18	0%	58.17	0%
	RCP8.5	80.52	0%	77.22	0%	55.12	0%

In addition, it is important to note that in conventional tillage practices, each pass of tillage can result in the loss of water availability (0.25 in) over time. This may have negative implications for soil moisture (as water may be restricted to the surface layer and thus get lost through evaporation). According to USDA, 75-85% of total farming acreage for the three dominant cash crops in Tennessee has a no-tillage practices history. Although there are conservation tillage practices, it accounted for 16.2 percent of the acreage seeded to the state's major crops (USDA NASS, 2018; USDA NASS, 2017). However, tillage alone is not responsible for lowering soil moisture, but the presence of the fragipan layer makes it relevant. The fragipan acts as a lid (restrictive layer), affecting water penetration below the layer. Runoff-driven erosion in the loess of western TN may get the fragipan further exposed to the surface since high erosion rates are associated with conventional tillage (Gimenez, et al., 1997). With the increasing trend of runoff in the fragipan region due to low infiltration, the rate of lowering of the surface layer (above fragipan) increases (Wilson, et al., 2022). However, the fragipan soils exist predominantly in MLRA 134 and are approximately within the top 2 m of the soil profile in this region (Bockheim & Hartemink, 2013). In most locations, the fragipan layer is below historical tillage depths, typically 30 cm, and therefore, soil moisture remains intact (Wilson, et al., 2022).

The major crops cultivated in Tennessee, such as soybean, corn, cotton, hay, and wheat, have varying water requirements throughout their growth cycles. Historically, in West Tennessee, corn typically utilizes 20 inches of water during its growth period. Given effective rainfall of 14 inches and a soil water availability of 3 inches, the irrigation requirement for corn would be 3 inches. If an irrigation system applies 0.5 inches per application, it implies that the field would need to be irrigated approximately six times during the growing season to optimize yield (Leib & Grant, 2018). Based on historical averages, soybean's water needs vary depending on its growth stage, necessitating between 0.5 and 1.5 inches of water per irrigation application (Leib, et al., 2018). Conversely, cotton experiences a rapid increase in water use from 1.0 to 1.7 inches per week, with an average of approximately 1.6 inches per week (Leib, et al., 2018). Considering the projections for the Obion watershed, which indicate an average soil water content depletion of 0.35-0.52 inches in 2050 and 2090 (Figure 5), irrigation water use may rise by 33%-100%, depending on the specific crop types.

Similarly, in the Nolichucky watershed, an average soil moisture depletion of 0.13-1.0 inches could significantly increase irrigation water requirements for various crops in the future. Since irrigators typically base management decisions on half the plant's available water, these changes can be critical in agricultural management.

Soil Moisture Hotspots

To identify spatial water extreme hotspots, Python scripts and GIS were used to analyze field capacity, critical ratio, and wilting point during the extreme months in the three time periods. In the Obion watershed, soil moisture is lowest during the 2046-2055 period under both scenarios, with a slight increase during the 2090-2099 period. In the Nolichucky watershed, there was a slight reduction in soil moisture levels for both the RCP4.5 and RCP8.5 scenarios. Soil moisture hotspots in the west-central Obion and western valleys of Nolichucky are the most extreme during the 2046-2055 period for both scenarios **(Figure 3-6)**. Previous study agrees with this research that croplands use the most water in the soil and contribute to the low moisture hotspots in each watershed (Tao, et al., 2003). In addition, it is observed that the forested mountains and clayey soils in the eastern region of Nolichucky hold most of the soil moisture due to heavy precipitation.

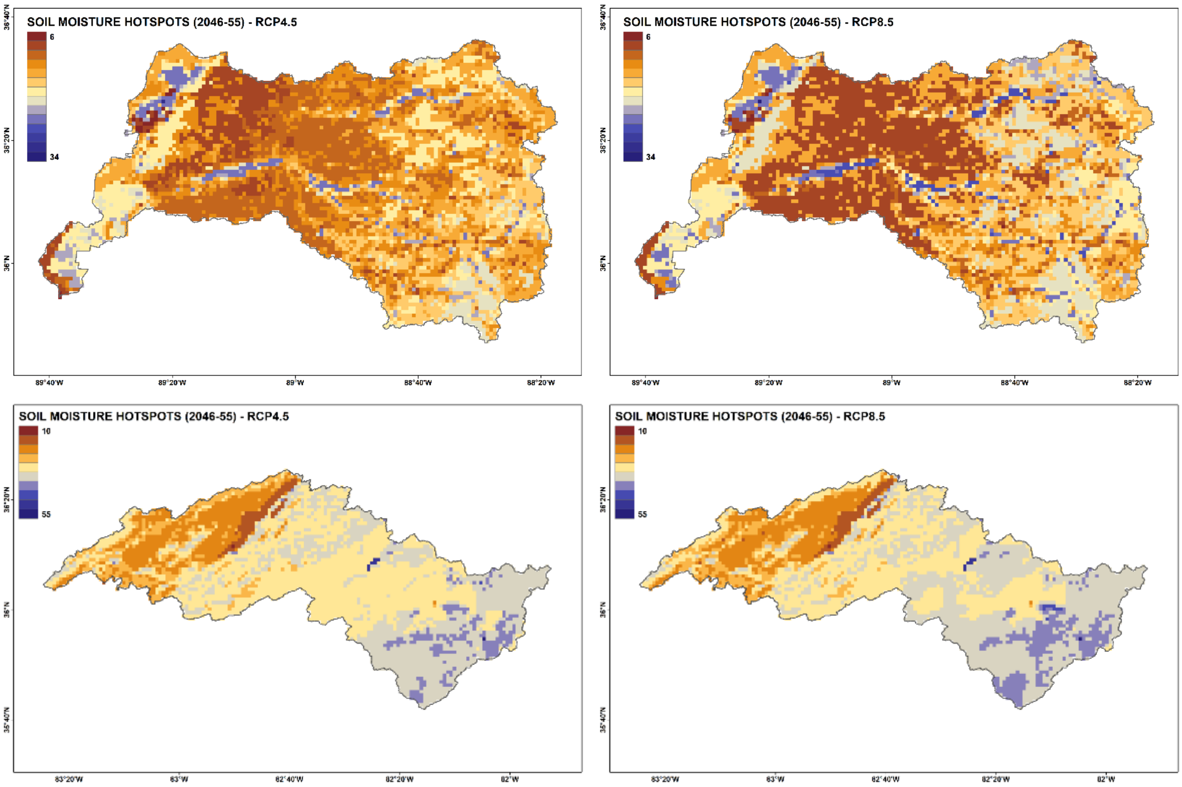

Figure 3-6 Soil Moisture Hotspots Extremes during 2046-55 for RCP4.5 & RCP8.5 Scenarios

Despite their distinct characteristics, this comparison highlights the high-water risk for both watersheds, particularly for croplands. Furthermore, the analysis revealed differences in water extremes within each watershed based on land cover, emphasizing the need for tailored plans and implementations that account for sub-regional variations.

3.4.4 Spatial Extremes' Impacting Factors

Soil moisture correlation analysis is done for RCP8.5 using SEM in IBM SPSS to identify factors impacting spatial extremes **(Figure 3-7)**. Croplands are a major area of concern due to potential impacts on productivity and irrigation requirements, as indicated by the hotspot analysis.

Hydrological processes

Cropland soil moisture is significantly influenced by hydrological parameters, with field capacity playing a key role (Korres, et al., 2010; Kim, 2013). In the Obion watershed, there is a high spatial correlation (0.89) between soil moisture and field capacity, while in Nolichucky, the correlation is lower (0.44) (Figure 6). Low soil moisture in Nolichucky's croplands may be due to factors such as the low infiltration of runoff because of the presence of mountainous rock or reduced water-holding capacity caused by the gradient. The Obion croplands have a negative correlation (0.04) between soil moisture and water-holding capacity, indicating high water-holding capacity corresponding to low porosity. Conversely, the Nolichucky croplands have a positive correlation (0.62) due to high porosity in a closed aquifer scenario, allowing the mountainous rock to hold and reserve water. Hydraulic conductivity did not show a significant relationship with soil moisture at the macro scale resolution in either watershed. The hydrological processes show strong positive correlations (0.81 and 0.74) with soil moisture in the Obion and Nolichucky watersheds, respectively, emphasizing the importance of high field capacity and porosity in reducing the need for cropland irrigation, whereas hydraulic conductivity might have minimal impact.

Soil Textures

Previous studies have highlighted the significant impact of soil and vegetation properties on soil moisture variability (Srivastava, et al., 2021; Guzha, et al., 2018). In the case of the two watersheds under consideration, cropland soil moisture shows a high correlation (0.53-0.57) with clay content,

Obion Watershed	Nolichucky Watershed

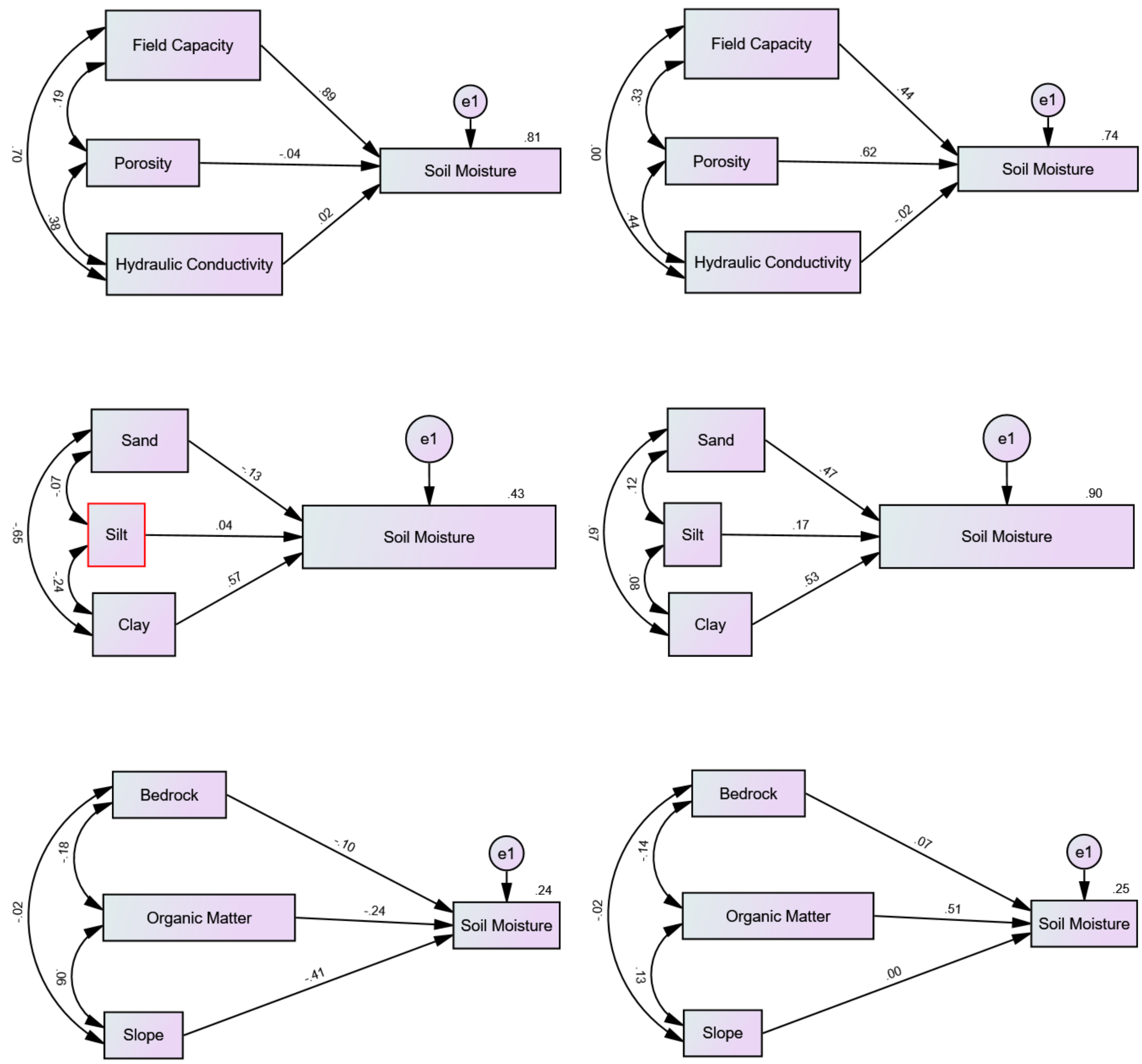

Figure 3-7 a. Correlations of Hydrological processes, b. Soil textures and c. Watershed Attributes with Soil Moisture for Obion & Nolichucky Watersheds

indicating high water holding capacity, which aligns with previous findings (Vories, et al., 2007). However, Nolichucky cropland soil moisture also shows a mild correlation with sand content, which can enhance water infiltration and storage. Other studies have also found a strong correlation between soil moisture spatial pattern and sand content, similar to the Nolichucky watershed (Korres, et al., 2010). Overall, soil textures have a significant impact on soil moisture, with clay content showing a strong positive correlation in both watersheds. Thus, a high percentage of clay soils in croplands could reduce irrigation requirements significantly in future water extreme scenarios.

Watershed Attributes

Several studies have shown that watershed attributes, such as slope and bedrock depth, have weak correlations with soil moisture spatial variation (Zhu, et al., 2012; Qiu, et al., 2010; Korres, et al., 2013). The Obion croplands exhibit a weak negative correlation between bedrock depth and soil moisture, suggesting that the presence of bedrock at the top layers of alluvial soil may increase water holding capacity. In contrast, the Nolichucky croplands show a weak positive relationship between bedrock depth and soil moisture, indicating that the presence of bedrock at the top layers of rocky soil may reduce intrusion and water content capacity. The Obion croplands also exhibit a weak negative correlation of 0.24 between soil moisture and organic matter, while the Nolichucky croplands show a mild positive correlation of 0.51. However, the negative correlation between soil moisture and organic matter in the Obion croplands may be an anomaly due to the study's resolution. In general, the presence of organic matter in alluvial soils may reduce water availability, while in rocky soils, it may increase water content. In the Obion croplands, the slope has a mild negative correlation of 0.41 with soil moisture, while there is no significant correlation in the Nolichucky croplands due to the high gradient geographical system. Overall, watershed attributes have positive weak correlations with soil moisture in the Obion and Nolichucky croplands. From the assessment, it is evident that the impact of organic matter on irrigation may vary based on the specific cropland's soil type, whether it is alluvial or rocky.

Based on the standardized regression analysis **(Table 3-8)**, field capacity, percentage of clay soils, and organic matter are the most important factors affecting crop irrigation.

Table 3-8 Standardized regression estimates of Hydrological processes, Soil textures, and Watershed processes with Soil moisture.

Groups	Category	Relationship Parameters		Obion (n=2421)		Nolichucky (n=980)	
				r	p	r	p
Hydrological processes	Regression Correlations	Soil Moisture	Field Capacity	0.89	***	0.44	***
		Soil Moisture	Porosity	-0.04	***	0.62	***
		Soil Moisture	Hydraulic Conductivity	0.02	0.16	-0.02	0.40
	Correlations	Porosity	Hydraulic Conductivity	0.38	***	0.44	***
		Field Capacity	Porosity	0.19	***	0.33	***
		Field Capacity	Hydraulic Conductivity	0.70	***	0.00	0.92
	Group	Soil Moisture		0.81			0.74
Soil textures	Regression Correlations	Soil Moisture	Sand	-0.13	***	0.47	***
		Soil Moisture	Silt	0.04	.03	0.18	***
		Soil Moisture	Clay	0.57	***	0.53	***
	Correlations	Silt	Clay	-0.24	***	0.08	***
		Sand	Silt	-0.07	***	0.12	***
		Sand	Clay	-0.65	***	0.68	***
	Group	Soil Moisture		0.43		0.90	
Watershed attributes	Regression Correlations	Soil Moisture	Bedrock	-0.10	***	0.07	0.01
		Soil Moisture	Organic Matter	-0.24	***	0.51	***
		Soil Moisture	Slope	-0.41	***	0.00	0.87
	Correlations	Slope	Organic Matter	0.06	.002	0.13	***
		Organic Matter	Bedrock	-0.18	***	-0.14	***
		Slope	Bedrock	-0.02	.29	-0.02	0.49
	Group	Soil Moisture		0.24		0.25	

Previous studies have suggested that changes in organic matter concentrations can have a significant impact on land management practices and crop irrigation (Li, et al., 2019; Mbava, et al., 2020). As a result, it may be worth exploring management strategies to regulate organic matter content in croplands and assess whether this could potentially reduce the irrigation requirements during future water extreme scenarios.

3.5 CONCLUSION

The predicted increase in temperature of 2.7-6.4°C and change in precipitation by 1-4% for both watersheds in Tennessee is likely to have a significant impact on seasonal patterns and water balance. Runoff extreme months suggest a shift in the growing season by a month from August-October to July-September at Obion and from September-November to August-October at the Nolichucky watershed. Such shifts in the growing season for the RCP-4.5 and RCP-8.5 scenarios are expected to negatively impact future crop production. As the optimal temperature and precipitation season for crop growth changes, extreme scenarios are likely to reduce crop yield. Furthermore, in both watersheds, compared to the baseline scenario, the average soil moisture is decreasing, and the ranges of monthly maximum and minimum values suggest a substantial number of extreme values below the average wilting point in the top two soil layers, especially during the extreme months of August, September, and October. Therefore, there is a significant risk of crop yield being impacted during this growing period in the Obion and Nolichucky watersheds due to low soil water content.

High temperatures and low precipitation have a combined impact on soil moisture, as observed from the hot moments. The Obion watershed experiences temperatures as high as 36-43°C during July-August and precipitation approaching zero during August-October. This overlapping impact lowers soil moisture below the average wilting point of croplands during the growing season, which could potentially impact crop yields. In fact, during 2046-55, 34-46% of the growing season for Obion is predicted to be below the average wilting point, highlighting the need for irrigation or the use of water-efficient crops. It is also observed that the available water in soil before irrigation decreases significantly for future scenarios, indicating a 60% increase in irrigation demand for the major crops of Tennessee. The hotspot analysis revealed that the central part of Obion has the lowest moisture content, while the eastern region of Nolichucky has the highest. Forest land tends to have higher soil moisture levels in both watersheds, whereas croplands have lower levels, emphasizing the need for better soil moisture management strategies in croplands to ensure optimal crop production.

The statistical models reveal that certain hydrological process parameters, such as high field capacity and porosity, can significantly reduce the need for irrigation in croplands. Similarly, the presence of a high percentage of clay soils can also significantly reduce the water requirements in croplands. In contrast, the correlations between the watershed attributes and soil moisture are weak, and the impact of organic matter on irrigation requirements varies depending on the specific soil type in each cropland. Therefore, the primary factors affecting the spatial extremes of cropland irrigation requirements are likely to be field capacity, percentage of clay soils, and organic matter content.

The broader implication of the study would be implementing an effective management plan to increase the organic matter content in croplands, which has the potential to significantly reduce irrigation requirements during water scarcity in the future. Therefore, it is essential to conduct an analysis of water-efficient crops and organic matter management techniques for extreme climate scenarios in multiple watersheds following a similar methodology. However, a limitation of the study is the unavailability of high temporal resolution data on soil moisture for multiple land covers within the watershed, which could be conducted on another watershed with local measurements. Incorporating such data could significantly improve the accuracy of future projections. Further research should also focus on more localized aspects of climate change impacts, such as the lowering of water reservoirs, increased agricultural irrigation demands, and severe bank erosion based on the current findings, to ensure effective adaptation strategies are implemented.

REFERENCES

Acharya, A., Piechota, T. C. & Tootle, G., 2012. Quantitative Assessment of Climate Change Impacts on the Hydrology of the North Platte River Watershed, Wyoming. *Journal of Hydrologic Engineering,* 17(10), pp. 1071-1083.

Anand, J., Gosain, A., Khosa, R. & Srinivasan, R., 2018. Regional scale hydrologic modeling for prediction of water balance, analysis of trends in streamflow and variations in streamflow: The case study of the Ganga River basin. *Journal of Hydrology: Regional Studies,* Volume 16, p. 32–53.

Arora, V. K. & Boer, G. J., 2001. Effects of simulated climate change on the hydrology of major river basins. *JGR Atmospheres,* 106(D4), pp. 3335-3348.

Berg, A. & Sheffield, J., 2018. Climate Change and Drought: the Soil Moisture Perspective. *Current Climate Change Reports,* 4(2), pp. 180-191.

Block, P. J., Filho, F. A. S., Sun, L. & Kwon, H., 2009. A Streamflow Forecasting Framework using Multiple Climate and Hydrological Models. *Journal of the American Water Resources Association,* 45(4).

Briggs, L. J. & Shantz, H. L., 1912. The wilting coefficient and its indirect determination. *Botanical Gazette,* 53(1), p. 20–37.

Chu, X. et al., 2019. Macro-scale grid-based and subbasin-based hydrologic modeling: joint simulation and cross-calibration. *Journal of Hydroinformatics,* 21(1), pp. 77-91.

Coffel, E. et al., 2019. Future Hot and Dry Years Worsen Nile Basin Water Scarcity Despite Projected Precipitation Increases. *Earth's Future,* 7(8), pp. 967-977.

Collins, W. e. a., 2008. *Evaluation of the HadGEM2 model,* FitzRoy Road, Exeter, UK: Met Office Hadley Centre Technical Note no. HCTN 74.

Dunkerley, D., 2019. Sub-Daily Rainfall Intensity Extremes: Evaluating Suitable Indices at Australian Arid and Wet Tropical Observing Sites. *Water,* 11(2616).

Dunne et al., J. P., 2006. ' 'GFDL's ESM2 Global Coupled Climate–Carbon Earth System Models. Part I: Physical Formulation and Baseline Simulation Characteristics. *Journal of Climate,* Volume 19, p. 643–674.

Earman, S. & Dettinger, M., 2011. Potential impacts of climate change on groundwater resources – a global review. *Journal of Water and Climate Change,* 2(4), p. 213–229.

Fazey, I. et al., 2020. Transforming knowledge systems for life on Earth: Visions of future systems and how to get there. *Energy Research & Social Science,* 70(101724).

Furtak, K. & Wolińska, A., 2023. The impact of extreme weather events as a consequence of climate change on the soil moisture and on the quality of the soil environment and agriculture – A review. *Catena,* 231(107378).

Gao, H., Tang, Q. & Ferguson, C. R., 2010. Estimating the water budget of major US river basins via remote sensing. *International Journal of Remote Sensing,* 31(14), p. 3955–3978.

Georgakakos, K. P. & Smith, D. E., 2001. Soil moisture tendencies into the next century for the conterminous United States. *Journal of Geophysical Research,* 106(D21), pp. 27,367-27,382.

Ghaneeizad, S. et al., 2018. Development of a Distributed Hydrologic Model for a Region with Fragipan Soils to Study Impacts of Climate on Soil Moisture: A Case Study on the Obion River Watershed in West Tennessee. *Geosciences,* 8 (10)(364).

Guzha, A. et al., 2018. Impacts of land use and land cover change on surface runoff, discharge and low flows: Evidence from East Africa. *Journal of Hydrology: Regional Studies,* Volume 15, p. 49–67.

Hamman, J. J. et al., 2018. The Variable Infiltration Capacity model version 5 (VIC-5): infrastructure improvements for new applications and reproducibility. *Geosciences Model Development,* Volume 11, pp. 3481-3496.

Haugh, C. J., 2012. Effects of Groundwater Withdrawals Associated with Combined-Cycle Combustion Turbine Plants in West Tennessee and Northern Mississippi, Reston, VA: U.S. Geological Survey.

Hayhoe et al., K., 2008. Regional climate change projections for the Northeast USA. *Mitigation and Adaptation Strategies for Global Change,* Volume 13, pp. 425-436.

He et al., M., 2019. Potential Changes in Runoff of ' 'California's Major Water Supply Watersheds in the 21st Century. *MDPI: Water,* 11(8).

Hejazi et al., M. I., 2015. 21st century United States emissions mitigation could increase water stress more than the climate change it is mitigating. *PNAS,* 112(34), p. 10635–10640.

Hoyle, R. H., 1995. The structural equation modeling approach: Basic concepts and fundamental issues. In: *Structural equation modeling: Concepts, issues, and applications.* s.l.:Sage Publications, Inc., pp. 1-15.

Ibragimov, N. et al., 2007. Water use efficiency of irrigated cotton in Uzbekistan under drip and furrow irrigation. *Agricultural Water Management,* 90(1–2), pp. 112-120.

JAMSTEC, 2014. WCRP CMIP5: The MIROC team MIROC-ESM-CHEM model output collection, Japan: Centre for Environmental Data Analysis.

Khatri, K. B., Strong, C., Kochanski, A. K. & Burian, S., 2018. Water Resources Criticality Due to Future Climate Change and Population Growth: Case of River Basins in Utah, USA. *Journal of Water Resources Planning and Management,* 144(8).

Kim, D., 2013. Incorporation of multi-scale spatial autocorrelation in soil moisture–landscape modeling. *Physical Geography,* 34(6), p. 441–455.

Korres, W., Koyama, C. N., Fiener, P. & Schneider, K., 2010. Analysis of surface soil moisture patterns in agricultural landscapes using Empirical Orthogonal Functions. *Hydrol. Earth Syst. Sci.,* Volume 14, p. 751–764.

Korres, W., Reichenau, T. & Schneider, K., 2013. Patterns and scaling properties of surface soil moisture in an agricultural landscape: An ecohydrological modeling study. *Journal of Hydrology,* Volume 498, p. 89–102.

Leib, B. G. & Grant, T., 2018. *Irrigation Water Management (IWM)-A Simple Analogy,* University of Tennessee – Extension, Knoxville, TN, W809-A (peer-reviewed): s.n.

Leib, B. G., Grant, T. & Raper, T. B., 2018. *The basics of cotton irrigation in Tennessee,* University of Tennessee – Extension, Knoxville, TN, W809-C (peer-reviewed): s.n.

Leib, B. G., Grant, T., Shekoofa, A. & McClure, M. A., 2018. *The basics of soybean irrigation in Tennessee,* University of Tennessee – Extension, Knoxville, TN, W809-B (peer-reviewed): s.n.

Liang, X., Lettenmaier, D. P., Wood, E. F. & Burges, S. J., 1994. A simple hydrologically based model of land surface water and energy fluxes for general circulation models. *J. Geophys. Res.,* 99(D7), p. 14415–14428.

Li, M. et al., 2019. Effect of land management practices on the concentration of dissolved organic matter in soil: A meta-analysis. *Geoderma,* Volume 344, pp. 74-81.

Liu, D. et al., 2014. Impact of initial soil moisture anomalies on climate mean and extremes over Asia. *JGR Atmospheres,* Volume 119, pp. 529-545.

Lobanova, A. e. a., 2018. Hydrological impacts of moderate and high-end climate change across European river basins. *Journal of Hydrology: Regional Studies,* Volume 18, p. 15–30.

Mbava, N. et al., 2020. Factors affecting crop water use efficiency: A worldwide meta-analysis. *Agricultural Water Management,* 228(105878).

McCabe, D. M. W. a. G. J., 1999. Estimates of runoff using water-balance and atmospheric general circulation models. *Journal of the Americal Water Resources Association,* 35(6).

McLaughlin, S. B., Wullschleger, S. D., Sun, G. & Nosal, M., 2007. Interactive effects of ozone and climate on water use, soil moisture content and streamflow in a southern Appalachian forest in the USA. *New Phytologists,* Volume 174, pp. 125-136.

Meixner, T. et al., 2016. Implications of projected climate change for groundwater recharge in the western United States. *Journal of Hydrology,* Volume 534, pp. 124-138.

Morgan, C., Norman, J. & Lowery, B., 2003. Estimating Plant-Available Water Across a Field with an Inverse Yield Model. *Soil Science Society of America Journal,* 67(2), pp. 620-629.

Qiu, Y. et al., 2010. Spatial prediction of soil moisture content using multiple-linear regressions in a gully catchment of the Loess Plateau, China. *Journal of Arid Environments,* Volume 74, p. 208–220.

Rahman, S. et al., 2019. Projected changes of inundation of cyclonic storms in the Ganges–Brahmaputra–Meghna delta of Bangladesh due to SLR by 2100. *Journal of Earth System Science,* 128(145).

Rai, R. K., Singh, V. P. & Upadhyay, A., 2017. Chapter 17 - Soil Analysis. In: *Planning and Evaluation of Irrigation Projects: Methods and Implementation.* s.l.:Academic Press, pp. 505-523.

Raje, D., Priya, P. & Krishnan, R., 2013. Macroscale hydrological modelling approach for study of large scale hydrologic impacts under climate change in Indian river basins. *Hydrological Processes,* 28(4).

Razmara, P. et al., 2016. Risk Assessment of Climate Change Impacts on Runoff in Urmia Lake Basin, Iran. *Journal of Hydrologic Engineering,* 21(8).

Rouzi, A. et al., 2018. Water Efficient Alternative Crops for Sustainable Agriculture along the Tarim Basin: A Comparison of the Economic Potentials of Apocynum pictum, Chinese Red Date and Cotton in Xinjiang, China. *Sustainability,* 10(1).

Roy et al., B., 2021. Climate-induced flood inundation for the Arial Khan River of Bangladesh using open-source SWAT and HEC-RAS model for RCP8.5-SSP5 scenario. *SN Applied Sciences,* 3(648).

Ryberg, K. R., Lin, W. & Vecchia, A. V., 2014. Impact of Climate Variability on Runoff in the North-Central United States. *J. Hydrol. Eng.,,* 19(1), pp. 148-158.

Saha et al., P., 2020. A sustainability analysis on the trends and frequency of the channel flow of a carp breeding river against human interventions and governing public–private partnership (PPP) as adaptation. *SN Applied Sciences,* 2(969).

Saha, P. et al., 2019. A sustainability study of the flow regulation impacts by dams in a carp breeding river using the hydrodynamic model and building block analysis. *SN Applied Sciences,* 1(1429).

Sanchez-Gomez, E., Somot, S. & Mariotti, A., 2009. Future changes in the Mediterranean water budget projected by an ensemble of regional climate models. *GEOPHYSICAL RESEARCH LETTERS,* 36(L21401).

Schaake, J., 2000. *Average hydraulic properties of ARS soil texture classes,* Silver spring, Maryland: Office of Hydrology, National Weather Service/NOAA, .

Schilling, K. et al., 2015. Effects of Land Cover on Streamflow Variability in a Small Iowa Watershed: Assessing Future Vulnerabilities. *American Journal of Environmental Sciences,* 11(4), pp. 186-198.

Seneviratne, S. et al., 2010. Investigating soil moisture–climate interactions in a changing climate: A review. *Earth-Science Reviews,* 99(3-4), pp. 125-161.

Sepulchre, P. et al., 2019. IPSL-CM5A2. An Earth System Model designed for multi-millennial climate simulations. *Geoscientific Model Development.*

Sheffield et al., J., 2013. North American climate in CMIP5 experiments. Part I: Evaluation of historical simulations of continental and regional climatology. *Journal of Climate,* Volume 26, pp. 9209-9244.

Spinoni, J. e. a., 2019. A new global database of meteorological drought events from 1951 to 2016. *Journal of Hydrology: Regional Studies,* 22(100593).

Srivastava, A. et al., 2021. The role of landscape morphology on soil moisture variability in semi-arid ecosystems. *Hydrological Processes,* Volume 35.

Tao, F., Yokozawa, M., Hayashi, Y. & Lin, E., 2003. Future climate change, the agricultural water cycle, and agricultural production in China. *Agriculture, Ecosystems & Environment,* 95(1), pp. 203-215.

Troy, T., Wood, E. & Sheffield, J., 2008. An efficient calibration method for continental-scale land surface modeling.. *Water Resour. Res.,* Volume 44, p. 1–13.

Trudel, M., Doucet-Généreux, P., Leconte, R. & Côté, B., 2016. Vulnerability of Water Demand and Aquatic Habitat in the Context of Climate Change and Analysis of a No-Regrets Adaptation Strategy: Study of the Yamaska River Basin, Canada. *Journal of Hydrologic Engineering,* 21(2).

USDA, 2018. *2018 Tennessee Tillage Systems,* Nashville, TN: National Agricultural Statistics Service Eastern Mountain Region, USDA.

UW, 2021. *VIC.* [Online]
Available at: https://vic.readthedocs.io/en/master/Documentation/Definitions/

Vories, E. D. et al., 2007. Estimating the impact of delaying irrigation for midsouth cotton on clay soil. *Transactions of the ASABE. 50(3):,* 50(3), pp. 929-937.

Wilson, C. G. et al., 2018. The Importance of Soil Moisture and Soil Organic Carbon on Yield Gaps. s.l., American Geophysical Union.

Wrzesien, M. L. & Pavelsky, T. M., 2020. Projected Changes to Extreme Runoff and Precipitation Events From a Downscaled Simulation Over the Western United States. *Front. Earth Sci.,* Volume 7.

Yin, J. et al., 2018. Large increase in global storm runoff extremes driven by climate and anthropogenic changes.. *Nat Commun,* 9(4389).

Zheng, H., Chiew, F. H., Charles, S. & Podger, G., 2018. Future climate and runoff projections across South Asia from CMIP5 global climate models and hydrological modelling. *Journal of Hydrology: Regional Studies,* Volume 18, p. 92–109.

Zhu, Q. et al., 2012. Monitoring and prediction of soil moisture spatial–temporal variations from a hydropedological perspective: a review. *Soil Research,* 50(8), pp. 625-637.

CHAPTER-4

FIELD-BASED INVESTIGATION OF SOIL MOISTURE DYNAMICS AND THEIR INFLUENCE ON SHEAR STRESS AND ERODIBILITY COEFFICIENTS FOR ENHANCED BANK EROSION PREDICTION

RESEARCH QUESTION

How do temporal variations in naturally occurring soil moisture influence critical shear stress and the erodibility coefficient of cohesive streambank soils?

ABSTRACT

Streambank erosion is a geomorphological process with significant implications for ecological and socio-economic systems. This process is driven by dynamic interactions during high flows between shear stress (τ) and soil properties of resistance. Quantifying resistance requires determining critical shear stress (τ_c) and an erodibility coefficient (K_d), which are often considered static values. However, limited research has indicated that seasonal soil moisture fluctuations may impact erosion resistance parameters (τ_c and K_d) in natural settings, leaving critical gaps in understanding how these factors interact dynamically. This study analyzed field-based measurements, offering insights into seasonal soil moisture dynamics and their influence on erosion mechanisms in a real-world setting. Field-based jet erosion tests (JET) were conducted on the banks of Conner Creek, Knox County, Tennessee, to measure τ_c and K_d across varying soil moisture levels (0.10-0.39 m/m) under natural hydrological conditions. The results reveal U-shaped quadratic trends in the relationships between SM and both τ_c and K_d. Statistical correlations suggest these findings are significant, with coefficients of determination (r^2) of 0.61 for τ_c-SM and 0.51 for K_d-SM, indicating moderate to strong fits. This study emphasizes the critical role of soil moisture dynamics and highlights the distinct mechanisms governing τ_c and K_d in influencing erosion processes. The findings provide a potential pathway for improving erosion rate estimations if integrated into predictive models.

4.1 INTRODUCTION

Bank erosion is a pressing geomorphological process that leads to infrastructure damage, socio-economic disruption, and environmental degradation (Poesen, 2018). Driven primarily by precipitation, soil water availability and increased flow rates (Vietz et al., 2018), bank erosion poses a major soil degradation threat. Current projections of more extreme weather in the future, including heavier and more frequent rainfall and runoff events, may accelerate this process, potentially increasing global hydrological erosion rates by 30 to 66% (Borrelli et al., 2020). This escalation could intensify sediment transport and destabilize riverbanks, further amplifying the risk of infrastructure damage and ecological disruption, necessitating costly rehabilitation and conservation efforts (Duró et al., 2020; Florsheim et al., 2008; Wynn and Mostaghimi, 2006). Advancing research into bank erosion mechanisms and quantification is crucial for sustaining stream systems and developing effective and integrated management strategies (Poesen, 2018; Sarker et al., 2011).

Streambank erosion occurs primarily due to three interconnected processes: fluvial erosion, mass failures, and subaerial processes (Couper & Maddock, 2001). Fluvial erosion involves hydraulic forces that remove soil and sediment from the bank face,

influenced by factors like flow depth, near-bank velocity, and boundary resistance (Saadon et al., 2021; Sutarto, 2018). This erosion can undercut banks, leading to mass failures where gravity-driven collapse occurs as shear strength diminishes due to changes in pore water content and pressure (Lawler & Lawler, 1995; Pizzuto, 2009). Subaerial processes, which pre-condition banks for fluvial erosion, include soil weakening and weathering from moisture fluctuations, impacting soil particle cohesion (Simon & Rinaldi, 2000; Thorne & Tovey, 1981). However, subaerial processes remain under-researched due to a lack of models incorporating drying and wetting cycles (Couper & Maddock, 2001). Seasonal hydrograph shifts and changing soil moisture levels often drive these cycles, underscoring the need for further study.

Erosion parameters like flow shear stress (τ), the soil erodibility coefficient (K_d), and the soil critical shear stress (τ_c) are key drivers of fluvial erosion, influenced by channel morphology, soil properties, and flow dynamics (Millar & Quick, 1998). While τ varies with flow conditions and channel planform, τ_c represents a threshold determined by bank material properties, such as particle size, cohesion, and soil moisture (Duan, 2005; Yu et al., 2015). τ_c is generally treated as constant for a given bank material in most models and equations, but seasonal flow variations and soil moisture changes can dynamically influence both τ and τ_c, directly affecting erosion estimates (Chen & Duan, 2006; Dietrich & Richards, 1987; Ferguson et al., 2003). K_d, which reflects the susceptibility of bank material to erosion once shear stress exceeds critical shear, depends on soil texture, moisture content, and vegetation cover, and varies with hydrologic events and subaerial processes (Daly et al., 2015; Moragoda et al., 2022; Wynn et al., 2008). Understanding the interactions between erosion parameters and hydrologic conditions is crucial for predicting erosion rates, especially with seasonal shifts affecting streambank stability (Saha et al., 2024; Schnauder & Sukhodolov, 2012). Various techniques for estimating shear strength parameters include a rotating cylinder apparatus (Moore & Masch, 1962), hole erosion tests (HET) (Wan & Fell, 2004), cohesive strength meters (CSM) (Tolhurst et al., 1999), and jet erosion tests (JETs), with JETs being the most typical means used for in-situ measurements of Tc and Kd in recent literature. JET tests employ controlled water jet pressure to assess erosion response (Hanson & Cook, 2004). However, JET outcomes can vary significantly depending on field and laboratory conditions, requiring multiple test points to obtain reliable averages that account for site-specific soil property variations (Akinola et al., 2019). These JET tests provide shear stress and erodibility coefficient data, which are essential for accurately predicting streambank erosion rates under varying soil water conditions.

Soil moisture plays a critical role in stream bank erosion by influencing soil resistance and erosion rates (Larionov et al., 2018). Past studies showed that several factors, including the composition, orientation, bulk density of the soil, and particle size distribution, influence the effect of water content on soil erodibility (Grissinger, 1966a; Larionov et al., 2014). Dry soil exhibits a high erosion rate because surface particles are loosely bound and easily detached due to surface cracks and weak cohesion. As moisture increases to an optimal range (0.19–0.30 m/m), the erosion rate decreases because matric suction enhances soil cohesion, stabilizing the soil structure and making particles less prone to detachment (Allen et al., 1999; Nachtergaele & Poesen, 2002). Beyond this moisture threshold, the erosion rate rises again as soils approach saturation, where the buildup of positive pore-water pressure reduces effective stress (σ′=σ−u) by pushing soil particles apart and weakening inter-particle cohesion (Hanson & Simon, 2001). These alterations in shear strength make the soil more susceptible to hydraulic forces, accelerating erosion rates (Moragoda et al., 2022). However, most current erosion models do not fully account for these dynamic changes in shear strength due to fluctuating soil moisture levels, particularly under seasonal variations. This relationship may be important for improving bank erosion estimates, but further investigation is needed to confirm its significance. In-situ JET tests are valuable for measuring real-time changes in K_d and τ_c across moisture gradients, though their measurements are significantly influenced by soil moisture. While wetter conditions generally increase particle detachment and erosion rates, there is an optimum moisture range where erosion resistance is highest, whereas excessively dry conditions promote erosion due to surface cracking and weakened cohesion (Hanson & Cook, 2004; Klavon et al., 2017b; Simon et al., 2010).

Seasonal dynamics add complexity to bank erosion processes, as moisture variations throughout the year influence soil cohesion. For example, in temperate climates, winter months often bring elevated stream flows and high-water tables due to precipitation, which enhance erosion through increased hydraulic pressures on the bank soil (Henshaw et al., 2013). Extreme precipitation events, exacerbated by climate change, could intensify erosion rates by enhancing flow shear strength and flooding (de Souza Dias et al., 2022; Grove et al., 2013; Zaimes & Schultz, 2015), which would rapidly raise soil water content. However, the interpretation of bank erosion rates and their drivers remains challenging, as temporal variability in parameters such as soil moisture and shear strength parameters are rarely incorporated into models (Chassiot et al., 2020). Therefore, further research should focus on the temporal effects on fluvial erodibility parameters, particularly in how soil moisture and seasonal changes alter these coefficients, to refine predictive models and enhance the sustainability of riverbank environments under evolving climate scenarios.

Although previous studies have examined the influence of soil moisture on erosion rate, shear stress, or erodibility coefficients, many are limited to controlled laboratory settings and lack detailed field-based assessments across naturally fluctuating soil moisture conditions (Grissinger, 1966; Larionov et al., 2014; Moragoda et al., 2022). Although laboratory studies have advanced our understanding of erosion parameter estimates, they often fail to account for the variability introduced by soil-specific properties and natural hydrological conditions due to limited data availability (Larionov et al., 2018; Mahalder et al., 2022). Seasonal soil moisture fluctuations, influenced by precipitation and stream dynamics, could play a pivotal role in erosion processes. However, the extent to which these relationships hold across varying soil types and environmental conditions is not well understood. Research gaps persist in understanding how real-time seasonal changes in soil moisture impact these critical erosion parameters in streambank settings, where moisture levels can vary significantly due to natural hydrological processes.

The objective of this study is to establish a reliable relationship between seasonal soil moisture variability and erosion resistance parameters, advancing our site-specific understanding of bank erosion dynamics. This study directly addresses scientific gaps by examining the effects of seasonal soil moisture variability on shear stress and erodibility coefficients using field-based JET tests in natural streambank environments. It is important to recognize that the relationships between soil moisture, shear stress, and erodibility coefficients are influenced by soil properties such as texture, cohesion, and hydrological regimes. This underscores the need for localized assessments and adaptability in erosion modeling approaches. By integrating in-situ jet test data with seasonal soil moisture readings, this approach offers practical advancements for hydrological modeling and environmental management by improving erosion rate predictions, and providing more reliable, context-specific estimates than laboratory-based methods alone.

4.2 MATERIALS AND METHODS

4.2.1 Study Site Characteristics

The study sites selected for investigating soil moisture dynamics and their influence on shear stress and erodibility coefficients are located along Conner Creek in Knox County, Tennessee **(Figure 4-1)**. Connor Creek's watershed, with a drainage area of 3.64 sq km, is located at approximately 35°56'15" N latitude and 84°11' W longitude. The stream has a typical width of approximately 1.93 m with a reach slope of 0.007 m/m. The watershed features diverse soil types, such as gravelly loam, loamy sand, loam, and silty clay loam, with most streambanks dominated by silt loam. Landcover diversity includes pastures (10.8%), mixed forests (6.4%) of deciduous and evergreen species, and rapidly urbanizing areas (81.0%) consisting of residential zones, schools, and commercial developments. This urbanization has significantly altered natural hydrology by reducing infiltration and intensifying stormwater runoff to the creek, increasing erosion potential.

The watershed experiences flashy hydrographs due to extensive impervious surfaces from urbanized developments, which amplify runoff and lead to higher peak discharges and flow velocities during storms. Flow depths recorded from the USGS field gauge at the creek exhibited a trend of almost no flow during the dry season to a maximum of 1.62 m—nearing bankfull conditions during monsoon over the past five years. The creek has a documented history of erosion, including bank undercutting and sediment detachment during high-flow periods, particularly in urbanized sections . These erosion issues at the creek in an urbanized environment provide an ideal setting to investigate how seasonal soil moisture variability and hydrological changes influence erosion resistance. The interplay of urban runoff, diverse soil properties, and variable landcover directly aligns with the study's objective to understand the relationships between soil moisture, shear stress, and erodibility coefficients.

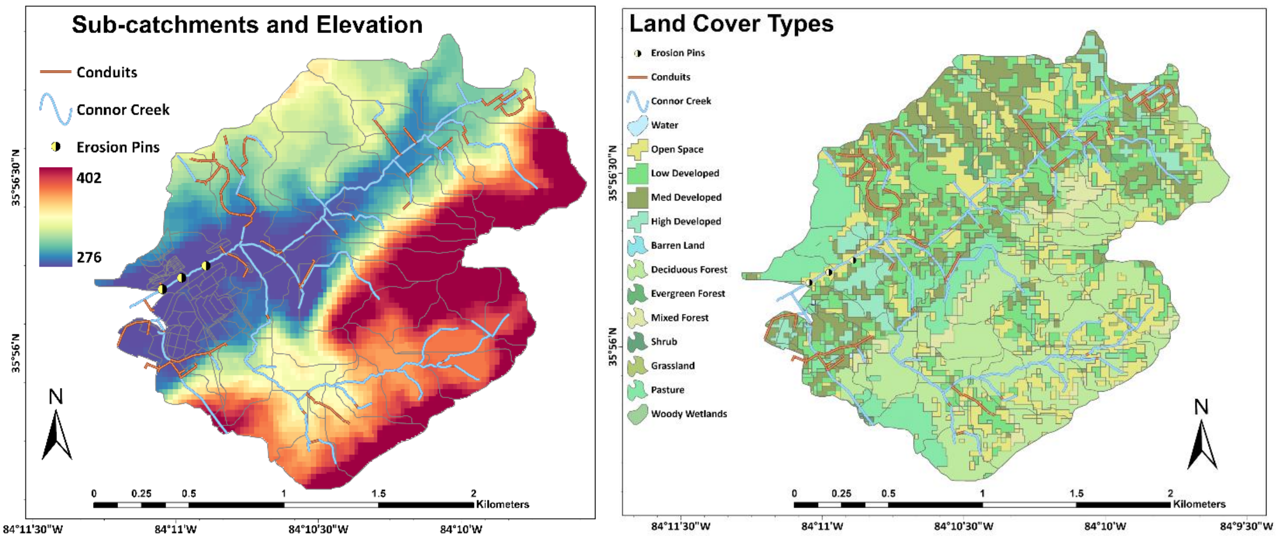

Figure 4-1 Location of bank erosions at the selected study site in Knoxville, Tennessee a. Elevation, and b. Land Cover.

4.2.2 Study Design

This study employs a field-based methodology to investigate the temporal variability of volumetric moisture content in soil water conditions and its influence on shear stress and erodibility coefficients. To capture real-time soil moisture variations, a portable soil moisture digital meter was used during field tests to allow measurements of soil water content at each test location and time, enabling correlations between soil moisture and erosion parameters. During each JET test, the Spectrum Field Scout TDR 300 Soil Moisture Meter was used for in-situ soil moisture measurements, providing instantaneous readings of root-zone moisture using Time-Domain Reflectometry (TDR) technology. The submerged JET test device **(Figure 4-2)** is commonly used to measure erosion rates in fine-grained, in situ soils subjected to hydraulic forces (Hanson & Simon, 2001). This apparatus directs a water jet with a known head (representing applied stress) onto the streambank, causing erosion to occur at a measurable rate. As erosion progresses, the distance between the jet nozzle and the eroding surface increases, which in turn reduces the applied shear stress. Over time, the erosion rate beneath the jet diminishes asymptotically, eventually approaching zero (Daly et al., 2013; Hanson & Cook, 2004). By analyzing field data, the critical shear stress and erodibility coefficient of the soil can be determined as the point where erosion ceases entirely.

Figure 4-2 The JET Device installed at the bank of Conner Creek, Knox County, TN

The National Sedimentation Laboratory (NSL) designed mini-JET device is utilized in the field for soil erodibility testing, which is a compact version of the standard JET apparatus. This JET device was utilized at approximately 36 data points across the study sites with a pressure head of 8-12 PSI, with measurements taken during different seasons throughout the year. These field measurements were processed using the Blaisdell model to compute critical shear stress (τ_c) and erodibility coefficients (K_d) (Blaisdell et al., 1981). This model is selected as it provides better estimates of the erosion parameters compared to other models(Mahalder et al., 2022).

Statistical analysis was performed by incorporating soil moisture measurements, critical shear stress, and erodibility coefficients to assess trends and correlations. Scatter plots were generated to visualize relationships among these variables, and statistical tests such as Least Squares Regression Analysis were conducted to evaluate the strength and reliability of the observed trends.

The methodology for this study is summarized in a workflow diagram **(Figure 4-3)**, illustrating each step from data collection to analysis. This integrated methodology provides valuable insights into the processes governing streambank erosion and supports the development of more accurate predictive models.

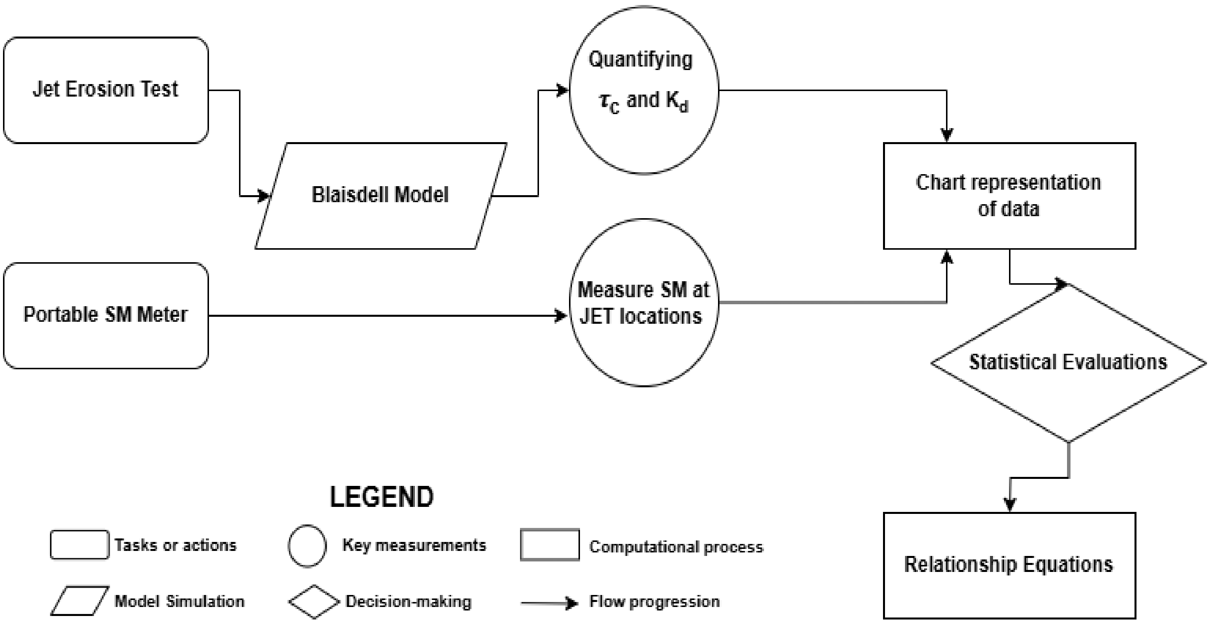

Figure 4-3 Methodology Flow Chart of the study.

4.2.3 Data Collection

Bank materials, a key factor of bank stability, were identified using laboratory hydrometer tests as a silt loam from the USDA soil texture category. The hydrometer analysis determined the soil composition as 42.5% silt, 35.4% sand, and 22.1% clay. Variable critical shear stress and erodibility coefficients were measured across 36 data points by employing in-situ JET devices under altering soil water conditions. These estimates were derived using the Blaisdell method across a range of soil moisture conditions (residual moisture of 9.5% to saturation of 39%) in 0.1-3.0% intervals to capture variability in erosion behavior under different soil moisture scenarios. During each JET test, an In-situ portable SM digital meter records soil moisture measurements with an internal logger and Bluetooth technology. This methodology of continuous and small interval tests under varying soil moisture conditions ensures robust and representative estimates of erosion parameters essential for understanding the dynamics of soil moisture and erosion relationships. **Table 4-1** summarizes the input data sources, time duration, and their variability, which form the basis for understanding the dynamics of streambank erosion and its dependence on soil water properties.

Table 4-1 Description of the input data sources

Data Type	Duration	Source	Note
Bank materials	May, 2024	Hydrometer Lab test	Soil texture
Critical Shear Stress	October 2024 – September 2025	In-situ JET test Measurements	Estimated with Variation of SM levels
Erodibility coefficient	October 2024 – September 2025	In-situ JET test Measurements	Estimated with Variation of SM levels
Soil Moisture	October 2024 – September 2025	In-situ portable SM digital meter	Ranges from dry to saturated conditions

4.2.4 Statistical Analysis

Coefficient of Determination

Statistical analyses were conducted to evaluate the relationships between soil moisture levels and the resulting shear stress and erodibility coefficients. Least Squares Regression Analysis was performed to quantify the strength and direction of the relationships, using the following correlation coefficient ranges: greater than 0.80 as very strong positive, 0.60–0.79 as strong positive, 0.40–0.59 as moderate positive, 0.20–0.39 as weak positive, and 0–0.19 as very weak positive as described by different studies (Jung et al., 2020).

$$r^2 = 1 - \frac{SS_{Res}}{SS_{Tot}} \qquad (1)$$

Here, y_i are actual observed values, $\hat{y_i}$ are predicted values from the model and y_i are mean of observed variables X and Y. Also, SS_{Res} = $\sum(y_i - \hat{y_i})^2$ are the sum of squares of residuals and SS_{Tot} = $\sum(y_i - \bar{y})^2$ are the total sum of squares. These analyses aimed to validate the observed relationships between soil moisture, shear stress, and erodibility coefficients. These methods offer a framework to establish the statistical strength and practical significance of the results.

Statistical Significance

To determine the statistical significance of the relationships between soil moisture levels and the resulting shear stress and erodibility coefficients, we computed the p-values associated with the correlation coefficients. The statistical significance of these relationships was assessed using a two-tailed t-test, where the t-statistics were calculated as:

$$t = \frac{r\sqrt{n-2}}{\sqrt{1-r^2}} \frac{SS_{Res}}{SS_{Tot}} \qquad (2)$$

where r is the Pearson correlation coefficient, and n is the sample size. The statistical significance p-value is calculated using the cumulative distribution function (CDF) of the t-distribution from t-statistics and degrees of freedom, df = n-2.

4.3 RESULTS AND DISCUSSIONS

4.3.1 Relationship Between SM with τ_c and K_d

The scatter plot of critical shear stress (τ_c) versus soil moisture (SM) exhibits a U-shaped trend, with the right side of the curve slightly higher than the left in **Figure 4-4a**, which coincides with the shape of past studies for silty clay loam soil (Akin et al., 2024; Singh & Thompson, 2016b). At low soil moisture levels (close to 10%), τ_c values are high (8.5 Pa), suggesting that the soil exhibits strong resistance to shear forces in these conditions. As soil moisture increases to intermediate levels (20–30%), τ_c decreases, reaching its lowest value of 0.06 Pa at about 24%. This indicates a significant reduction in the soil's shear resistance, likely due to a reduction in inter-particle cohesion as moisture increases. Beyond 30% soil moisture, τ_c rises again (9.06 Pa), reflecting increased resistance to shear forces in highly saturated soils, potentially due to the effects of additional hydraulic energy required to mobilize soil particles under saturated conditions. The observed erosion rate vs. soil moisture plot (Figure 4c) shows a similar relationship pattern to other previous studies (Grissinger, 1966; Larionov et al., 2014; Moragoda et al., 2022). The values along the x-axis of $\tau_c \approx 0$ could be due to highly erodible soil patches, disturbed soil structure, or measurement limitations in the JET test. Variability in saturation, pore pressure effects, or instrument sensitivity might also contribute to these anomalies.

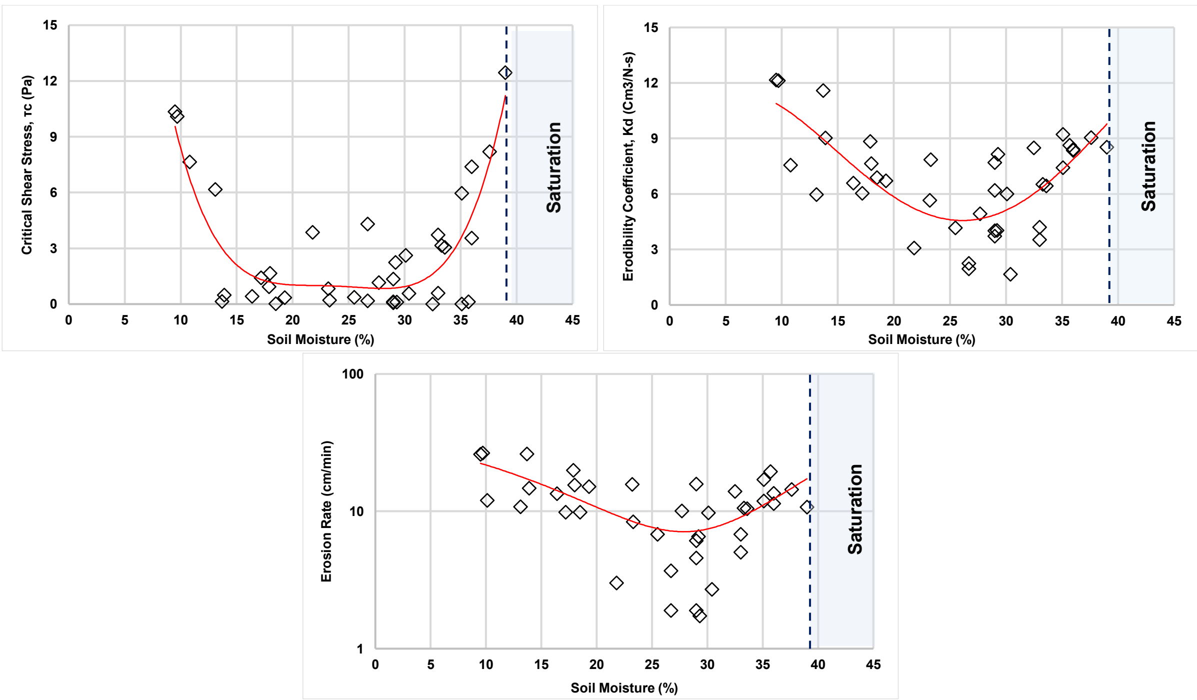

Figure 4-4 The variability of (a) critical shear stress (τ_c), (b) erodibility coefficients (K_d), and (c) erosion rate with dynamic soil water content

The erodibility coefficient (K_d) versus soil moisture (SM) plot shows a quadratic relationship in **Figure 4-4b**, but it follows a U-shaped curve slightly different from τ_c, where the left side of the curve is higher than the right, similar to other lab studies (Larionov et al., 2014; Moragoda et al., 2022). At low soil moisture levels (<15%), K_d values are relatively high, suggesting that, despite increased shear resistance (τ_c), dry soil particles may still be susceptible to erosion due to localized weaknesses such as surface cracks or dryness. When these cracks widen, intermolecular forces (van der Waals forces) weaken due to the increasing distances between particles, making it more susceptible to particle detachment (Larionov et al., 2018). As soil moisture increases to intermediate levels (15–30%), K_d decreases, indicating lower susceptibility to erosion. This reflects a temporary stabilization in the soil structure as moisture levels rise, reducing the ease of particle detachment. At higher soil moisture levels (>30%), K_d increases again, indicating greater susceptibility to erosion in saturated conditions. This trend corresponds to the elevated hydraulic forces acting on fully saturated soils, which weaken soil cohesion and make particle detachment easier, even as τ_c values begin to rise.

This study highlights the interplay between soil moisture (SM), critical shear stress (τ_c), and erodibility coefficient (K_d) to explain the observed erosion dynamics transitioning from unsaturated to partially saturated, and fully saturated soils. In the vadose zone (unsaturated), pore-water pressure (PWP) plays a pivotal role in controlling soil strength (Casagli et al., 1999). At low soil moisture levels (near 10%), matric suction (negative PWP) (μ_a−μ_w) dominates, significantly enhancing apparent cohesion (c_a) and increasing τ_c. This is due to cohesion forces binding soil particles, resulting in high inter-particle friction and increased resistance to hydraulic forces (Kemper & Rosenau, 1984; Li et al., 2022). However, these conditions can also lead to localized weaknesses, such as surface cracks, that increase K_d by making surface particles more susceptible to detachment (Tang et al., 2020). This dual effect underscores the complex nature of erosion dynamics in dry soils, where high shear strength coexists with localized erosion vulnerabilities.

As SM increases to intermediate levels (20–30%), matric suction diminishes, leading to reduced cohesion and effective stress (Pandya & Sachan, 2020). This causes a drop in τ_c, reflecting weaker soil resistance. At the same time, K_d remains low due to the limited presence of positive pore-water pressure as the saturation of soil pores is incomplete, which restricts the transmission of hydraulic forces that contribute to soil particle detachment (Dong et al., 2023). This intermediate state represents a balance between suction-dominated and saturation-dominated conditions, where the soil exhibits temporary stability with minimal erosion susceptibility.

When soil moisture approaches full saturation (35–40%), pore-water pressure transitions from negative (matric suction) to positive, significantly altering soil properties. Positive pore-water pressure reduces effective stress, weakening soil cohesion, and inter-particle friction. However, in fully saturated soils, capillary cohesion and particle realignment enhance resistance to particle detachment, requiring higher hydraulic energy to mobilize and detach particles, which increases τc as the soil resists erosion under elevated hydraulic energy (Topçu et al., 2024). Experimental evidence shows that τ_c increases under saturated conditions for fine-grained soils due to increased cohesive forces from capillary tension and particle interlocking, which counteract the weakening effects of positive pore pressure. At the same time, K_d increases with higher soil moisture content, indicating greater susceptibility to erosion as the soil becomes more saturated. A recent study (Akin et al., 2024) found that the relationship between K_d and soil water mass varies by soil type. For silty clay loam (similar to this study), K_d follows a curvilinear U-shaped trend, reaching a higher value after reaching optimum infiltration point (Hanson & Robinson, 1993). In contrast, other soils as sandy and clay loam shows a linear increase in K_d with increasing infiltration.

4.3.2 Statistical Relationship & Correlations

The quadratic relationships derived from the plots of soil moisture dynamics with critical shear stress (τ_c) and erodibility coefficients (K_d) are:

$$\tau_c = 0.0002 \times SM^4 - 0.02 \times SM^3 - 0.75 \times SM^2 - 11.78 \times SM + 70 \quad (3)$$

$$K_d = -0.00004 \times SM^4 + 0.004 \times SM^3 - 0.14 \times SM^2 - 1.31 \times SM + 7.89 \quad (4)$$

The coefficient of determination (r^2) for the quadratic relationship between τ_c and soil moisture is 0.75 (r=0.86), indicating a moderately strong fit, suggesting 75% of the variability in τ_c can be explained by changes in soil moisture. This implies that soil moisture is a driver of critical shear stress but not the sole determinant. For K_d and soil moisture, the r^2 value is 0.52 (r=0.72), reflecting a moderate fit where 52% of the variability in K_d is attributable to soil moisture. The slightly lower r^2 for K_d suggests a larger set of influencing factors, including localized hydraulic forces such as preferential flow paths and seepage erosion, soil structural variability like aggregated versus dispersed soil structures and layering effects, and micro-scale particle cohesion influenced by clay content, organic matter binding, and electrochemical interactions between particles.

For the relationship between critical shear stress (τ_c) and soil moisture (SM), the coefficient of determination was $r^2 = 0.75$, yielding a correlation coefficient of $r = 0.86$. With a sample size of 39, the computed t-statistic was 10.43, corresponding to a p-value of 1.44×10^{-12}. Similarly, for the relationship between the erodibility coefficient (Kd) and soil moisture, the coefficient of determination was $r^2 = 0.52$, with a correlation coefficient of $r = 0.72$. The corresponding t-statistics were 6.37, yielding a p-value of 1.99×10^{-7}. Since both p-values are significantly lower than conventional significance thresholds (0.05, 0.01, and 0.001), the relationships between soil moisture and both critical shear stress and erodibility coefficient are statistically significant. These findings confirm that soil moisture variations have a substantial impact on bank erosion processes.

The residuals in both relationships indicate that other factors, such as soil texture and vegetation cover, also contribute to the variability. These relationships could be employed to assess the altering τ_c and K_d in relation to variable seasonal soil moisture dynamics in an erosion framework or model.

4.3.3 Relationship Between K_d and τ_c

Critical shear stress (τ_c) is fundamentally governed by the shear strength of the soil, which is determined by effective stress, cohesion, and frictional resistance (Hanson & Simon, 2001). Conversely, the erodibility coefficient (K_d) measures how easily soil particles can be detached by hydraulic forces, which depends more on the balance of cohesive forces at the particle scale and the energy available for detachment (Simon & Collison, 2001). The relationship between τ_c and K_d varies significantly across soil moisture conditions, highlighting the distinct physical mechanisms governing these parameters **(Figure 4-5)**.

At low soil moisture levels (SM<20%), the relationship between τ_c and K_d is weak and less significant, as reflected in the nearly flat or slightly positive trend. These conditions align with findings by Hanson & Simon (2001), who noted that cohesive soils in low-moisture environments exhibit complex interactions between surface and subsurface processes. At intermediate soil moisture levels (SM=20%–30%), the relationship between τ_c and K_d shows an inverse trend. This range represents a transition between suction-dominated and saturation-dominated states. This balance between weakening cohesion and reduced detachment susceptibility reflects findings by Moragoda et al. (2022), who observed stabilization of erosion resistance at moderate moisture levels. At high soil moisture levels (SM>30%), the relationship between τ_c and K_d shows a weak inverse trend. This behavior aligns with observations by Thoman and Niezgoda (2008), who reported consistently high K_d values in saturated cohesive soils. These findings highlight the multi-scale nature of erosion dynamics, where both τ_c and K_d respond differently to changes in soil moisture, pore-water pressure, and soil structure. Understanding these dynamics is crucial for accurately modeling erosion processes and designing effective management strategies for streambank stability. The distinct dependencies of τ_c and K_d on soil conditions underscore the importance of treating them as independent parameters when assessing erosion susceptibility.

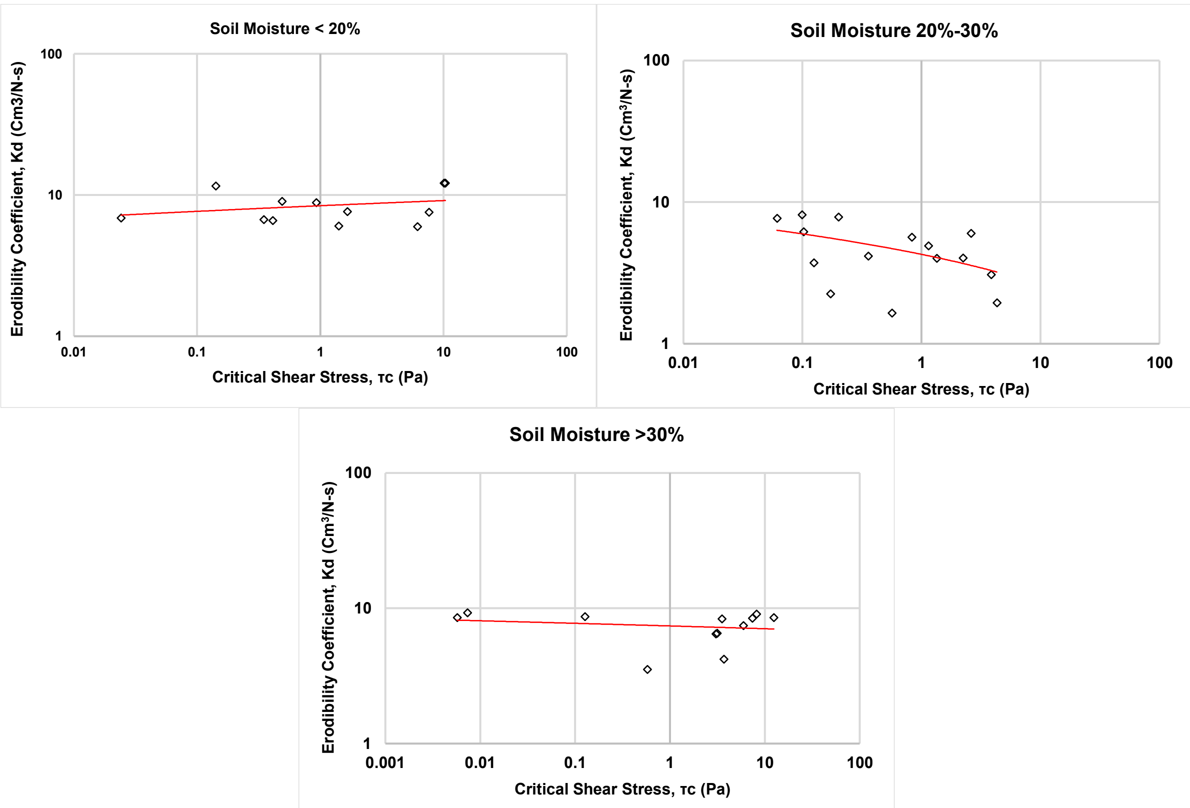

Figure 4-5 The relationship between critical shear stress (τ_c) and erodibility coefficients (K_d) for soil moisture ranges of (a) less than 20%, (b) 20-30%, and (c) greater than 30%

4.4 CONCLUSIONS

This study presents a field-based analysis of the relationship between soil moisture (SM), critical shear stress (τ_c), and the erodibility coefficient (K_d) and their role in streambank erosion processes. The results confirm that both τ_c and K_d exhibit a U-shaped relationship with soil moisture, with high values at extreme low and high moisture levels and a minimum at intermediate moisture conditions. Field-based JET test conducted at 36 locations along Conner Creek, Knoxville, TN, captured soil moisture variations ranging from 10% to 39% (0.10-0.39 m/m). The lowest τ_c was observed at 24% SM (0.06 Pa), while the highest τ_c values occurred at 10% (8.5 Pa) and 39% (9.06 Pa), indicating that moisture extremes contribute to increased resistance against erosion. Similarly, Kd values exhibited an inverse U-shaped trend, with a minimum occurring in the 15–30% SM range ($K_d \approx 2.1 \times 10^{-3}$ $cm^3/N{\cdot}s$) and increasing at both drier **(**$K_d \approx 8.99 \times 10^{-3}$ $cm^3/N{\cdot}s$ at 15% SM**)** and saturated conditions **(**$K_d \approx 5.24 \times 10^{-3}$ $cm^3/N{\cdot}s$ at 39% SM**)**. Statistical analysis showed significant relationships between soil moisture and both τ_c ($r^2 = 0.75$, $p < 0.001$) and K_d ($r^2 = 0.52$, $p < 0.001$), confirming that soil moisture plays a substantial role in controlling bank erosion susceptibility. These findings provide insights into the non-linear dynamics of soil moisture and their impact on erosion processes specific to silty clay loam soil. The results emphasize that soil moisture is a critical driver of erosion susceptibility, influencing both soil strength and the ease of particle detachment.

This study highlights the need to integrate soil moisture dynamics into erosion prediction models. Most erosion models assume τ_c to be constant for a given soil type; however, this study provides evidence that τ_c and K_d vary dynamically with SM, particularly under seasonal and hydrological fluctuations. Incorporating soil moisture-dependent τ_c and K_d values into predictive frameworks could improve bank erosion estimates and enhance mitigation strategies for unstable streambanks.

While this study provides valuable insights, several limitations should be acknowledged. First, the data used to derive the relationships between SM, τ_c, and K_d were constrained by spatial and temporal variability, which may limit the generalization of the findings to other sites with different soil textures or hydrological conditions. Future research should address these limitations by expanding data collection to include diverse soil types, and hydrological regimes. Another promising direction for future research is developing more dynamic models that incorporate temporal changes in soil moisture with variable critical shear stress (τ_c) and erodibility coefficients (K_d), which could improve predictions of erosion susceptibility under changing climate conditions. In conclusion, this study underscores the importance of soil moisture dynamics in shaping erosion processes and suggests a possible means to improve erosion estimation models. By addressing the identified limitations and building on the findings, future research can contribute to more effective erosion management strategies and sustainable land use practices.

REFERENCES

Akin, A. A., Nguyen, G., & Sheshukov, A. Y. (2024). Infiltration-Based Variability of Soil Erodibility Parameters Evaluated with the Jet Erosion Test. Water 2024, Vol. 16, Page 981, 16(7), 981. https://doi.org/10.3390/W16070981

Akinola, A. I., Wynn-Thompson, T., Olgun, C. G., Mostaghimi, S., & Eick, M. J. (2019). Fluvial Erosion Rate of Cohesive Streambanks Is Directly Related to the Difference in Soil and Water Temperatures. Journal of Environmental Quality, 48(6), 1741–1748. https://doi.org/10.2134/jeq2018.10.0385

Allen, P. M., Arnold, J., & Jakubowski, E. (1999). Prediction of stream channel erosion potential. Environmental and Engineering Geoscience, 5(3), 339–351. https://doi.org/10.2113/gseegeosci.v.3.339

Blaisdell, F. W., Hebaus, G. G., & Anderson, C. L. (1981). Ultimate Dimensions of Local Scour. Journal of the Hydraulics Division, 107(3), 327–337. https://doi.org/10.1061/JYCEAJ.0005630

Borrelli, P., Robinson, D. A., Panagos, P., Lugato, E., Yang, J. E., Alewell, C., Wuepper, D., Montanarella, L., & Ballabio, C. (2020). Land use and climate change impacts on global soil erosion by water (2015-2070). PNAS, 117(36), 21994–22001. https://doi.org/10.1073/pnas.2001403117/-/DCSupplemental

Casagli, N., Rinaldi, M., Gargini, A., & Curini, A. (1999). Pore water pressure and streambank stability: Results from a monitoring site on the Sieve River, Italy. Earth Surface Processes and Landforms, 24(12), 1095–1114. https://doi.org/10.1002/(SICI)1096-9837(199911)24:12<1095::AID-ESP37>3.0.CO;2-F

Chassiot, L., Lajeunesse, P., & Bernier, J. F. (2020). Riverbank erosion in cold environments: Review and outlook. Earth-Science Reviews, 207. https://doi.org/10.1016/j.earscirev.2020.103231

Chen, D., & Duan, J. G. (2006). Modeling width adjustment in meandering channels. Journal of Hydrology, 321(1–4), 59–76. https://doi.org/10.1016/J.JHYDROL.2005.07.034

Couper, P. R., & Maddock, I. P. (2001). Subaerial river bank erosion processes and their interaction with other bank erosion mechanisms on the River Arrow, Warwickshire, UK. Earth Surface Processes and Landforms, 26(6), 631–646. https://doi.org/10.1002/ESP.212

Daly, E. R., Fox, G. A., Al-Madhhachi, A. T., & Miller, R. B. (2013). A Scour Depth Approach for Deriving Erodibility Parameters from Jet Erosion Tests. Transactions of the ASABE, 56(6), 1343–1351. https://doi.org/10.13031/TRANS.56.10350

Daly, E. R., Miller, R. B., & Fox, G. A. (2015). Modeling streambank erosion and failure along protected and unprotected composite streambanks. Advances in Water Resources, 81, 114–127. https://doi.org/10.1016/J.ADVWATRES.2015.01.004

de Souza Dias, V., de Faria, K. M. S., da Luz, M. P., & Formiga, K. T. M. (2022). Investigation and Quantification of Erosions in the Margins of Water Bodies: A Systematic Review. Water, 14(11). https://doi.org/10.3390/w14111693

Dietrich, W. E., & Richards, K. S. (1987). River Channels: Environment and Process.

Dong, J. gui, Xu, J., & Xiang, G. xing. (2023). Pore Water Distribution in Unsaturated Soil. Indian Geotechnical Journal, 53(2), 291–299. https://doi.org/10.1007/S40098-022-00672-6/METRICS

Duan, J. G. (2005). Analytical Approach to Calculate Rate of Bank Erosion. Journal of Hydraulic Engineering, 131(11), 980–990. https://doi.org/10.1061/(ASCE)0733-9429(2005)131:11(980)/ASSET/6481FB3A-6BA1-4A15-AF07-50F471B69580/ASSETS/IMAGES/2.JPG

Duró, G., Crosato, A., Kleinhans, M. G., Roelvink, D., & Uijttewaal, W. S. J. (2020). Bank Erosion Processes in Regulated Navigable Rivers. Journal of Geophysical Research: Earth Surface, 125(7). https://doi.org/10.1029/2019JF005441

Ferguson, R. I., Parsons, D. R., Lane, S. N., & Hardy, R. J. (2003). Flow in meander bends with recirculation at the inner bank. Water Resources Research, 39(11), 1322. https://doi.org/10.1029/2003WR001965

Florsheim, J. L., Mount, J. F., & Chin, A. (2008). Bank Erosion as a Desirable Attribute of Rivers. BioScience, 58(6), 519–529. https://doi.org/10.1641/B580608

Grissinger, E. H. (1966a). Resistance of selected clay systems to erosion by water. Water Resources Research, 2(1), 131–138. https://doi.org/10.1029/WR002I001P00131

Grissinger, E. H. (1966b). Resistance of selected clay systems to erosion by water. Water Resources Research, 2(1), 131–138. https://doi.org/10.1029/WR002i001p00131

Grove, J. R., Croke, J., & Thompson, C. (2013). Quantifying different riverbank erosion processes during an extreme flood event. Earth Surface Processes and Landforms, 38(12), 1393–1406. https://doi.org/10.1002/ESP.3386

Hanson, G. J., & Cook, K. R. (2004). APPARATUS, TEST PROCEDURES, AND ANALYTICAL METHODS TO MEASURE SOIL ERODIBILITY IN SITU. Applied Engineering in Agriculture, 20(4), 455–462. https://doi.org/10.13031/2013.16492

Hanson, G. J., & Robinson, K. M. (1993). The Influence of Soil Moisture and Compaction on Spillway Erosion. Transactions of the ASAE, 36(5), 1349–1352. https://doi.org/10.13031/2013.28469

Hanson, G. J., & Simon, A. (2001). Erodibility of cohesive streambeds in the loess area of the Midwestern USA. Hydrological Processes, 15(1), 23–38. https://doi.org/10.1002/HYP.149

Hathaway, A. (2024). Knox County Stormwater Monitoring Plan.

Henshaw, A. J., Thorne, C. R., & Clifford, N. J. (2013). Identifying causes and controls of river bank erosion in a British upland catchment. CATENA, 100, 107–119. https://doi.org/10.1016/J.CATENA.2012.07.015

Jung, C., Lee, Y., Lee, J., & Kim, S. (2020). Performance Evaluation of the Multiple Quantile Regression Model for Estimating Spatial Soil Moisture after Filtering Soil Moisture Outliers. Remote Sensing 2020, Vol. 12, Page 1678, 12(10), 1678. https://doi.org/10.3390/RS12101678

Kemper, W. D., & Rosenau, R. C. (1984). Soil Cohesion as Affected by Time and Water Content. Soil Science Society of America Journal, 48(5), 1001–1006. https://doi.org/10.2136/SSSAJ1984.03615995004800050009X

Klavon, K., Fox, G., Guertault, L., Langendoen, E., Enlow, H., Miller, R., & Khanal, A. (2017). Evaluating a process-based model for use in streambank stabilization: insights on the Bank Stability and Toe Erosion Model (BSTEM). Earth Surface Processes and Landforms, 42(1), 191–213. https://doi.org/10.1002/esp.4073

Larionov, G. A., Bushueva, O. G., Dobrovol'skaya, N. G., Kiryukhina, Z. P., Krasnov, S. F., & Litvin, L. F. (2014). Effect of the water temperature and soil moisture on the erodibility of chernozem samples: A model experiment. Eurasian Soil Science, 47(7), 734–739. https://doi.org/10.1134/S1064229314070096/METRICS

Larionov, G. A., Bushueva, O. G., Gorobets, A. V., Dobrovolskaya, N. G., Kiryukhina, Z. P., Krasnov, S. F., Litvin, L. F., Maksimova, I. A., & Sudnitsyn, I. I. (2018). Experimental Study of Factors Affecting Soil Erodibility. Eurasian Soil Science, 51(3), 336–344. https://doi.org/10.1134/S1064229318030067/METRICS

Lawler, D. M., & Lawler, D. M. (1995). Effects of Scale on Interpretation and Management of Sediment and Water Quality (Proceedings of alioulderSymposium. 226, 175. https://www.researchgate.net/publication/246545439

Li, M., Liu, Q., Zhang, H., Wells, R. R., Wang, L., & Geng, J. (2022). Effects of antecedent soil moisture on rill erodibility and critical shear stress. CATENA, 216, 106356. https://doi.org/10.1016/J.CATENA.2022.106356

Mahalder, B., Schwartz, J. S., Wynn-Thompson, T. M., Palomino, A. M., & Zirkle, J. (2022). Comparison of Erodibility Parameters for Cohesive Streambank Soils between In Situ Jet Test Device and Laboratory Conduit Flume. Journal of Hydraulic Engineering, 148(1). https://doi.org/10.1061/(ASCE)HY.1943-7900.0001938

Millar, R. G., & Quick, M. C. (1998). Stable Width and Depth of Gravel-Bed Rivers with Cohesive Banks. Journal of Hydraulic Engineering, 124(10), 1005–1013. https://doi.org/10.1061/(ASCE)0733-9429(1998)124:10(1005)

Moore, W. L., & Masch, F. D. (1962). Experiments on the scour resistance of cohesive sediments. Journal of Geophysical Research, 67(4), 1437–1446. https://doi.org/10.1029/JZ067I004P01437

Moragoda, N., Kumar, M., & Cohen, S. (2022). Representing the role of soil moisture on erosion resistance in sediment models: Challenges and opportunities. Earth-Science Reviews, 229, 104032. https://doi.org/10.1016/j.earscirev.2022.104032

Nachtergaele, J., & Poesen, J. (2002). Spatial and temporal variations in resistance of loess-derived soils to ephemeral gully erosion. European Journal of Soil Science, 53(3), 449–463. https://doi.org/10.1046/j.1365-2389.2002.00443.x

Pandya, S., & Sachan, A. (2020). Variation of collapse potential and stiffness degradation with matric suction of compacted unsaturated cohesive soil. International Journal of Geotechnical Engineering, 14(1), 35–48. https://doi.org/10.1080/19386362.2017.1398368

Pizzuto, J. (2009). An empirical model of event scale cohesive bank profile evolution. Earth Surface Processes and Landforms, 34(9), 1234–1244. https://doi.org/10.1002/esp.1808

Poesen, J. (2018). Soil erosion in the Anthropocene: Research needs. Earth Surface Processes and Landforms, 43(1), 64–84. https://doi.org/10.1002/esp.4250

Saadon, A., Abdullah, J., Muhammad, N. S., Ariffin, J., & Julien, P. Y. (2021). Predictive models for the estimation of riverbank erosion rates. CATENA, 196, 104917. https://doi.org/10.1016/J.CATENA.2020.104917

Saha, P., Hathaway, J., Schwartz, J. S., Wilson, C. G., Abban, B. K., & Papanicolaou, A. N. T. (2024). Climate Change Impacts on Spatiotemporal Soil Water Extremes in Geophysically Diverse Watersheds: A Comparison between East and West Tennessee Watersheds. Journal of Hydrologic Engineering, 29(3). https://doi.org/10.1061/jhyeff.heeng-6117

Sarker, M. H., Akter, J., Sarker, M. H., & Ferdaous, M. R. (2011). River bank protection measures in the Brahmaputra-Jamuna River: Bangladesh Experience Md Ruknul Ferdous River bank protection measures in the Brahmaputra-Jamuna River: Bangladesh Experience. https://www.researchgate.net/publication/263125674

Schnauder, I., & Sukhodolov, A. N. (2012). Flow in a tightly curving meander bend: effects of seasonal changes in aquatic macrophyte cover. Earth Surface Processes and Landforms, 37(11), 1142–1157. https://doi.org/10.1002/ESP.3234

Simon, A., & Rinaldi, M. (2000). Channel instability in the loess area of the midwestern United States. Journal of the American Water Resources Association, 36(1), 133–150. https://doi.org/10.1111/j.1752-1688.2000.tb04255.x

Simon, A., Thomas, R. E., & Klimetz, L. (2010). COMPARISON AND EXPERIENCES WITH FIELD TECHNIQUES TO MEASURE CRITICAL SHEAR STRESS AND ERODIBILITY OF COHESIVE DEPOSITS.

Singh, H. V., & Thompson, A. M. (2016). Effect of antecedent soil moisture content on soil critical shear stress in agricultural watersheds. Geoderma, 262, 165–173. https://doi.org/10.1016/J.GEODERMA.2015.08.011

Sutarto, T. E. (2018). A Short Review on Various Techniques for Measuring Stream Bank Soil Erosion Strength. Proceedings - 2018 International Conference on Applied Science and Technology, ICAST 2018, 252–258. https://doi.org/10.1109/iCAST1.2018.8751560

Tang, C. S., Cheng, Q., Leng, T., Shi, B., Zeng, H., & Inyang, H. I. (2020). Effects of wetting-drying cycles and desiccation cracks on mechanical behavior of an unsaturated soil. CATENA, 194, 104721. https://doi.org/10.1016/J.CATENA.2020.104721

Thorne, C. R., & Tovey, N. K. (1981). Stability of composite river banks. Earth Surface Processes and Landforms, 6(5), 469–484. https://doi.org/10.1002/ESP.3290060507

Tolhurst, T. J., Black, K. S., Shayler, S. A., Mather, S., Black, I., Baker, K., & Paterson, D. M. (1999). Measuring the in situ Erosion Shear Stress of Intertidal Sediments with the Cohesive Strength Meter (CSM). Estuarine, Coastal and Shelf Science, 49, 281–294. http://www.idealibrary.comon

Topçu, S., Savaş, H., & Tosun, H. (2024). Effect of stress conditions on concentrated leak erosion resistant of fine-grained soils with different characteristics. Acta Geotechnica, 19(12), 7967–7988. https://doi.org/10.1007/S11440-024-02376-Y/FIGURES/23

Vietz, G. J., Lintern, A., Webb, J. A., & Straccione, D. (2018). River Bank Erosion and the Influence of Environmental Flow Management. Environmental Management, 61(3), 454–468. https://doi.org/10.1007/S00267-017-0857-9/METRICS

Wan, C. F., & Fell, R. (2004). Investigation of Rate of Erosion of Soils in Embankment Dams. Journal of Geotechnical and Geoenvironmental Engineering, 130(4), 373–380. https://doi.org/10.1061/(ASCE)1090-0241(2004)130:4(373)

Wynn, T. M., Henderson, M. B., & Vaughan, D. H. (2008a). Changes in streambank erodibility and critical shear stress due to subaerial processes along a headwater stream, southwestern Virginia, USA. Geomorphology, 97(3–4), 260–273. https://doi.org/10.1016/J.GEOMORPH.2007.08.010

Wynn, T. M., Henderson, M. B., & Vaughan, D. H. (2008b). Changes in streambank erodibility and critical shear stress due to subaerial processes along a headwater stream, southwestern Virginia, USA. Geomorphology, 97(3–4), 260–273. https://doi.org/10.1016/j.geomorph.2007.08.010

Wynn, T., & Mostaghimi, S. (2006). The effects of vegetation and soil type on streambank erosion, Southwestern Virginia, USA. Journal of the American Water Resources Association, 42(1), 69–82. https://doi.org/10.1111/j.1752-1688.2006.tb03824.x

Yu, M. hui, Wei, H. yan, & Wu, S. bai. (2015). Experimental study on bank erosion and interaction with near-bank bed evolution due to fluvial hydraulic force. International Journal of Sediment Research, 30(1), 81–89. https://doi.org/10.1016/S1001-6279(15)60009-9

Zaimes, G. N., & Schultz, R. C. (2015). Riparian land-use impacts on bank erosion and deposition of an incised stream in north-central Iowa, USA. CATENA, 125, 61–73. https://doi.org/10.1016/J.CATENA.2014.09.013

CHAPTER-5

DYNAMIC EROSION MODELING OF STREAMBANKS: INTEGRATING SOIL MOISTURE–BASED PREDICTIONS OF CRITICAL SHEAR STRESS AND ERODIBILITY COEFFICIENTS INTO BSTEM

RESEARCH QUESTION

Can erosion models better capture seasonal streambank erosion variability by integrating critical shear stress (τc) and erodibility coefficient (Kd) as functions of dynamic soil moisture?

ABSTRACT

Improved prediction of streambank erosion requires reliable estimation of erosion resistance parameters, critical shear stress (τ_c) and the erodibility coefficient (K_d), which are often assumed static in conventional models. However, field conditions reveal that these parameters vary dynamically with soil moisture. This study presents a modified approach to the Bank Stability and Toe Erosion Model (BSTEM), incorporating field-derived polynomial relationships between soil moisture and τ_c-K_d to reflect real-time hydrologic variability. Sensitivity analyses of Manning's roughness (n) for a range of 0.025 to 0.065 in both default and modified dynamic model showed variation of over 200 cm in predicted retreat, indicating the importance of selecting correct value for erosion estimation. With the calibrated manning's n, dynamic model outputs were compared against traditional static approaches under both dry and wet conditions. Statistical analysis demonstrated that the dynamic model achieved higher p-values on both t-test and ANOVA ($p \geq 0.79$) and lower variance (Anova $F \leq 0.08$) at sites 1 and 3, outperforming static models especially during early and late-season soil moisture transitions. These findings highlight the critical role of soil moisture in controlling erosion resistance and demonstrate the value of integrating hydrologically responsive parameters into predictive frameworks. This modified BSTEM approach offers both improved accuracy and enhanced process realism and can serve as a scalable modeling tool for streambank management under dynamic environmental conditions.

5.1 INTRODUCTION

Streambank erosion is a complex and dynamic process primarily influenced by variations in flow conditions, soil moisture, and geotechnical properties (Fox & Wilson, 2010; Simon & Collison, 2001). It commonly occurs on the cut bank in meandering rivers or channels, where hydraulic forces interact with vulnerable bank materials (Gaskin et al., 2003). The interplay between hydrological forces and soil characteristics, including water content, cohesion, slope, and root reinforcement, makes accurate erosion prediction challenging. As climate change intensifies, alterations in precipitation patterns (both extreme rainfall and increased dry periods) and streamflow regimes are expected to shift the timing and magnitude of erosion events (Biron et al., 2014). This highlights the importance of considering dynamic hydrologic drivers in erosion estimation framework which may offer improved predictive insight. Such additions to models may allow better predictions of erosion timing and magnitude, as well as the development of more effective strategies to mitigate streambank failure and sediment-related impacts.

Erosion models often rely on constant values for critical shear stress (τ_c) and erodibility coefficient (K_d), which may not reflect the temporal variability of soil properties under field conditions. This assumption can introduce significant uncertainty, particularly in parameters τ_c and K_d, which are known to fluctuate with changes in soil water content (Larionov et al., 2014; Moragoda et al., 2022), soil structure—such as aggregation, compaction, and layering (Clark & Wynn, 2007; Fox & Wilson, 2010; Rinaldi & Darby, 2007) and other environmental factors including temperature, pH and vegetation cover (Akinola et al., 2019; Daly et al., 2015; Hoomehr et al., 2018; Simon et al., 2010). Among these, soil moisture plays a particularly dynamic role by altering matric suction and pore pressure, which directly affect soil cohesion and resistance to detachment (Hanson & Robinson, 1993; Li et al., 2022; Moragoda et al., 2022; Simon & Collison, 2001; Singh & Thompson, 2016b).

One widely used erosion model is the Bank Stability and Toe Erosion Model (BSTEM). BSTEM applies static values of τ_c and K_d (Simon et al., 2000) derived from single-condition tests conducted during either wet or dry seasons. This approach may result in overestimation or underestimation of lateral bank retreat under varying hydrological conditions, as τ_c and K_d values may be unusually high or low depending on the seasonal conditions at the time of testing (Daly et al., 2015; Simon et al., 2010). BSTEM has been shown to predict lateral bank retreat inaccurately, particularly when it does not account for delayed water table response. The rapid decline in near-bank pore-water pressures under such conditions can falsely increase modeled bank stability (Midgley et al., 2012). Soil moisture directly affects pore-water pressure (PWP), where increased saturation raises positive PWP, reducing effective stress ($\sigma' = \sigma - u$) and weakening soil cohesion and erosion resistance (Simon & Collison, 2001). Integrating soil moisture–based variability into τ_c and K_d may improve the predictive accuracy and reliability of BSTEM, particularly in the context of seasonal dynamics (Daly et al., 2015; Klavon et al., 2017a; Moragoda et al., 2022).

Building on the limitations discussed in the previous section, it is essential to understand how sensitive BSTEM predictions are to both geotechnical and hydraulic parameters under natural variability. Several studies have demonstrated BSTEM's sensitivity to key input variables such as soil cohesion, internal friction angle, and Manning's n, all of which significantly influence predicted erosion rates and lateral retreat (Klavon et al., 2017a; Midgley et al., 2012). For instance, Parker et al. (2008) reported that variability in soil parameters, such as effective cohesion (c') ranging from 0 to 3.10 kPa and internal friction angle (ϕ') from 22.4° to 41.1°, exhibited a direct relationship with the factor of safety (FoS), while saturated unit weight (γ), varying between 18.6 and 19.3 kN/m^3, showed an inverse relationship with FoS in streambank stability simulations. Midgley et al. (2012) showed that using default or even site-measured soil parameters often underpredicted erosion unless specifically calibrated for cohesion, friction angle, and erodibility. Another study further emphasized that BSTEM's predictions of retreat and failure mechanisms are highly sensitive to erosion resistance, and hydraulic conditions (Konsoer et al., 2016).

These findings reinforce that BSTEM's accuracy is highly contingent on how well field-specific parameters are captured, including those that are known to vary seasonally. Yet, in practice, parameters like τc and Kd are typically input as fixed values despite their documented sensitivity to environmental factors. Daly et al. (2015) demonstrated that calibration of τc and Kd was critical for improving erosion predictions. Sensitivity studies have shown that changes in pore-water pressure (Cancienne et al., 2008) and matric suction (Pollen-Bankhead & Simon, 2010) exert major impacts on modeled factors of safety and erosion rates (estimated with τ_c and K_d). Given its direct influence on matric suction and pore-water pressure, soil moisture plays a particularly dynamic role in modulating effective stress, making it a key driver of variability in τ_c and K_d, and thus a critical factor in streambank erosion modeling (Moragoda et al., 2022; Simon & Collison, 2001; Singh & Thompson, 2016b). This underscores the need for incorporating dynamic soil moisture conditions into erosion models to better reflect real-world variability and improve prediction.

Field studies (Larionov et al., 2018; Moragoda et al., 2022) have shown that erosion parameters such as critical shear stress (τc) and the erodibility coefficient (Kd) exhibit non-linear, often U-shaped, relationships with soil moisture. At intermediate moisture levels, erosion resistance tends to be lowest, while higher resistance is observed in extremely dry soils due to matric suction or in saturated conditions due to increased hydraulic demand for particle mobilization. Similar patterns have also been observed in other studies that demonstrated how moisture extremes influence soil shear strength (Allen et al., 1999; Li et al., 2022; Nachtergaele & Poesen, 2002). Therefore, it is necessary to investigate whether explicitly incorporating this variability into erosion models can enhance their ability to predict streambank retreat under dynamic hydrologic conditions.

Despite this understanding, many models including BSTEM continue to apply τ_c and K_d as fixed values based on singular condition measurements (Daly et al., 2015; Klavon et al., 2017a; Simon & Rinaldi, 2000), which limits their capacity to represent temporal variability under real-world conditions. Chapter 4 of this study further established the measurable soil moisture-based relationships affecting erosion dynamics. Earlier studies also showed that incorporating soil moisture can improve the estimates of bank erosion rates (Konsoer et al., 2016; Parker et al., 2008). By integrating soil moisture–based functional relationships, this study advances a process-based modification to BSTEM that improves model realism, supports decision-making, and enables scenario testing under changing hydrological regimes.

The review above reveals key limitations in the current modeling approaches. Static representations of τ_c and K_d, derived from wet or dry season tests, fail to capture the temporal variability observed in field conditions (Daly et al., 2015; Khanal et al., 2016; Moragoda et al., 2022). While BSTEM provides a process-based framework, its predictive accuracy may be limited when key dynamic drivers such as soil moisture variability are not explicitly incorporated, a knowledge gap that needs to be investigated. Another overlooked but critical variable is Manning's n. Often treated as a calibration parameter, Manning's n significantly influences near-bank hydraulic shear stress and can affect lateral retreat predictions (Klavon et al., 2017a). This study explores whether incorporating soil moisture–driven variability in τ_c and K_d, along with evaluating the sensitivity of Manning's n, can improve BSTEM's predictive capability under fluctuating hydrological conditions. The objectives of the study are to- i) develop a dynamic erosion modeling approach for streambanks in BSTEM by incorporating soil moisture-based predictions of critical shear stress (τc) and erodibility coefficient (Kd) and ii) assess the sensitivity of the modified BSTEM model to variations in dynamic soil moisture-based τ_c and K_d with Manning's n, aiming to improve model accuracy for lateral retreat predictions based on a case study for a Tennessee Ridge and Valley stream.

5.2 MATERIALS AND METHODS

5.2.1 Study Site Characteristics

Connor Creek, located in Knox County, Tennessee, was selected as the field site for investigating dynamic soil moisture–driven variations in streambank erosion processes **(Figure 5-1)**. The watershed drains an area of approximately 3.64 km² and is geographically situated at 35°56'15" N latitude and 84°11' W longitude. The creek exhibits a typical bankfull width of approximately 1.93 meters and an average reach slope of 0.007 m/m, representing a small, low-gradient stream.

The streambanks are primarily composed of silt loam, underlain by soil textures including gravelly loam, loamy sand, loam, and silty clay loam. The watershed is heavily urbanized, with 81.0% of the area characterized by impervious surfaces associated with residential, educational, and commercial developments, while 10.8% consist of pasture and 6.4% of mixed deciduous and evergreen forests. This urbanization has substantially disrupted the natural hydrologic cycle, reduced infiltration rates and increasing runoff volumes, leading to more frequent high-flow events and elevated shear stresses on the streambanks.

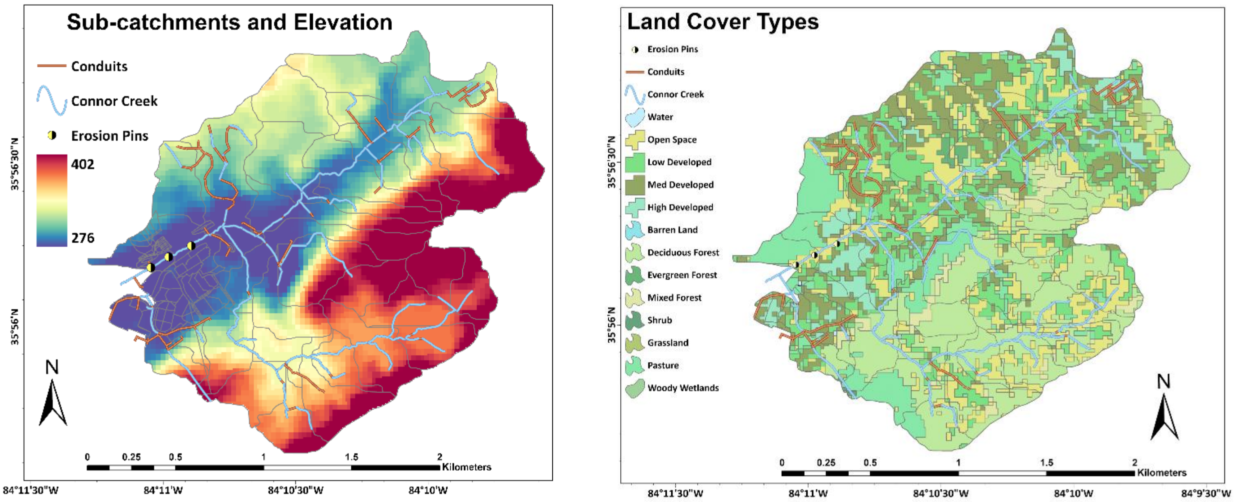

Figure 5-1 Location of bank erosions at the selected study site in Knoxville, Tennessee a. Elevation, and b. Land Cover.

Hydrological monitoring at a USGS field gauge has shown that Connor Creek exhibits highly variable hydrographs, with flow depths ranging from negligible baseflows during dry seasons to peaks of 1.62 meters during storm events, nearing bankfull conditions. Over the past five years, these flashy storms have resulted in documented cases of severe bank undercutting, mass wasting, and accelerated sediment detachment, particularly in urbanized sections of the creek. Field measurements documented seasonal variations in soil moisture (SM) at the study site, ranging from as low as 9.5% during extended dry periods to approximately 39% under saturated conditions. The strong contrasts in seasonal SM conditions, combined with urban-driven hydrological variability, directly support the study's objectives: to integrate dynamically varying critical shear stress (τ_c) and erodibility coefficient (K_d) estimates into the BSTEM framework, moving beyond conventional static parameter assumptions. Thus, Connor Creek serves as a natural laboratory for testing soil moisture–based dynamic erosion modeling strategies intended to enhance resilience planning under future hydrologic regimes.

Bank Erosion Sites

Three bank erosion sites have been selected at the Hardin Valley of Connor Creek, Knoxville, TN. After a thorough survey of the creek, erosion sites with tension cracks were identified. Using a measuring rod, three bank sites have been profiled using sub-sections across at a maximum interval of 1 ft **(Figure 5-2)**.

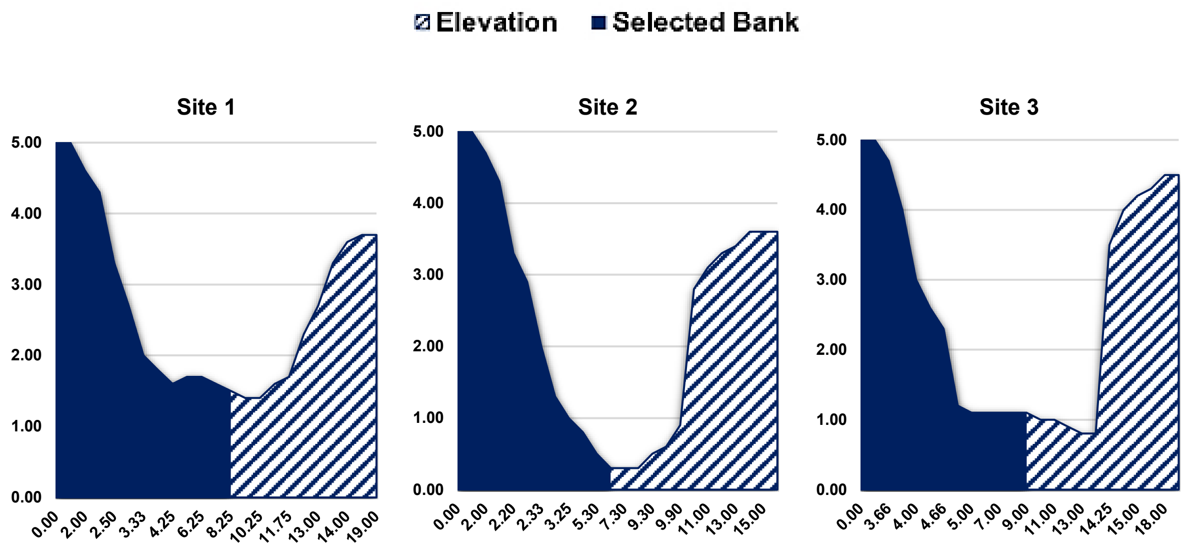

Figure 5-2 Bank and cross-section profiles for the selected sites.

5.2.2 Study Design

This study develops a dynamic erosion modeling framework by integrating soil moisture–based predictions of critical shear stress (τc) and erodibility coefficient (Kd) into the Bank Stability and Toe Erosion Model (BSTEM). In-situ Jet Erosion Tests (JETs) were conducted at 36 field locations to measure τc and Kd under varying soil moisture conditions, with estimates processed using the Blaisdell method. Soil moisture ranged from a residual content of 9.5% to saturation levels around 39%, allowing the capture of erosion behavior across realistic seasonal variability. Measurements were collected at 0.1–3.0% SM intervals to refine sensitivity to changes in hydrologic conditions. Relationships between SM, τ_c, and K_d were established based on seasonal field data collected at Connor Creek, TN (Chapter 4). The quadratic relationships derived from the plots of soil moisture dynamics with critical shear stress (τ_c) and erodibility coefficients (K_d) are:

$$\tau_c = 0.0002 \times SM^4 - 0.02 \times SM^3 - 0.75 \times SM^2 - 11.78 \times SM + 70 \quad (1)$$

$$K_d = -0.00004 \times SM^4 + 0.004 \times SM^3 - 0.14 \times SM^2 - 1.31 \times SM + 7.89 \quad (2)$$

Modifications will be made to the core model architecture of BSTEM to enable dynamic integration of soil moisture–based predictions for critical shear stress (τ_c) and erodibility coefficient (K_d), replacing conventional static parameterization. Specifically, quadratic relationships derived from empirical field data between soil moisture and erosion parameters will be embedded into the model's computational framework. To support this dynamic functionality, an additional soil moisture input column will be incorporated into the time-series worksheet of BSTEM, allowing real-time variation of τ_c and K_d during the simulation period. Custom coding adjustments will ensure the model reads and applies the evolving soil moisture conditions to update erosion resistance properties at each time step, enhancing the model's ability to capture seasonal and event-driven variability in streambank erosion processes.

A sensitivity analysis was performed by varying Manning's n for both the bank face and toe to evaluate how hydraulic roughness influences modeled lateral retreat under dynamic τ_c and K_d conditions. Manning's n values ranging from 0.025 to 0.065—consistent with literature-reported ranges for bare streambanks—were applied in the dynamic BSTEM simulations. The same range of Manning's n values was also used for simulations employing the default BSTEM configuration with static τc and Kd values derived from wet- and dry-season JET test measurements. Simulated total lateral retreat from each scenario was compared against field-observed retreat measurements at the Connor Creek study sites.

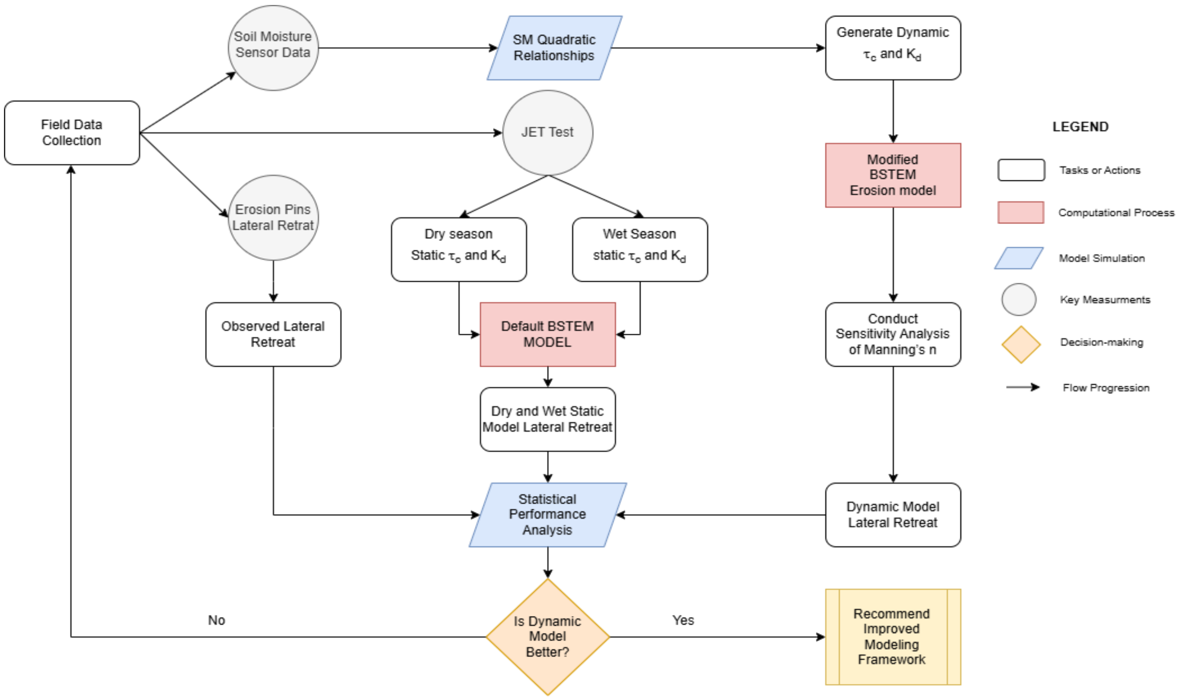

Figure 5-3 Methodology Flow Chart of the study.

The Manning's n range yielding the closest match to channel characteristics was selected for three modeling approaches as dynamic, Static A (Average WL condition- SM 17%), and Static B (High WL condition- SM 33%). For the Manning's n range, simulated lateral retreat rate (Lateral retreat per day, cm/day) over the selected periods of erosion transitions were extracted to evaluate whether the dynamic model captured seasonal erosion trends more accurately compared to static scenarios over a one-year period. Model performance was assessed using statistical metrics, including t-test and ANOVA, to quantify improvements associated with dynamic soil moisture–based modeling relative to conventional static approaches. This methodology is summarized in the workflow diagram **(Figure 5-3)**, providing a clear outline from field measurements to BSTEM dynamic modeling, sensitivity analysis, and validation against observed data.

5.2.3 Data Descriptions

To develop and simulate the dynamic version of the Bank Stability and Toe Erosion Model (BSTEM), a comprehensive dataset was compiled, encompassing bank geometry, soil materials, channel hydraulics, flow conditions, and erosion-resistance properties. **Table 5-1** summarizes the sources and nature of these input parameters. Bank geometry was obtained from detailed cross-section surveys using station-elevation readings with measuring rods, while the thickness and configuration of five soil layers were derived from in-field vertical profile measurements. Soil texture classifications for each layer were determined via hydrometer analysis conducted in the laboratory.

Table 5-1 Description of Input Data Sources for Dynamic Erosion Modeling

Data Type	**Description**	**Source**
Profile Cross-sections	Station and elevation with top of toe	Field survey with measuring rod
Bank Layer Thickness	Five (5) layers ending at base of bank toe	In-field Profile Measurement
Bank materials	Soil texture of five (5) layers	Hydrometer Laboratory Analysis
Water Flow (m^3/s)	Hourly	USGS Station and Field Gauge
Bank erosion	Three (3) Bank Sites	Erosion pin field monitoring
Soil Moisture	Three (3) Bank Sites	In-situ SM sensor network
Precipitation (mm)	Hourly	USGS Station 03535618
Temperature (°C)	Hourly	Oak Ridge Weather Station

Channel flow data was generated through simulations in the SWMM hydrologic model, calibrated using hourly streamflow records from USGS and field gauge stations. Critical shear stress (τc) and erodibility coefficient (Kd) values were not input as constants but computed dynamically from quadratic regression equations developed in Chapter 4, using time-series soil moisture data collected at three monitoring sites. These dynamic τc and Kd estimates were then applied across model time steps to reflect seasonal variability in bank resistance. Model performance was subsequently validated against in-field erosion pin measurements of lateral retreat collected between October 2023 and September 2024.

Soil Water Content

In this study, soil moisture sensors were installed at a depth of 3 feet at all three streambank erosion monitoring sites along Connor Creek. Measurements were collected continuously from October 2023 to September 2024, capturing seasonal soil moisture dynamics over a full annual cycle. The recorded soil water content is plotted in **Figure 5-4**, illustrating temporal variability across the sites. Values ranged from 0.10 m^3/m^3, representing the driest streambank conditions, to 0.39 m^3/m^3 under the wettest conditions. These measurements encompass the full range of field-observed moisture extremes and were used to parameterize the dynamic τc and Kd relationships integrated into the erosion modeling framework.

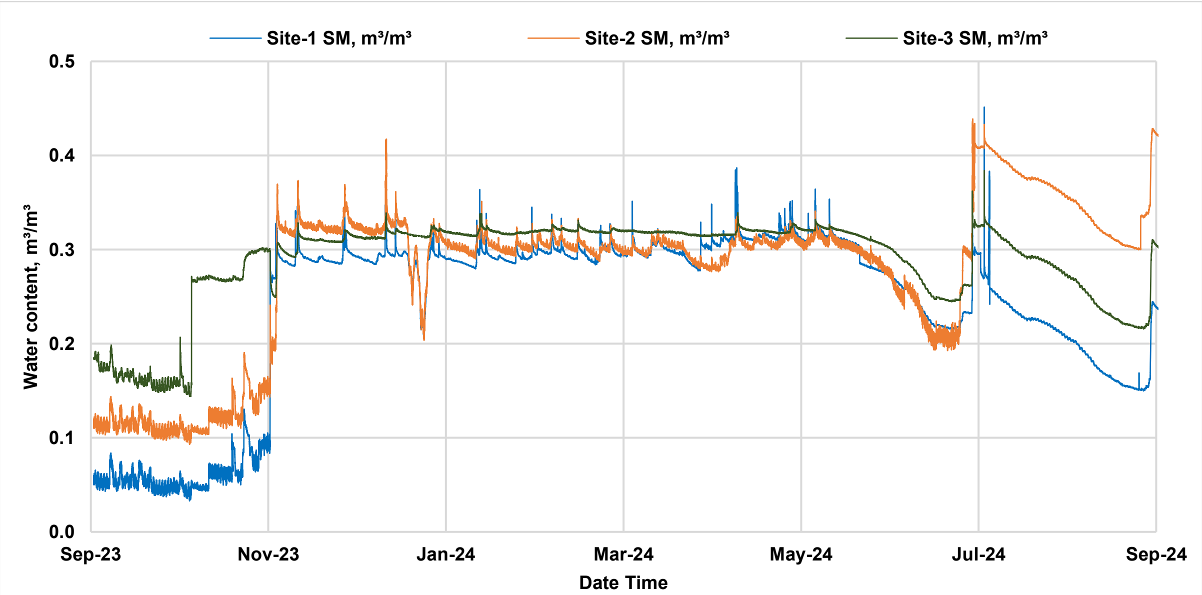

Figure 5-4 Soil water content of streambank sites at Connor Creek

Erosion Lateral Retreat

To quantify streambank erosion at the study locations, erosion monitoring was conducted using a network of three (3) steel erosion pins installed at the toe, face, and lip of each streambank site. The pins were embedded horizontally into the bank at benchmarked positions to serve as fixed references for measuring bank material loss over time. Initial measurements were recorded in June 2023, with subsequent readings collected periodically until September 2024. Because initial soil disturbance from pin installation may affect early readings, the first few months of data are typically excluded. Therefore, lateral retreat estimates were derived from changes observed between October 2023 and September 2024 **(Table 5-2)**.

The total lateral retreat at each site was assessed by comparing changes in exposed pin lengths from their original benchmark values. This data captured seasonal erosion trends across varying hydrological conditions and soil moisture scenarios and was used to validate both dynamic and static BSTEM simulations. The observed changes in lateral retreat over the one-year monitoring period are illustrated in **Figure 5-5**.

5.2.4 Erosion Model BSTEM

Multiple models are available for streambank erosion prediction, including CONCEPTS (Conservation Channel Evolution and Pollutant Transport System), CCHE2D, Delft3D, HEC-RAS, and BSTEM (Bank Stability and Toe Erosion Model) (Abdul-Kadir & Ariffin, 2012; Klavon et al., 2017b; Langendoen et al., 2001; Saha et al., 2019). Among these, BSTEM is particularly suited for this study due to its capability to simulate streambank erosion using coupled geotechnical and hydraulic processes, and more recently, its capacity to incorporate dynamic, time-series inputs.

Table 5-2 Description of the Bank sites

Erosion Sites	**Coordinates**		**Pin Benchmarks (In)**		
	Latitude	Longitude	Bank Toe	Bank Face	Bank Lip
1	35.937290	-84.181260	1.40	1.20	1.40
2	35.936730	-84.182690	1.70	1.10	1.00
3	35.936260	-84.183860	1.30	1.20	1.50

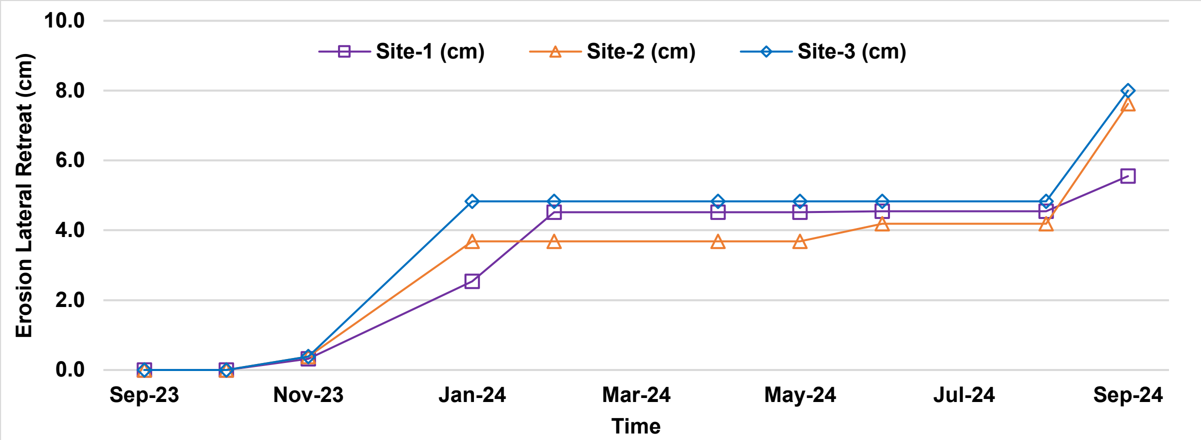

Figure 5-5 Temporal Trends of Streambank Lateral Retreat at Three Monitoring Sites

Modeling Framework

The BSTEM (Bank Stability and Toe Erosion Model) simulates streambank erosion by evaluating two primary processes: toe fluvial erosion and geotechnical mass failure **(Figure 5-6)**. These processes operate sequentially at each time step. At start of timestep, the model performs toe erosion of the streambank. The updated bank geometry is then used to compute the bank's stability via the factor of safety. If the bank is deemed unstable ($Fs < 1$), mass failure occurs, modifying the geometry. If the bank remains stable ($Fs \geq 1$), the model progresses to the next step. This iterative structure allows the model to dynamically simulate erosion over time, accounting for the interplay of fluvial and geotechnical processes and their feedback on bank geometry and resistance.

Parameter Initialization and Input Structure

In the default setup, critical shear stress (τc) and erodibility coefficient (Kd) are obtained from single-condition field Jet Erosion Tests (JETs). These values are assumed to remain constant throughout the simulation. In contrast, the dynamic configuration developed in this study derives τc and Kd from quadratic relationships with soil moisture, as established in the previous chapter. Time-series soil moisture measurements from field sensors are input into the model, and the derived equations dynamically update τ_c and K_d at each timestep. All other model inputs such as bank geometry, water level, flow data, and soil characteristics are derived from detailed field measurements. Bank geometry is determined from cross-sectional surveys, and the soil profile includes measurements of layer thickness, cohesion, and friction angle. Groundwater elevation and water level data are used to compute porewater pressures that influence both geotechnical stability and hydraulic erosion.

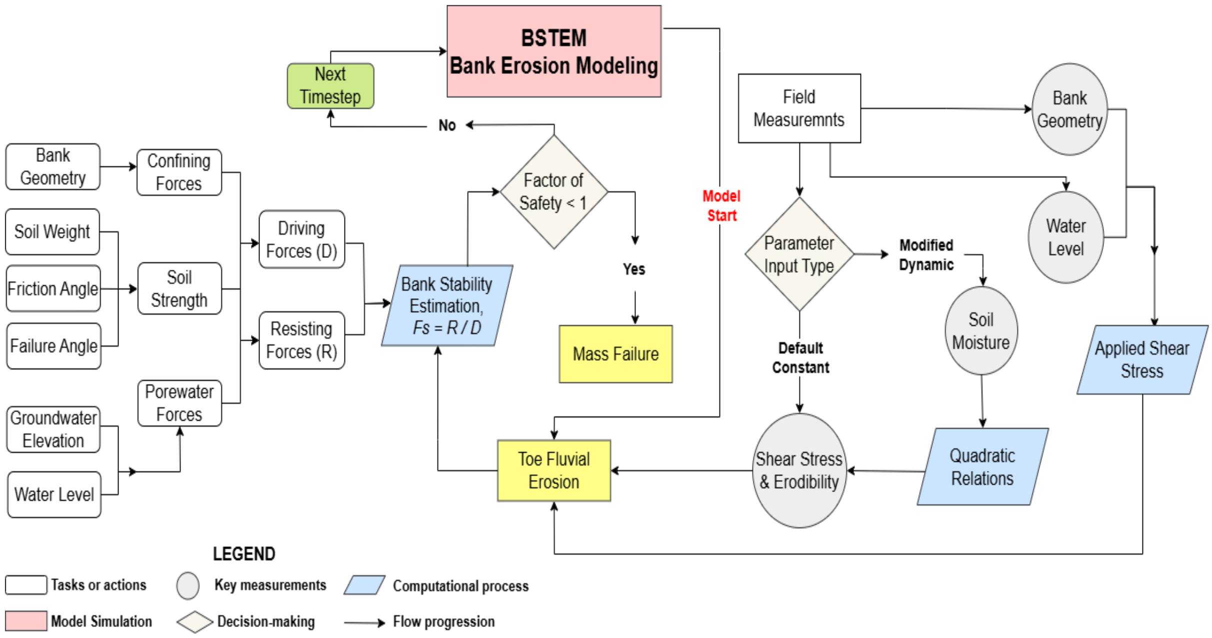

Figure 5-6 Dynamic BSTEM Erosion Model Schematics

Toe Fluvial Erosion Component

The fluvial erosion rate (ER) at the toe of the bank is estimated using the relationship:

$$ER = Kd * (\tau - \tau_c) \tag{3}$$

where τ is the applied shear stress, τc is the critical shear stress, and Kd is the erodibility coefficient.

The applied shear stress is computed as:

$$\tau = \frac{\gamma \times A \times S}{P} \tag{4}$$

where γ is the unit weight of water (9807 N/m³), A is the cross-sectional flow area, S is the channel slope, and P is the wetted perimeter. Once the erosion rate is computed, the erosion distance (ED) over a time step Δt is given by:

$$ED = ER * \Delta t \tag{5}$$

Bank Stability and Mass Failure Module

Once the bank toe has been eroded, BSTEM evaluates the stability of the bank using a factor of safety (Fs) based on limit equilibrium methods. Mass failure is predicted when Fs < 1.

The factor of safety is calculated as:

$$F_s = \frac{R}{D} \tag{6}$$

where R is the resisting force and D is the driving force. The resisting force includes soil shear strength and reduction due to porewater pressure:

$$R = \Sigma\,[Weight * Cos(\theta) * Tan(\varphi) - Porewater\ Force] \tag{7}$$

Driving forces incorporate gravitational forces acting on the bank geometry and confining angles:

$$D = \Sigma\,[\text{Weight} * \text{Sin}(\theta) - \text{Confining Force} * \text{Sin}(\alpha - \theta)] \tag{8}$$

Here, θ is the failure plane angle, φ is the internal friction angle, α is the confining force angle, and Weight is the self-weight of soil acting on the failure plane.

Confining Forces

Confining Force accounts for horizontal resistance acting against failure along the plane. In saturated soil conditions, the confining force is primarily hydrostatic and is calculated as:

$$F_c = \gamma_w \times h_w \times A \tag{9}$$

Here, γ_w = unit weight of water (9.807 kN/m^3), h_w = depth of water acting laterally (e.g., stream level relative to failure surface), A = area of the confining surface exposed to water pressure.

Porewater Forces

In the unsaturated ("vadose") zone, the porewater pressure is estimated by capillarity, referred to as matric pressure, suction or tension. Porewater pressure (μ_w) is calculated at the center of each soil layer based on static water pressure below the groundwater table as

$$\mu_w = \gamma_w \times h \tag{10}$$

Here μ_w, h and γ_w are porewater pressure (kPa), head of water (m) and unit weight of water (9.807 kN/m^3).

$$PWF = -9.807 \times [GW - (LTE - 0.5 \times (LTE - LBE)] \tag{11}$$

Here, LTE, LBE are Layer top and Bottom elevations of soil, and GW is the groundwater level.

Groundwater Elevation

Groundwater elevation is estimated using modified Richard's 1D infiltration equation considering two scenarios. When groundwater is the maximum elevation considering stream level,

$$GW = Min\ Elev. - \frac{(2 \times Seepage + 1) \times (MaxElev. - MinElev.)}{1 + \Delta t \times Ks \times SAT \times (MaxElev. - MinElev.)} \tag{12}$$

If the estimated groundwater is less than the minimum elevation and seepage is false,

$$GW = Min\,Elevation \tag{13}$$

When Groundwater is not at the maximum elevation considering stream level,

$$GW = Max\,Elev. - \frac{(2 \times Seepage + 1) \times (MaxElev. - MinElev.)}{1 + \Delta t \times Ks \times SAT \times (MaxElev. - MinElev.)} \tag{14}$$

If the estimated GW is greater than the maximum elevation and seepage is true,

$$GW = Max\,Elevation \tag{15}$$

Here, K_s = Saturated Hydraulic conductivity, SAT= Saturation coefficient and Seepage is -1 for True and 0 for false scenarios.

Limit Equilibrium Failure Modes

BSTEM integrates two equilibrium failure modes: horizontal layering and cantilever collapse. For horizontal layers, the factor of safety is calculated using the equation:

$$F_s = \frac{\sum_{i=1}^{I}\left(c_i' L_i + (\mu_a - \mu_w)_i L_i \tan\varphi_i^b + [W_i \cos\beta - \mu_{ai} L_i + P_i \cos(\alpha - \beta)] \tan\varphi_i'\right)}{\sum_{i=1}^{I}(W_i \sin\beta - P_i \sin[\alpha - \beta])} \tag{16}$$

where c' is effective cohesion, L is failure plane length, μa and μw are pore-air and pore-water pressures, φb is the unsaturated friction angle, W is soil weight, P is hydrostatic pressure, and β and α are slope angles. For cantilever failures, where b = 90°, the factor of safety becomes:

$$F_s = \frac{\sum_{i=1}^{I}\left(c_i' L_i + (\mu_a - \mu_w)_i L_i \tan\varphi_i^b + [P_i \sin\alpha - \mu_{ai} L_i] \tan\varphi_i'\right)}{\sum_{i=1}^{I}(W_i + P_i \cos\alpha)} \tag{17}$$

Failure Volume Estimation

The lateral retreat of the streambank is calculated as:

$$\text{LR} = \text{Current Geometry X} - \text{Initial Geometry X} \tag{18}$$

Finally, the erosion volume is estimated to understand the total volume of soil loss from the banks using the equation:

$$E_v = (X * Z) * ED \tag{19}$$

where (X * Z) represents the eroded cross-sectional area of the bank estimated from the current geometry.

5.2.5 Hydrological Model SWMM

Multiple hydrological models are available for simulating flow scenarios at watershed and local scales, including SWMM, VIC, HEC-HMS, and Arc-SWAT (Ghaneeizad et al., 2018; Saha et al., 2019). For this study, the Storm Water Management Model (PCSWMM 5.0.0.13) was selected due to its widespread acceptance in urban watershed modeling and its ability to represent complex hydraulic systems. Stream cross-section transects and node elevations were updated based on detailed field surveys to ensure geometric accuracy. Each sub-catchment was delineated and updated with observed land cover, including impervious surfaces from urban development.

The SWMM model was configured to use the dynamic wave routing method, which solves the full Saint-Venant equations to simulate unsteady flow conditions with high accuracy (Rossman, 2006). For infiltration, the modified Green-Ampt method was adopted to better represent initial abstraction and variable infiltration capacity during low-intensity rainfall events (Nye & Heineman, 2016). The model was calibrated using observed streamflow data at a downstream gauge to replicate the existing flow regime. Simulated outputs from SWMM—specifically, streamflow elevations—were extracted at the three bank erosion sites and used as hydrologic input for erosion modeling throughout the year.

5.2.6 Statistical Assessment of the Modified Model

To evaluate the predictive performance of the modified erosion model, a statistical comparison is conducted between observed and simulated lateral retreat values across three field sites. Four standard statistical metrics are employed to assess model prediction accuracy as Coefficient of Determination (R^2), Root Mean Square Error (RMSE), Mean Absolute Error (MAE), and Nash–Sutcliffe Efficiency (NSE). These metrics were chosen to capture both the accuracy of the predicted magnitude and the fidelity of the temporal erosion patterns relative to field observations.

Coefficient of Determination (R^2)

Coefficient of Determination (R^2) is estimated from the squared Pearson correlation coefficient, quantifies the degree of linear association between modeled and observed values

$$R^2 = \left[\frac{\sum_{i=1}^{n}(y_i - \bar{y})\,(x_i - \bar{x})}{\sqrt{\sum_{i=1}^{n}(y_i - \bar{y})^2} \cdot \sqrt{\sum_{i=1}^{n}(x_i - \bar{x})^2}}\right]^2 \tag{20}$$

Root Mean Square Error (RMSE)

Root Mean Square Error (RMSE) evaluates the typical magnitude of prediction error, with greater weight on larger deviations.

$$RMSE = \sqrt{\frac{1}{n}\sum_{i=1}^{n}(y^i - x^i)^2} \tag{21}$$

Mean Absolute Error (MAE)

Mean Absolute Error (MAE) captures the average absolute difference between modeled and observed values, giving equal weight to all errors.

$$MAE = \frac{1}{n}\sum_{i=1}^{n}\left|y^i - x^i\right| \tag{22}$$

Nash-Sutcliffe Efficiency (NSE)

Nash-Sutcliffe Efficiency (NSE) indicates the relative magnitude of residual variance compared to observed data variance. Values closer to 1 suggest better model performance.

$$NSE = 1 - \frac{\sum_{i=1}^{n}(y^i - x^i)^2}{\sum_{i=1}^{n}(y^i - \bar{y})^2} \tag{23}$$

Here, x is the predicted data, y is the observed data, n is the total number of events observed. These performance metrics are calculated at selected time events reflecting meaningful changes in erosion behavior, to more effectively capture the models' ability to predict both the magnitude and timing of erosion events. for a robust evaluation of model realism under variable soil moisture and flow conditions.

5.3 RESULTS

5.3.1 SWMM Model Outputs

Model Outputs

The hydrological model SWMM is calibrated from 01 Jan-30 June 2021 with a time step of 5 minutes **(Figure 5-7)**. The calibration uncertain parameters used in the model are sub-catchment width (ft), imperviousness (%), storage imperviousness (%), storage perviousness (%) and zero imperviousness (%). The model is calibrated with the observation point of the flow gauge downstream. The model calibration shows NSE of 0.57 and correlation coefficient (R) of 0.78.

Model Flow depths

Time-series flow depths were derived for each erosion location using the calibrated SWMM model. These depths serve as essential hydrodynamic input data for estimating erosion along the streambanks in BSTEM model. **Figure 5-8** illustrates the modeled water depths across three erosion sites from October 2023 through September 2024. The site-1 shows frequent and intense inflow events throughout the winter and early spring months, with depths often exceeding 0.8 m, suggesting a flashy hydrologic response. Site-2 exhibits a similar seasonal pattern, though with slightly weakened peaks. Meanwhile, Site-3 shows greater variability in flow depth, with notable peaks not only in late fall and early spring but also during late summer, possibly linked to convective storm activity.

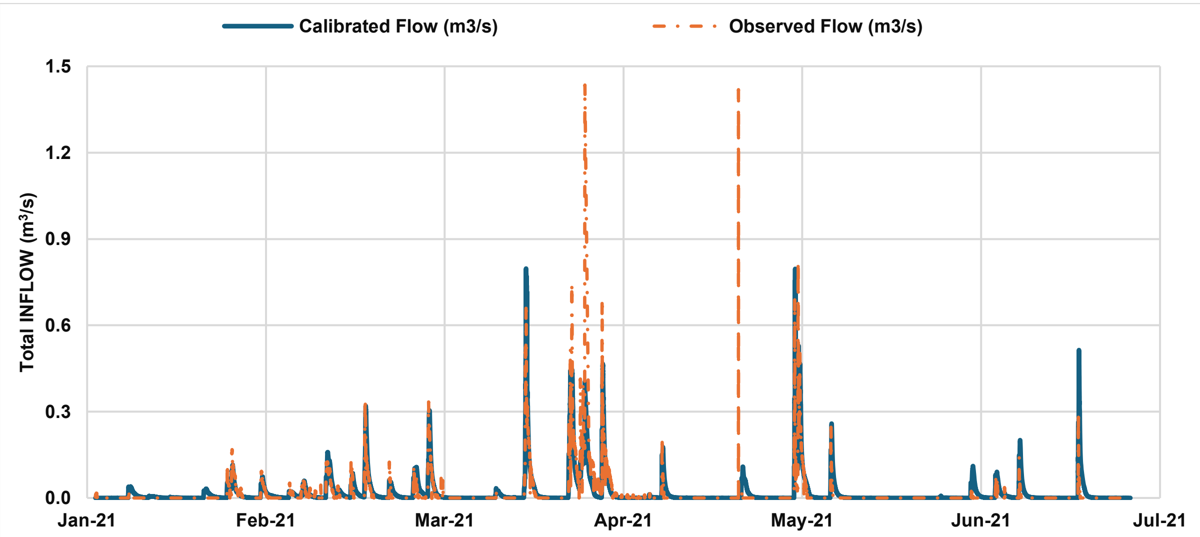

Figure 5-7 Calibration of flow downstream of Connor Creek watershed

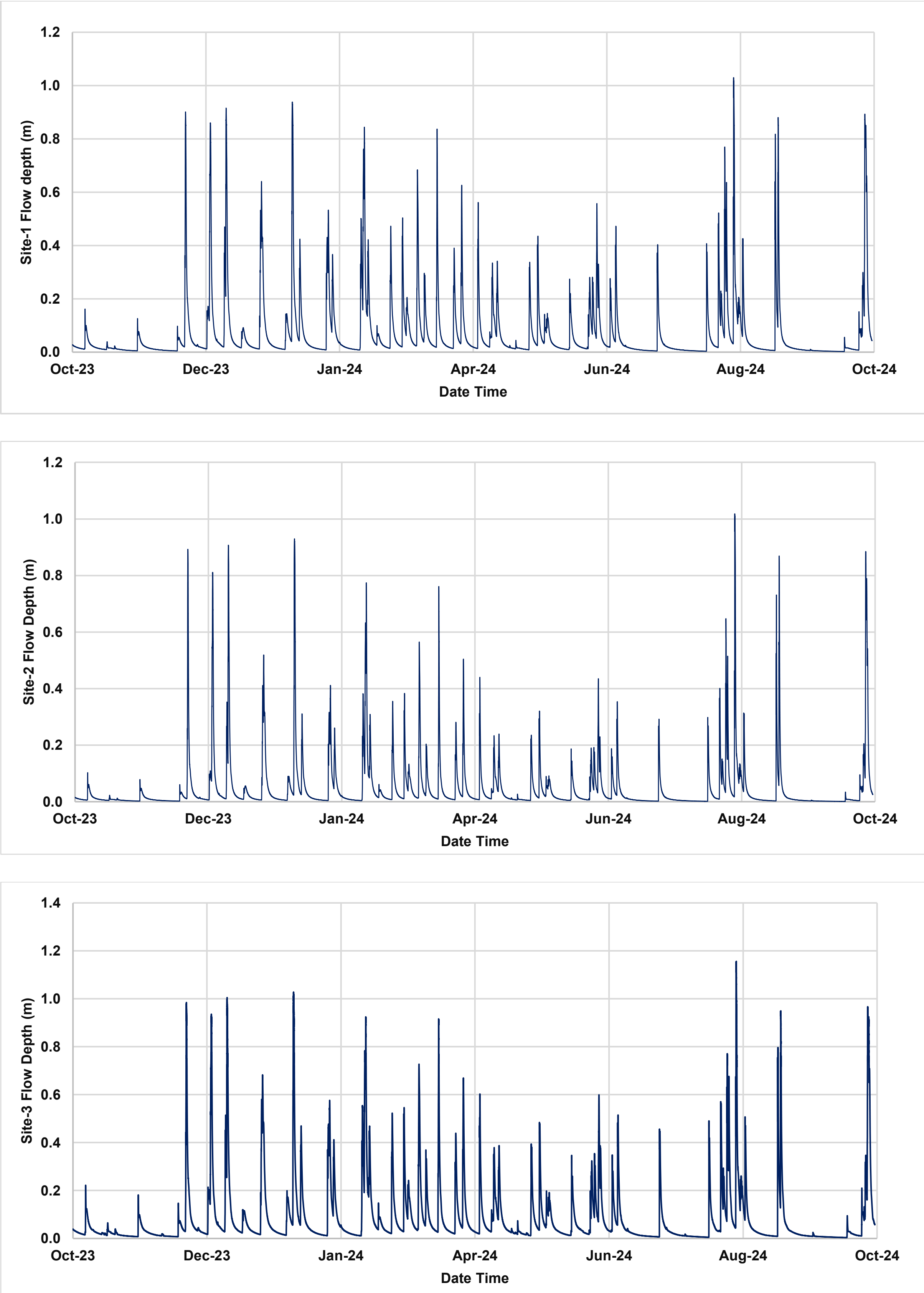

Figure 5-8 SWMM Model derived flow depths at each bank erosion sites

5.3.2 Impact of Roughness in Erosion Retreat

To evaluate the sensitivity of erosion predictions to hydraulic roughness, simulations were conducted at three field sites across a range of Manning's n values (0.025 to 0.065) **(Figure 5-9)**. Lateral retreats (LR) were estimated in BSTEM using three modeling approaches: (i) Dynamic, with soil moisture-responsive τ_c and K_d; (ii) Wet Static, using constant parameters under wet conditions (τ_c = 0.58 Pa, K_d = 3.52 cm^3/N-s); and (iii) Dry Static, using dry condition values (τ_c = 1.41 Pa, K_d = 6.03 cm^3/N-s). Across all three study sites, modeled lateral retreat (LR) exhibited a consistent inverse relationship with Manning's n, though the degree of sensitivity varied by site and model configuration. This variation is influenced by several site-specific characteristics, including differences in streambank geometry, stream elevation, and the range of soil moisture dynamics at each location. For instance, Site-1 has a moderately steep and concave bank profile with a mid-range toe elevation, where erosion is concentrated in a vertical zone, explaining the requirement of mid-range roughness value. Site-2 presents the steepest bank with a sharp toe and high bank height, making it more susceptible to concentrated shear stress and overprediction at low roughness values. Site-3 features a gently sloped and wide bank, distributing flow energy more evenly and leading to smoother and consistent retreat responses across Manning's n values.

These geometric differences shape how flow interacts with bank materials, influencing the effectiveness of erosion resistance parameters. On the context of erosion parameters, the dry static model, characterized by low τ_c and K_d, requires lower n values to maintain sufficient boundary shear stress and match observed retreat. In contrast, the wet static model, with higher τ_c and K_d, necessitates higher n values to suppress flow energy and mitigate overestimation caused by its greater erodibility. The dynamic model showed more consistent and stable behavior across the roughness range by adjusting τ_c and K_d in response to level of soil moisture variations, reducing reliance on n compensation. These findings emphasize that while modeled retreat decreases with increasing roughness, the scale and sensitivity of this response depend on how flow dynamics interact with site-specific geometry and parameter variability, highlighting the utility of dynamic modeling for improving predictive confidence.

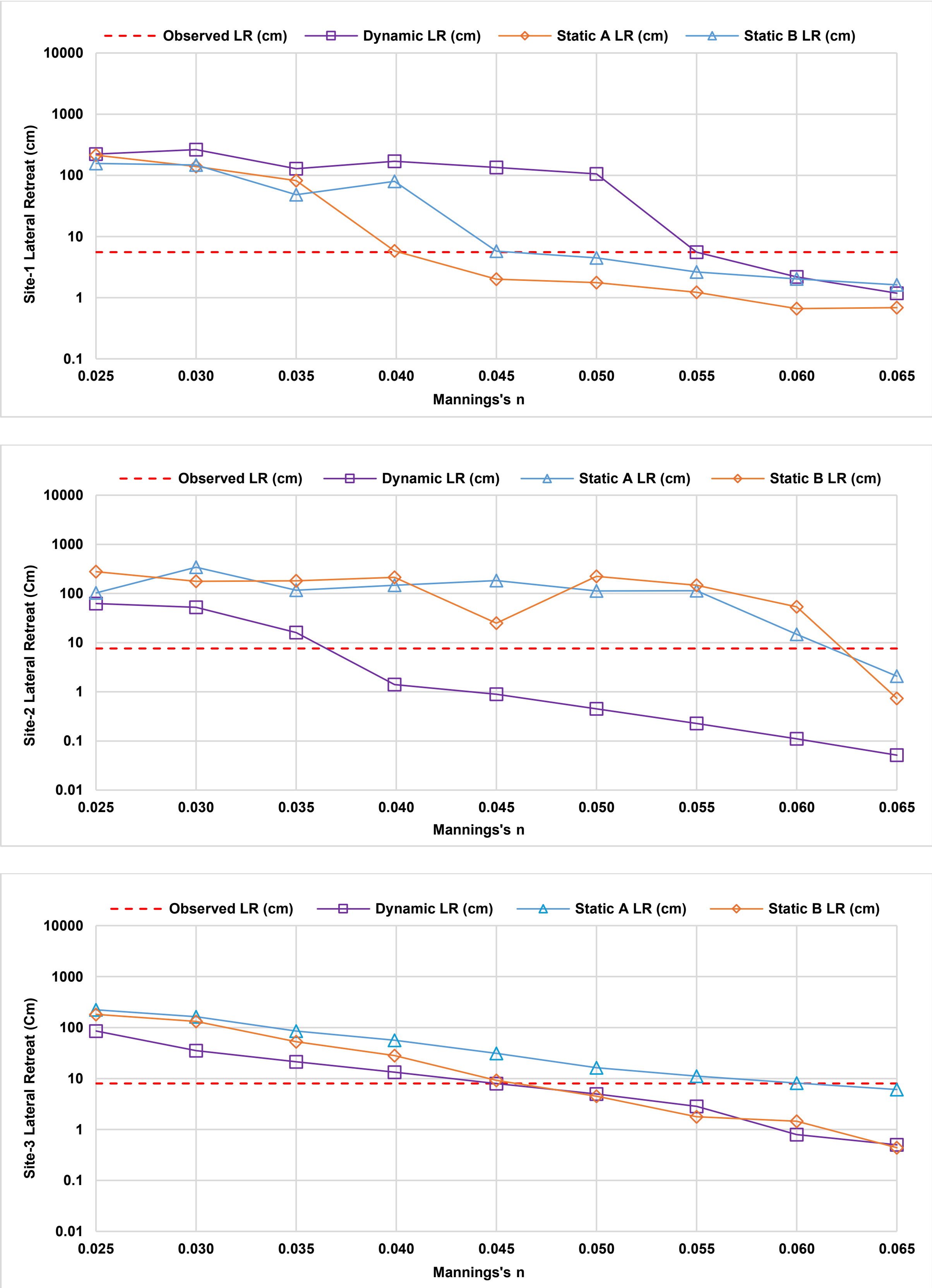

Figure 5-9 Modeled lateral retreat sensitivity to manning's n under dynamic and static soil moisture conditions at three streambank erosion sites

5.3.3 Impact of Soil Moisture on Temporal Erosion Prediction

To evaluate the accuracy of temporal erosion prediction, three modeling scenarios as dynamic, Static A (Average WL condition), and Static B (High WL condition), were assessed using field-observed lateral retreat at three sites over a one-year period **(Table 5-3)**. These scenarios were compared at three different Manning's n values (0.045, 0.050, 0.055), selected based on typical roughness values for channel characteristics as earth, winding, stones, and weeds (Chow, 1959). This assessment explores how dynamic and static values of τ_c and K_d affect erosion prediction accuracy across varying hydrologic and roughness conditions.

At Site-1 **(Figure 5-10)**, the dynamic model at Manning's n = 0.055 demonstrated the best agreement with observed retreat rates across all erosion transitions, supported by the highest NSE (0.91), lowest RMSE (0.61 cm), and MAE (0.40 cm), indicating minimal error and strong alignment with observed erosion behavior. At n = 0.045 and 0.050, although the dynamic model consistently overpredicted total retreat, it captured the initial and late season sharp erosion transitions at the correct timing. The static A model underestimated erosion during drier months during the initial erosion transition, while the static B model consistently underpredicted during all period of erosion transitions. At Site-2 **(Figure 5-11)**, none of the modeling approaches accurately replicated observed retreat across all three erosion periods, but the static B model at Manning's n = 0.055 showed the relatively best performance (COD = 0.81), though NSE remained negative (–0.76), reflecting poor temporal prediction overall. All models captured the early erosion event, but the dynamic model failed to reproduce the magnitude and underpredicted at high Manning's n range. Model performance at Site-2 remained weak across the accepted n values, and the closest match occurred at n ≈ 0.035, which falls outside the expected range for the site's channel characteristics. At Site-3 **(Figure 5-12)**, the dynamic model at n = 0.045 provided the most accurate timing and magnitude match across erosion phases, supported by the highest NSE (0.96) and lowest RMSE (0.50 cm) and MAE (0.29 cm) among all models. All models captured the initial retreat surge, but only the dynamic and static A tracked the rate of change closely. In the final period, the dynamic model produced a second erosion peak, while the static models failed to match the response accurately.

Table 5-3 Statistical comparison between observed and modeled lateral retreat rates across different Manning's n scenarios and modeling approaches.

Sites	Tests	Dynamic (0.045)	Static A (0.045)	Static B (0.045)	Dynamic (0.050)	Static A (0.05)	Static B (0.05)	Dynamic (0.055)	Static A (0.055)	Static B (0.055)
1	COD (r^2)	0.87	0.92	0.91	0.76	0.97	0.94	0.95	0.97	0.93
	RMSE (cm)	72.40	0.63	2.03	54.02	0.89	2.27	0.61	1.68	2.69
	MAE (cm)	56.35	0.42	1.63	39.27	0.70	1.83	0.40	1.34	2.20
	NSE	-1272.46	0.90	0.00	-708.03	0.81	-0.25	0.91	0.32	-0.75
2	COD (r^2)	0.77	0.84	0.68	0.74	0.80	0.64	0.70	0.50	0.81
	RMSE (cm)	3.28	56.91	5.69	3.55	50.15	82.24	3.69	33.63	61.92
	MAE (cm)	2.60	39.50	2.53	2.84	36.20	47.37	2.97	12.18	43.85
	NSE	-1.12	-638.24	-5.38	-1.49	-495.42	-1334.02	-1.69	-222.32	-755.89
3	COD (r^2)	0.96	0.81	0.90	0.84	0.93	0.76	0.94	0.91	0.77
	RMSE (cm)	0.50	10.60	1.15	2.47	0.71	3.91	3.16	1.90	3.58
	MAE (cm)	0.29	7.66	0.87	2.06	0.51	3.24	2.61	1.50	2.93
	NSE	0.96	-16.45	0.80	0.05	0.92	-1.38	-0.55	0.44	-0.99

In summary, the dynamic model showed superior capability in replicating erosion transitions, particularly during the early (Dec'23–Jan'24) and late (Aug–Sep'24) erosion periods. This was most evident at Site-1, where dynamic predictions aligned closely with observed retreat rates and timing, especially at Manning's n = 0.055. In contrast, Site-2 did not exhibit improved performance under the dynamic formulation since the closest match occurred near n = 0.035, which falls outside the expected range for the site's channel characteristics, limiting its validity. Static scenarios also performed poorly within the accepted roughness range, particularly in representing cumulative retreat, indicating a better calibration of the roughness. At Site-3, dynamic modeling at n = 0.045 yielded better agreement than statics, accurately capturing early erosion rise and maintaining reasonable estimates through drier conditions. Overall, the findings support that dynamic modeling improves temporal erosion prediction, but the benefit is maximized only when paired with appropriate hydraulic roughness values calibrated to site-specific conditions.

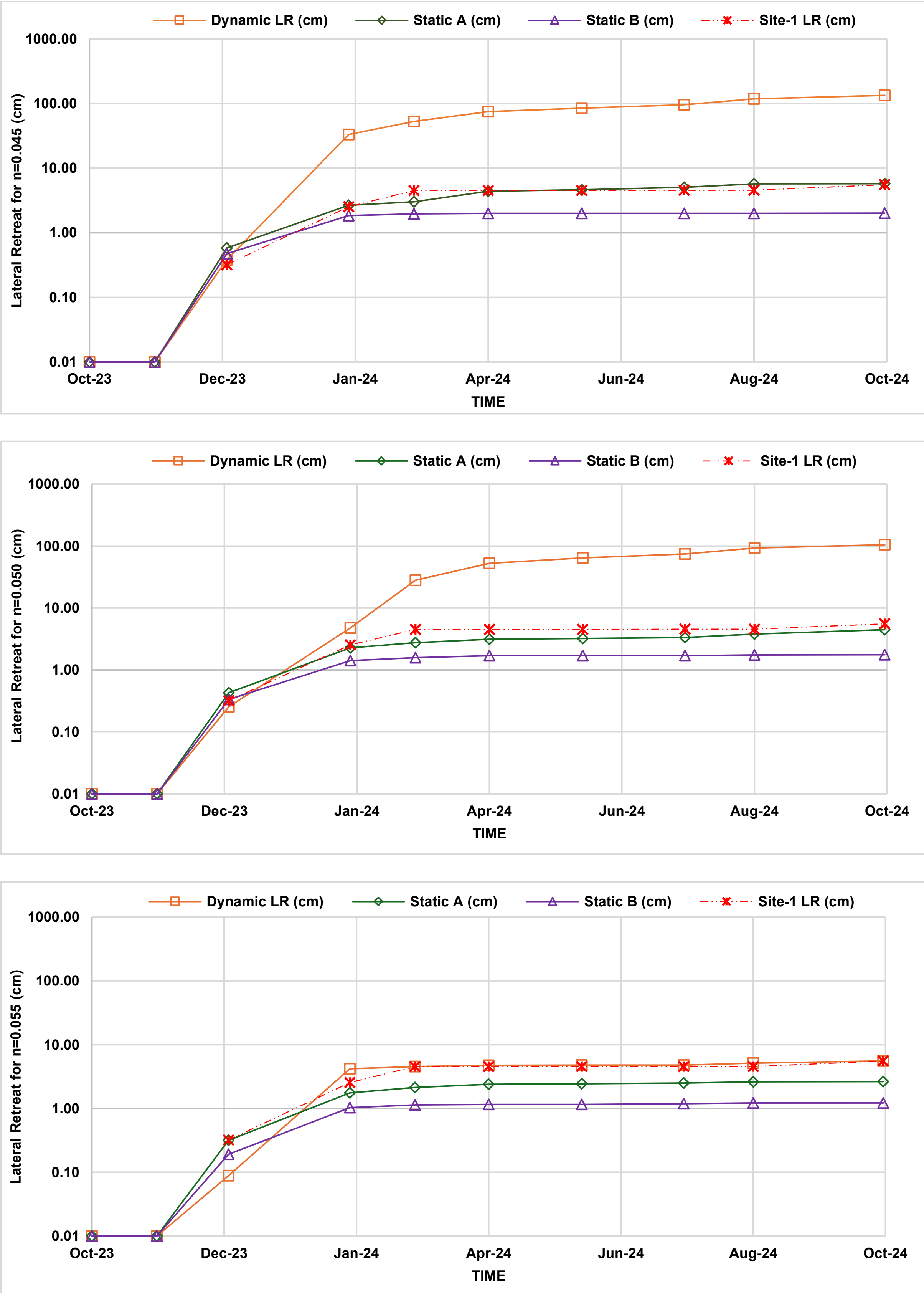

Figure 5-10 Comparison of modeled and observed cumulative lateral retreat at Site-1 under dynamic, Static A, and Static B scenarios at Manning's n = 0.045, 0.050, and 0.055.

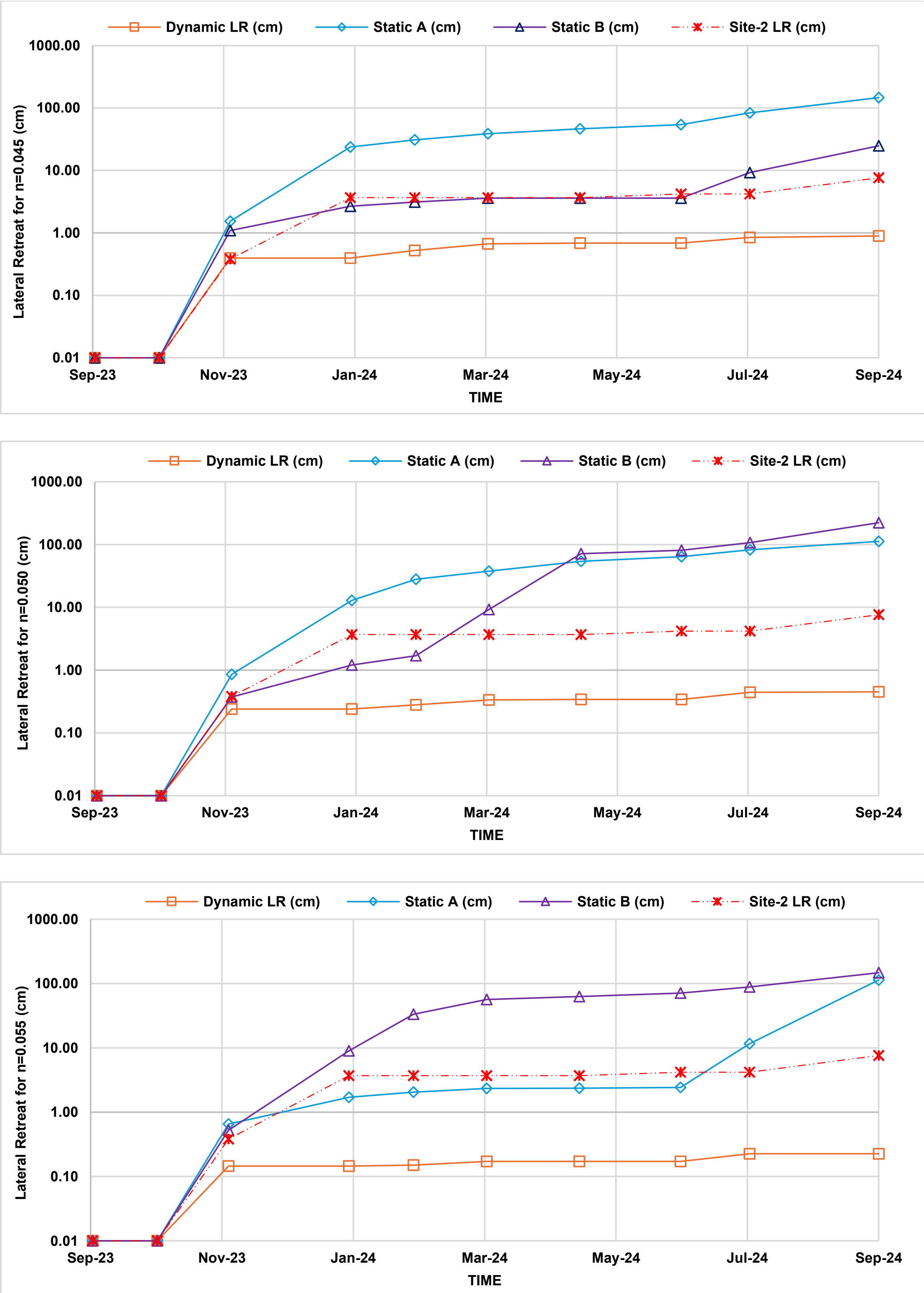

Figure 5-11 Comparison of modeled and observed cumulative lateral retreat at Site-2 under dynamic, Static A, and Static B scenarios at Manning's n = 0.045, 0.050, and 0.055.

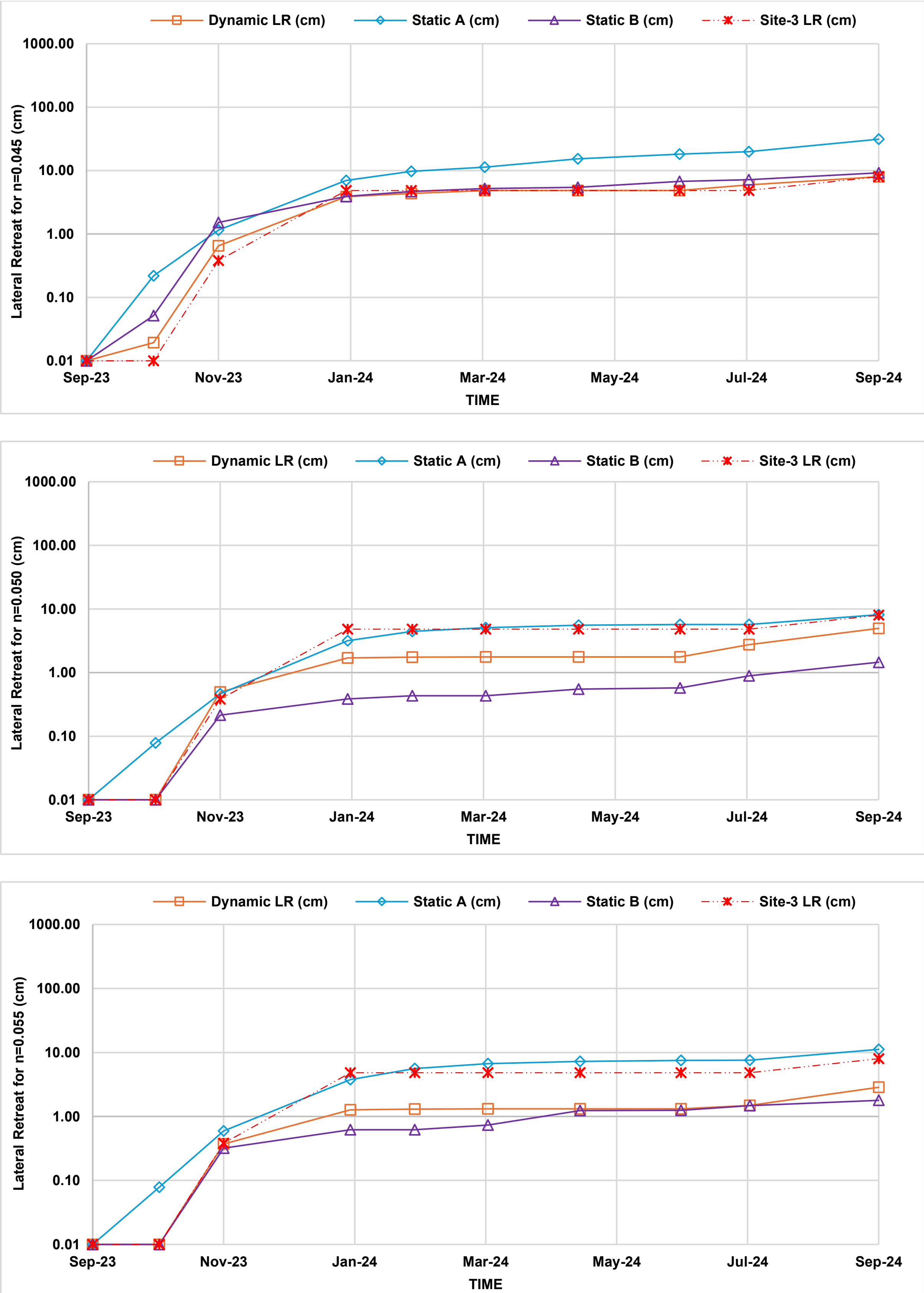

Figure 5-12 Comparison of modeled and observed cumulative lateral retreat at Site-3 under dynamic, Static A, and Static B scenarios at Manning's n = 0.045, 0.050, and 0.055.

5.3.4 Performance Assessment of Modified Model

To evaluate temporal prediction accuracy, modeled lateral retreat for three scenarios—dynamic, static B, and static A, based on $\tau_{c,}$ and K_d parameterization was compared to field-measured values over a one-year period **(Figure 5-13)**. At Site-1, the dynamic model closely tracked the observed retreat pattern, particularly capturing both early (Dec 2023–Jan 2024) and late (Aug–Oct 2024) erosion peaks. While the Static B model approximated the trend during the early phase, it slightly underpredicted the final months. The Static A model consistently underperformed, underestimating throughout the year. These trends are consistent with the statistical performance metrics, where the dynamic model yielded the highest accuracy (R^2 = 0.95; RMSE = 0.57 cm; NSE = 0.92), confirming its ability to respond to transitional soil moisture conditions. At Site-2, none of the models performed reasonably. While the Static B model had a relatively better statistical match (R^2 = 0.77; NSE = 0.47), all models failed to replicate the magnitude of the early erosion peak and underestimated the sharp retreat rise near the end. The dynamic model notably underpredicted erosion from January through September 2024 and only approached the observed values in October. This mismatch in both timing and magnitude is evident in the lower NSE (0.36) and R^2 (0.66), indicating limited responsiveness of the model under site-specific conditions. At Site-3, all models successfully captured the initial retreat surge (Nov–Jan), followed by a stabilization phase and eventual late-season increase. The dynamic model remained the most balanced, with the lowest MAE (0.30 cm) and highest NSE (0.96). Static models closely tracked the general pattern but both models slightly overpredicted during the final phase.

In summary, the dynamic model incorporating time-varying $\tau_{c,}$ and K_d based on soil moisture provided the best temporal accuracy at Site-1 and Site-3 by capturing both the magnitude and timing of key erosion transitions **(Table 5-4)**. At Site-2, all scenarios demonstrated difficulty in reproducing observed erosion transitions. Model performance varied by site, and while static models could approximate total retreat under specific conditions, they were less consistent in capturing the observed progression of erosion over time. These results underscore the importance of incorporating soil moisture variability in erosion modeling when temporal dynamics are critical.

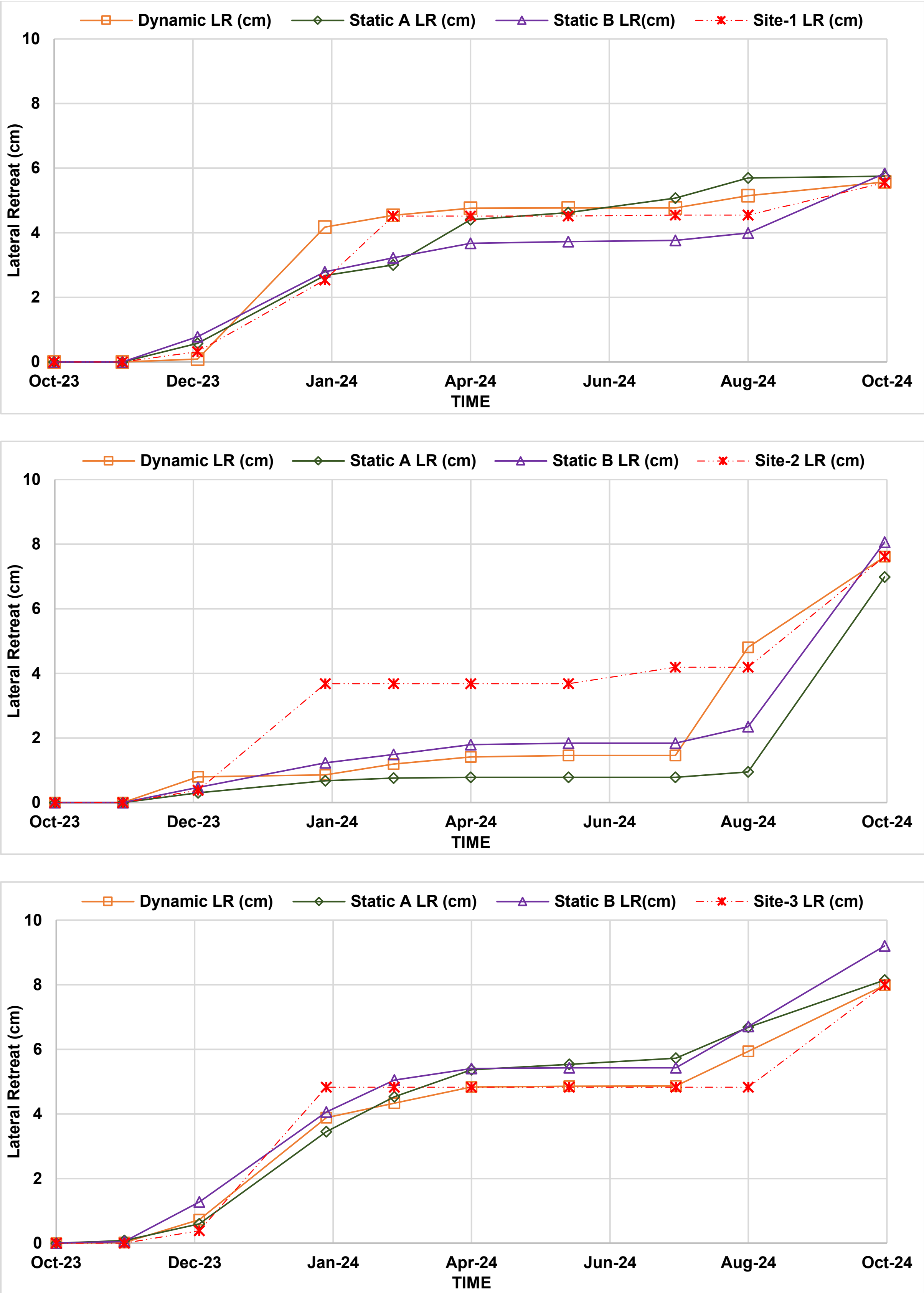

Figure 5-13 Time-series comparison of modeled and observed lateral retreat under dynamic, wet static, and dry static τ_c–K_d conditions

Table 5-4 Performance metrics of static and dynamic erosion models based on observed lateral retreat events

Sites	Scenarios	R^2	RMSE (cm)	MAE (cm)	NSE
Site-1	Dynamic	0.95	0.57	0.32	0.92
	Static A	0.92	0.64	0.40	0.91
	Static B	0.93	0.66	0.53	0.90
Site-2	Dynamic	0.66	1.80	1.36	0.36
	Static A	0.60	2.39	1.91	-0.12
	Static B	0.77	1.64	1.31	0.47
Site-3	Dynamic	0.96	0.50	0.30	0.96
	Static A	0.92	0.84	0.61	0.89
	Static B	0.95	0.86	0.68	0.88

5.4 DISCUSSIONS

Across all three study sites, Manning's n exhibited a strong inverse relationship with predicted lateral retreat, with model outputs varying by over 200 cm as hydraulic roughness increased from 0.025 to 0.065. This degree of variability was consistent across both dynamic and static τ_c–K_d scenarios, confirming that manning's n is a dominant control in erosion modeling uncertainty, particularly when field-calibrated values are unavailable. To better understand the statement, when a total Manning's n is specified in BSTEM, the model internally estimates the grain roughness component (n_g) using Strickler's equation for individual soil grain size (Chow, 1959) and adjusts the effective boundary shear stress using $n_g = n_0\ (n_g^2 / n^2)$. This correction isolates the grain-scale roughness contribution, allowing the model to more accurately compute the effective boundary shear stress acting on the bank surface. As a result, the sensitivity analysis revealed that even small changes in Manning's n directly alter the distribution of shear stress, and lead to large differences in predicted lateral retreat across all sites, highlighting how roughness directly governs erosion potential. While the models were run across a range of Manning's n values, this was done intentionally to evaluate how sensitive lateral retreat predictions are to hydraulic roughness under both static and dynamic τ_c–K_d configurations. This approach provides insight into how different scenarios with variable resistance approach interact with channel roughness to affect retreat estimates.

Soil moisture dynamics may have played a critical role in influencing the timing and intensity of observed lateral retreat across all sites. During early retreat at Site-1 (Dec'23–Jan'24), a rapid rise in soil moisture matched the sharp erosion that only the dynamic model captured at a closer time to the observed. Through the mid-period (Feb–Jul'24), soil moisture declined rapidly and raised again, requiring parameter flexibility that static models could not accommodate. In the late season (Aug–Sep'24), as moisture dropped again, the dynamic model captured the corresponding change in retreat magnitude, aligning closely with observations. At Site-2, during the early erosion spike (Dec'23–Jan'24), soil moisture increased sharply and could have triggered a surge in retreat, which all model failed to account. However, in the mid-season (Feb–Jul'24), soil moisture sharply declined and then rose again, and static models A and B underpredicted retreat due to their reliance on constant τ_c and K_d values unrepresentative of such transitions. In the late season (Aug–Sep'24), when moisture rose again, dynamic model best captured the observed erosion response. At Site-3, during the initial erosion event (Dec'23–Jan'24), soil moisture rapidly rose from 0.20 to over 0.30 m^3/m^3, corresponding to an erosion peak. Through the mid-period (Feb–Jul'24), as soil moisture declined slightly and remained stable, both Static models overpredicted retreat due to fixed resistance parameters. Finally, in the late season (Aug–Sep'24), when soil moisture rebounded, the dynamic model responded with a second erosion peak accurately, underscoring the need to simulate real-time moisture variability.

Significant variability in lateral retreat sensitivity across sites could also likely due to differing bank geometry characteristics such as slope angle, bank height, and concavity. Previous studies have documented that steeper and higher banks generate higher stress concentrations near the bank toe, intensifying erosion at these critical locations (Midgley et al., 2012; Rinaldi & Darby, 2007). For example, Site-3 exhibited pronounced sensitivity due to its steeper geometry and elevated soil moisture, where erosion transitions were closely tied to seasonal wetting. The dynamic model aligned well with observed retreat when matched with an appropriate Manning's n. In contrast, Site-2 exhibited a sharply concave bank profile with a steep lower face and narrow toe zone, which likely restricted shear stress distribution and delayed modeled retreat response. This confined geometry limits the ability of both static and dynamic models to initiate toe erosion and translate boundary stress into progressive lateral retreat, resulting in poor overall agreement despite capturing the late-season peak. Conversely, gentler, sloped banks like Site-1 allowed for more predictable shear stress distribution, where the dynamic model captured temporal changes in erosion effectively at a site-appropriate roughness. These geometry-driven variations directly influence the interaction between hydraulic roughness and boundary shear stress, affecting the optimal Manning's n necessary to match observed erosion. Consequently, accurate characterization of bank geometry is crucial when selecting roughness parameters, as geometry and roughness jointly dictate how shear stress distributes along streambank surfaces, directly influencing erosion potential and retreat patterns.

The temporal evaluation of modeled and observed lateral retreat further highlighted this advantage. Integrating time-varying τ_c and K_d based on measured soil moisture enhanced the model's ability to reciprocate the magnitude of seasonal erosion event dynamics. Notably, sudden bank erosion events following sharp rise or fall in soil moisture, such as in January 2024 and July 2024, were most accurately captured by the dynamic model. These events represent transitional conditions where changes in soil moisture directly alter τ_c and K_d, shifting the bank material from more resistant to more erodible states, thereby intensifying lateral retreat. Static models, represented to either dry or wet conditions of τ_c and K_d, struggle to simulate the dynamic erosion transitions during the opposite conditions or to incorporate sudden changes in the soil water conditions. This suggests that soil moisture dynamics serve as a critical driver in the streambank erosion process, enhancing resistance under certain conditions by increasing soil strength, while also accelerating erosion when thresholds are reduced during saturation or drying transitions.

Seasonal and episodic hydrologic events, such as storm-driven rapid infiltration, sudden wetting fronts, and prolonged drought conditions, strongly impact soil moisture dynamics, and consequently soil erosion (Simon et al., 2011; T. M. Wynn et al., 2004). The observed temporal mismatches between static model predictions and actual erosion events in this study emphasize the critical importance of incorporating event-scale hydrologic inputs into erosion models. Static parameterizations struggle to accurately predict erosion during transitional hydrologic periods, particularly when rapid changes in moisture alter erosion resistance parameters abruptly. The dynamic model demonstrated superior temporal performance in capturing rapid shifts in soil cohesion and erodibility at Sites 1 and 3, particularly during transitional soil moisture conditions.

In fluvial erosion modeling, three fundamental factors—boundary shear stress (hydraulically controlled by Manning's n), critical shear stress, and erodibility coefficient (both soil strength parameters), independently and interactively influence erosion processes. Specifically, Manning's n governs the hydraulic component by modulating boundary shear stress as a function of streamflow depth and roughness, whereas soil moisture-driven variations in τ_c and K_d reflect temporal shifts in the strength and erosion resistance of bank materials. Lammers et al. (2017) demonstrated through a sensitivity analysis in BSTEM that Manning's n is one of the most influential parameters, after streambank geometry, affecting streambank retreat predictions, contributing up to 8.8% of variability for erodible cohesive (silty) soils. In comparison, the erodibility coefficient (Kd) and critical shear stress (τc) contributed 5.3% and 4.8%, respectively. These findings are supported by current study that hydraulic roughness and erosion resistance parameters play a substantial role in erosion modeling and should be carefully characterized or calibrated, especially in heterogeneous field conditions.

5.5 CONCLUSIONS

This study evaluated the dynamic behavior of critical shear stress (τ_c) and the erodibility coefficient (K_d) as functions of soil moisture and integrated these relationships into the BSTEM framework to improve streambank erosion modeling. Field-derived quadratic relationships between soil moisture with τc and Kd were incorporated into a modified version of BSTEM, allowing erosion resistance to respond dynamically to hydrologic variability. The modified dynamic BSTEM model outperformed static configurations by more accurately replicating the timing and scale of observed retreat patterns. While Manning's n remained a dominant factor in model sensitivity—causing retreat variability up to 200 cm across tested ranges (n = 0.025–0.065), the inclusion of soil moisture-driven τ_c and K_d notably reduced overestimation or underestimation of erosion under fixed parameter input. At Site-1 and Site-3, dynamic LR matched observed retreat closely across months at intermediate n values (0.045–0.055), reflecting realistic channel resistance. Quantitative performance evaluation confirmed that the dynamic model achieved higher goodness-of-fit across metrics ($R^2 \geq 0.95$; RMSE < 0.60 cm) and lower error spread compared to static models, particularly during early and late-season erosion transitions. Static models either delayed erosion transition or missed late-season surges depending on their τ_c–K_d assumptions. In contrast, Site-2 remained less predictable for all configurations, likely due to complex bank geometry that limits toe stress translation and delays retreat initiation. This suggests that optimal performance of the dynamic model is achieved when Manning's n is aligned with site-specific channel characteristics.

Recommendations for future work include expanding this approach to other soil types, dominant with clay and sand, to test the generalizability of the derived relationships. In addition, long-term monitoring across diverse hydro-climatic zones would allow for refining and validating moisture–erosion functions under a broader range of conditions. Future assessments should also consider how roughness calibration and spatial variability in soil texture may influence the robustness of dynamic τ_c–K_d relationships. Ultimately, this study demonstrates that coupling soil moisture data with erosion resistance parameters can significantly advance the temporal accuracy and process realism of streambank erosion modeling.

REFERENCES

Abdul-Kadir, M. A., & Ariffin, J. (2012). Advances on Bank Erosion Studies: A Review. ASM Sci. J., 6(2), 128–137.

Akinola, A. I., Wynn-Thompson, T., Olgun, C. G., Mostaghimi, S., & Eick, M. J. (2019). Fluvial Erosion Rate of Cohesive Streambanks Is Directly Related to the Difference in Soil and Water Temperatures. Journal of Environmental Quality, 48(6), 1741–1748. https://doi.org/10.2134/jeq2018.10.0385

Biron, P. M., Buffin-Bélanger, T., Larocque, M., Choné, G., Cloutier, C. A., Ouellet, M. A., Demers, S., Olsen, T., Desjarlais, C., & Eyquem, J. (2014). Freedom Space for Rivers: A Sustainable Management Approach to Enhance River Resilience. Environmental Management, 54(5), 1056–1073. https://doi.org/10.1007/S00267-014-0366-Z/FIGURES/9

Chow, V. T. (1959). Open-channel hydraulics. McGraw-Hill Book Co., New York, N.Y.

Clark, L. A., & Wynn, T. M. (2007). Methods for Determining Streambank Critical Shear Stress and Soil Erodibility: Implications for Erosion Rate Predictions. Transactions of the ASABE, 50(1), 95–106. https://doi.org/10.13031/2013.22415

Daly, E. R., Miller, R. B., & Fox, G. A. (2015). Modeling streambank erosion and failure along protected and unprotected composite streambanks. Advances in Water Resources, 81, 114–127. https://doi.org/10.1016/J.ADVWATRES.2015.01.004

Fox, G. A., & Wilson, G. V. (2010). The Role of Subsurface Flow in Hillslope and Stream Bank Erosion: A Review. Soil Science Society of America Journal, 74(3), 717–733. https://doi.org/10.2136/sssaj2009.0319

Gaskin, S. J., Pieterse, J., Shafie, A. Al, & Lepage, S. (2003). Erosion of undisturbed clay samples from the banks of the St. Lawrence River. Canadian Journal of Civil Engineering, 30(3), 585–595. https://doi.org/10.1139/l03-008

Ghaneeizad, S., Papanicolaou, A. T., Abban, B., Wilson, C., Giannopoulos, C., Lambert, D., Walker, F., & Hawkins, S. (2018). Development of a distributed hydrologic model for a region with fragipan soils to study impacts of climate on soil moisture: A case study on the obion river watershed in West Tennessee. Geosciences (Switzerland), 8(10). https://doi.org/10.3390/geosciences8100364

Hanson, G. J., & Robinson, K. M. (1993). The Influence of Soil Moisture and Compaction on Spillway Erosion. Transactions of the ASAE, 36(5), 1349–1352. https://doi.org/10.13031/2013.28469

Hoomehr, S., Akinola, A. I., Wynn-Thompson, T., Garnand, W., & Eick, M. J. (2018). Water Temperature, pH, and Road Salt Impacts on the Fluvial Erosion of Cohesive Streambanks. Water 2018, Vol. 10, Page 302, 10(3), 302. https://doi.org/10.3390/W10030302

Klavon, K., Fox, G., Guertault, L., Langendoen, E., Enlow, H., Miller, R., & Khanal, A. (2017a). Evaluating a process-based model for use in streambank stabilization: insights on the Bank Stability and Toe Erosion Model (BSTEM). Earth Surface Processes and Landforms, 42(1), 191–213. https://doi.org/10.1002/ESP.4073

Klavon, K., Fox, G., Guertault, L., Langendoen, E., Enlow, H., Miller, R., & Khanal, A. (2017b). Evaluating a process-based model for use in streambank stabilization: insights on the Bank Stability and Toe Erosion Model (BSTEM). Earth Surface Processes and Landforms, 42(1), 191–213. https://doi.org/10.1002/esp.4073

Lammers, R. W., Bledsoe, B. P., & Langendoen, E. J. (2017). Uncertainty and sensitivity in a bank stability model: implications for estimating phosphorus loading. Earth Surface Processes and Landforms, 42(4), 612–623. https://doi.org/10.1002/ESP.4004

Langendoen, E. J., Simon, A., & Thomas, R. E. (2001). CONCEPTS - A Process-Based Modeling Tool to Evaluate Stream-Corridor Restoration Designs. Proceedings of the 2001 Wetlands Engineering and River Restoration Conference, 1–11. https://doi.org/10.1061/40581(2001)109

Larionov, G. A., Bushueva, O. G., Dobrovol'skaya, N. G., Kiryukhina, Z. P., Krasnov, S. F., & Litvin, L. F. (2014). Effect of the water temperature and soil moisture on the erodibility of chernozem samples: A model experiment. Eurasian Soil Science, 47(7), 734–739. https://doi.org/10.1134/S1064229314070096/METRICS

Li, M., Liu, Q., Zhang, H., Wells, R. R., Wang, L., & Geng, J. (2022). Effects of antecedent soil moisture on rill erodibility and critical shear stress. CATENA, 216, 106356. https://doi.org/10.1016/J.CATENA.2022.106356

Midgley, T. L., Fox, G. A., & Heeren, D. M. (2012). Evaluation of the bank stability and toe erosion model (BSTEM) Evaluation of the bank stability and toe erosion model (BSTEM) for predicting lateral retreat on composite streambanks for predicting lateral retreat on composite streambanks. https://doi.org/10.1016/j.geomorph.2011.12.044

Moragoda, N., Kumar, M., & Cohen, S. (2022). Representing the role of soil moisture on erosion resistance in sediment models: Challenges and opportunities. Earth-Science Reviews, 229, 104032. https://doi.org/10.1016/j.earscirev.2022.104032

Nye, T., & Heineman, M. (2016). Modified Green-Ampt Method in EPA SWMM EWRI 2016. EWRI.

Rinaldi, M., & Darby, S. E. (2007). Modelling river-bank-erosion processes and mass failure mechanisms: progress towards fully coupled simulations. Developments in Earth Surface Processes, 11, 213–239. https://doi.org/10.1016/S0928-2025(07)11126-3

Rossman, L. A. (2006). Storm Water Management Model Quality Assurance Report: Dynamic Wave Flow Routing.

Saha, P., Islam, M., Oyshi, J. T., Khanum, R., & Nishat, A. (2019). A sustainability study of the flow regulation impacts by dams in a carp breeding river using the hydrodynamic model and building block analysis. SN Applied Sciences, 1(11). https://doi.org/10.1007/s42452-019-1417-0

Simon, A., & Collison, A. J. C. (2001). Pore-water pressure effects on the detachment of cohesive streambeds: seepage forces and matric suction. Earth Surface Processes and Landforms, 26(13), 1421–1442. https://doi.org/10.1002/ESP.287

Simon, A., Curini, A., Darby, S. E., & Langendoen, E. J. (2000). Bank and near-bank processes in an incised channel. Geomorphology, 35(3–4), 193–217. https://doi.org/10.1016/S0169-555X(00)00036-2

Simon, A., Thomas, R. E., & Klimetz, L. (2010). COMPARISON AND EXPERIENCES WITH FIELD TECHNIQUES TO MEASURE CRITICAL SHEAR STRESS AND ERODIBILITY OF COHESIVE DEPOSITS.

Singh, H. V., & Thompson, A. M. (2016). Effect of antecedent soil moisture content on soil critical shear stress in agricultural watersheds. Geoderma, 262, 165–173. https://doi.org/10.1016/J.GEODERMA.2015.08.011

CHAPTER-6

SUMMARY AND CONCLUSIONS

This dissertation investigated the interplay between soil moisture dynamics and streambank erosion processes, addressing critical knowledge gaps in erosion modeling under temporally and spatially variable hydrological conditions. The work was structured into three core studies that collectively explored soil moisture extremes, their influence on erosion resistance parameters, and the development of a dynamic erosion modeling framework.

Chapter 3 focused on the spatio-temporal variability of soil moisture extremes across geophysically distinct watersheds in Tennessee. Results revealed that climate-induced variability in precipitation and temperature patterns significantly alters soil moisture dynamics, contributing to both prolonged dry spells and increased instances of saturation. Spatial heterogeneity in soil water responses was linked to watershed physiography, highlighting the necessity of region-specific analyses when projecting hydrological risks under future climate scenarios.

Chapter 4 advanced the understanding of erosion resistance by examining the influence of seasonal soil moisture variations on critical shear stress (τ_c) and the erodibility coefficient (K_d) at natural streambanks. Field-based JET test conducted across a range of soil moisture conditions demonstrated statistically significant nonlinear relationships between soil moisture and both τ_c and K_d. Specifically, U-shaped trends were identified, with reduced erosion resistance at both low and high soil moisture extremes, and enhanced resistance at intermediate moisture levels. These findings confirmed that treating τ_c and K_d as static parameters in erosion modeling may overlook key variability driven by hydrologic conditions.

Chapter 5 integrated these empirical insights into a modified BSTEM model. Using field-derived polynomial functions of τ_c and K_d with soil moisture, dynamic erosion modeling was conducted across three monitored sites. Compared to traditional static parameter scenarios, the dynamic model improved the accuracy of seasonal erosion predictions in cohesive silty clay streambanks. Sensitivity analysis demonstrated that while Manning's roughness (n) remains the most influential parameter in lateral retreat estimation, incorporating dynamic τ_c and K_d significantly reduced variance and enhanced the model's responsiveness to changing hydrologic conditions. The findings were further supported by performance comparisons using observed retreat data, showing that the dynamic model better captured erosion timing and magnitude, particularly under transitional soil moisture regimes.

This dissertation made several novel contributions to the field of streambank erosion modeling by explicitly incorporating soil moisture dynamics into the estimation of erosion resistance parameters. It demonstrated, for the first time at field scale, that τ_c and K_d exhibit nonlinear responses to naturally varying soil moisture, with reduced resistance observed at both dry and saturated extremes. The study developed and validated a modified BSTEM framework that integrates these dynamic τ_c and K_d functions, significantly improving the accuracy of modeled lateral retreat compared to static parameter approaches. By coupling real-time soil moisture variability with resistance parameters, this work enhances temporal dynamics in erosion modeling and provides a modified tool for more reliable streambank stability assessment under changing hydrologic conditions.

Building on these findings, future research should aim to generalize the soil moisture–erosion relationships across a broader range of soil types, including clays, sands, and mixed textures, to assess the universality of the developed functions. Long-term monitoring assessments are also recommended to capture interannual trends and improve model robustness under flashy peaks or extreme hydrologic events. Additionally, expanding the dynamic parameterization to mass failure modules and other erosion prediction frameworks could facilitate broader application in stream restoration design.

APPENDIX

Appendix A-1 Temperature Frequency percentiles of Obion Watershed

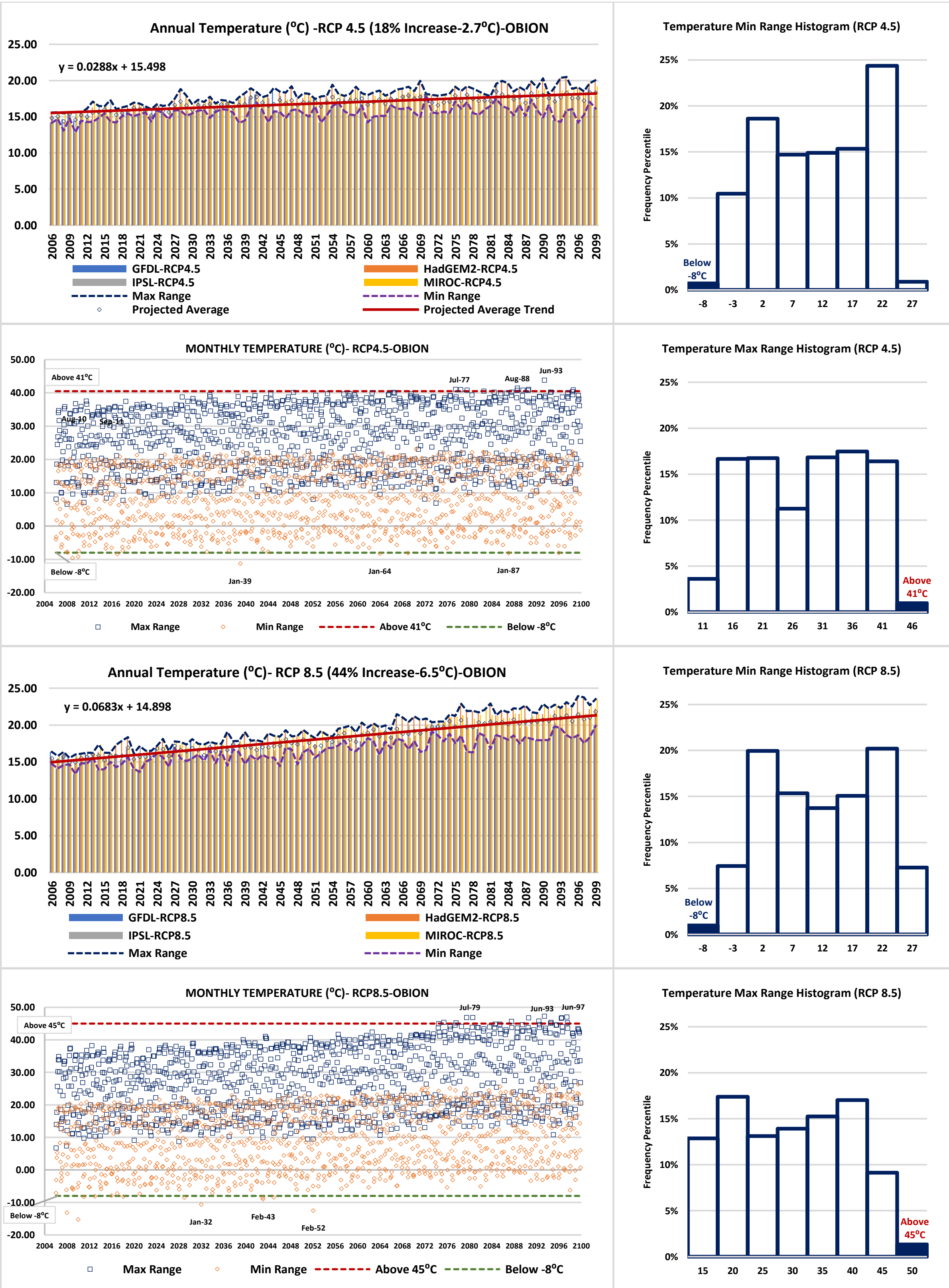

Figure A-1 Annual and monthly temperature trends and frequency percentiles of Obion

Appendix A-2 Temperature Frequency percentiles of Nolichucky Watershed

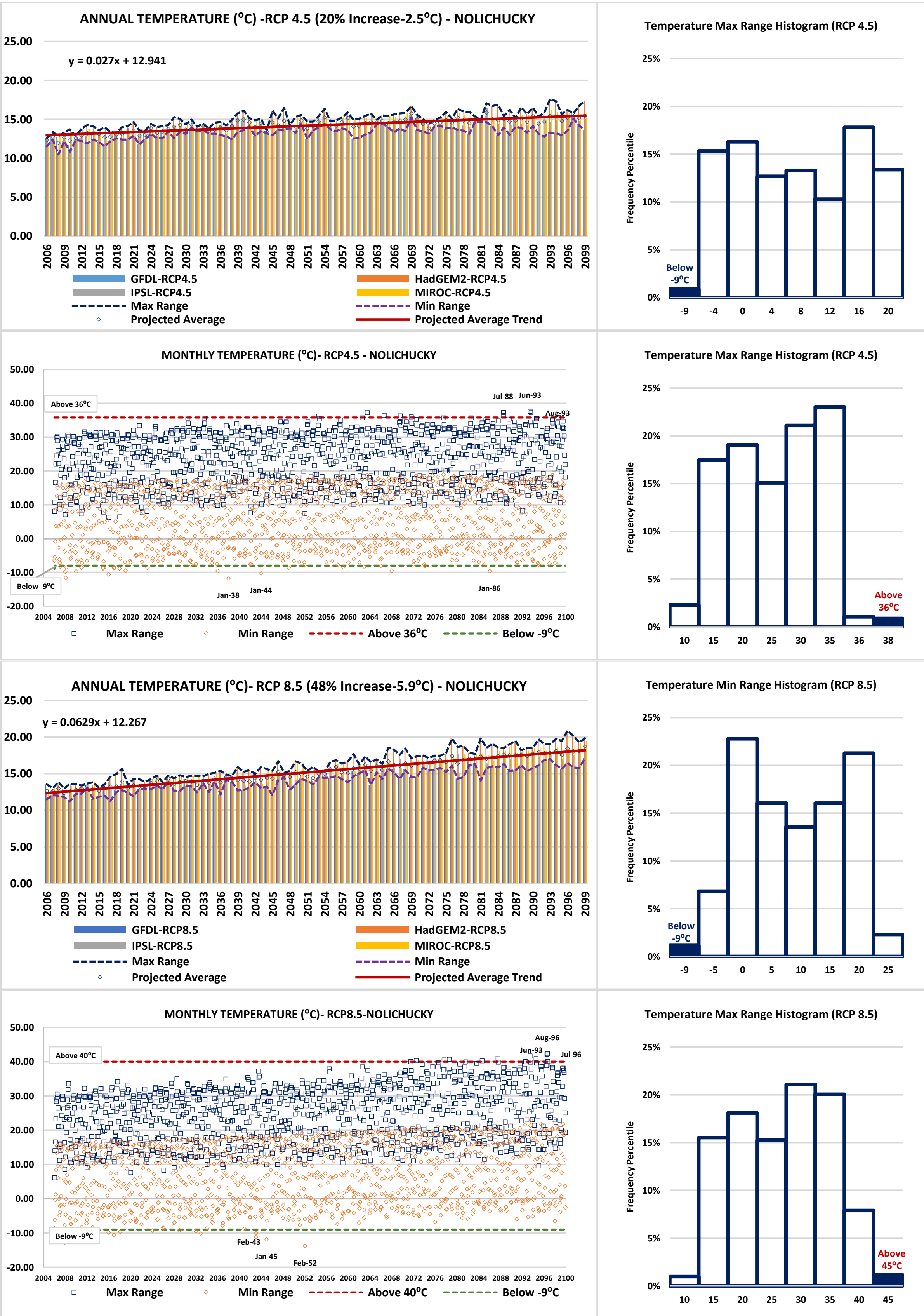

Figure A-2 Annual and monthly temperature trends and frequency percentiles of Nolichucky

Appendix A-3 Precipitation Frequency percentiles of Obion Watershed

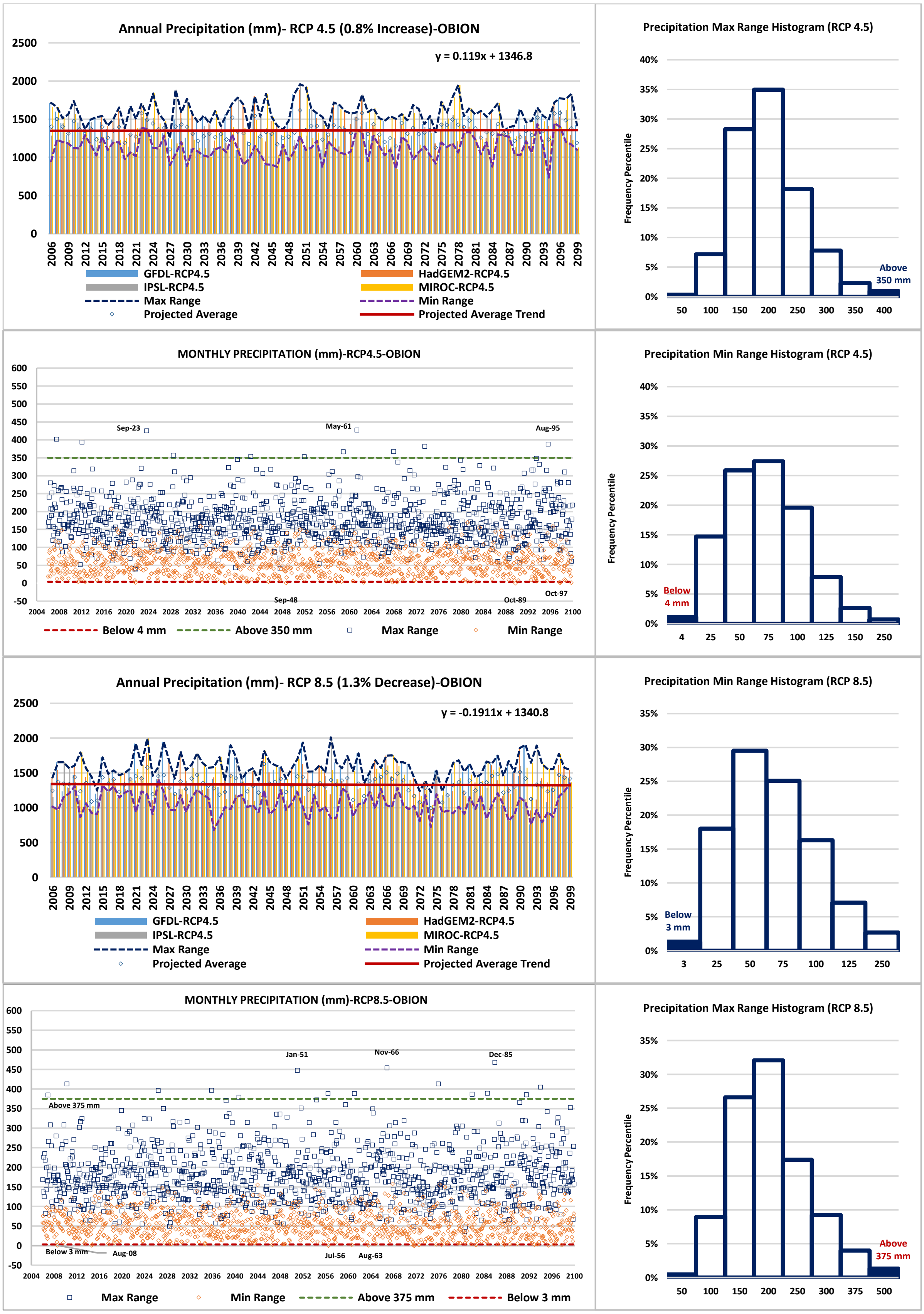

Figure A-3 Annual and monthly precipitation trends and Frequency percentiles of Obion

Appendix A-4 Precipitation Frequency percentiles of Nolichucky Watershed

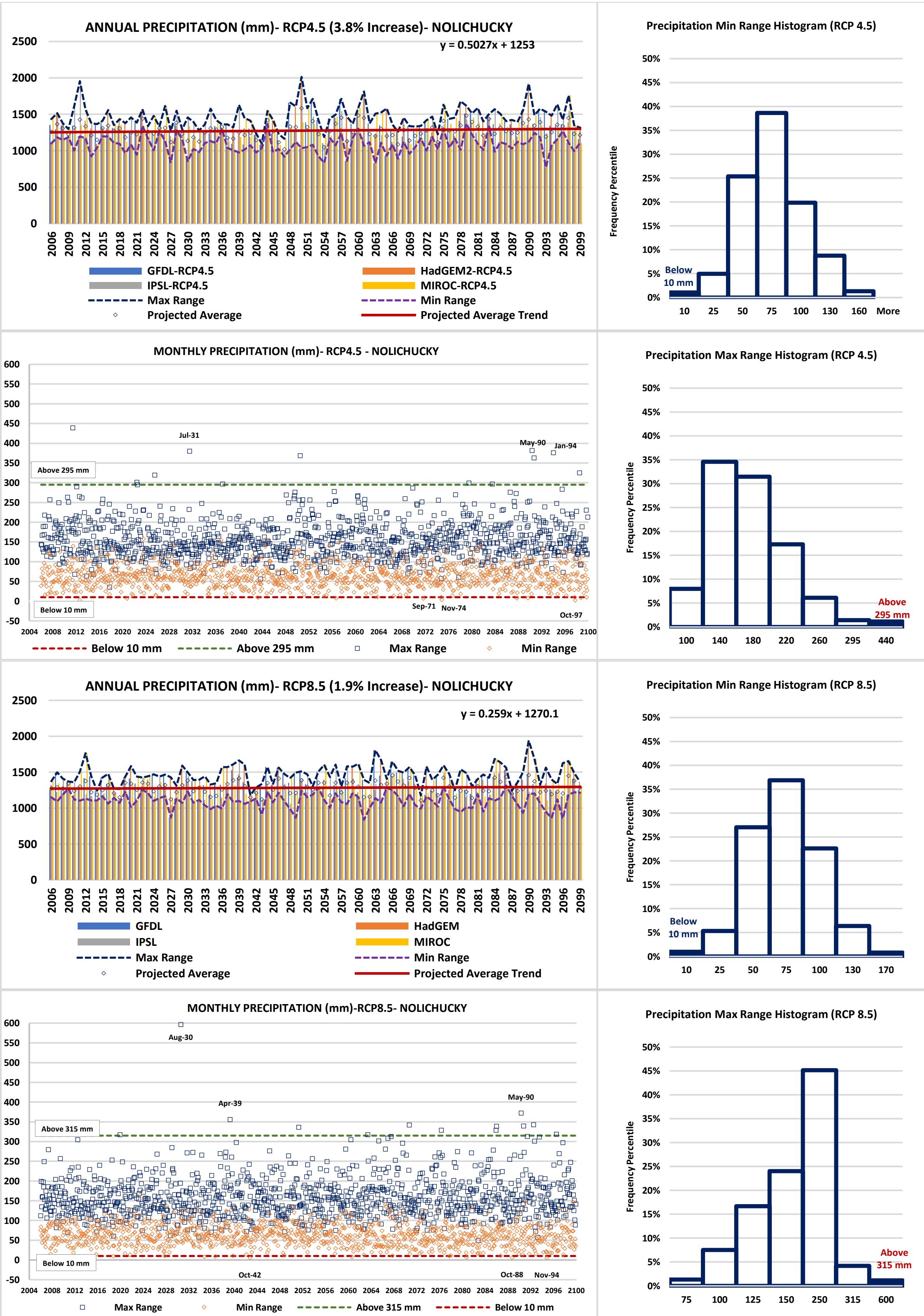

Figure A-4 Annual and monthly precipitation trends and Frequency percentiles of Nolichucky

Appendix A-5 Connor Creek Jet Test Estimates

Table A-1 Comparison of field-derived and function generated critical shear stress and erodibility coefficients in relation to real-time soil moisture

Sites	SM (%)	τ_c (Pa)	K (Cm3/N-s)	Pred τ_c (Pa)	Pred K (Cm3/N-s)
1	29.00	0.102	6.18	0.86	4.87
2	29.00	0.125	3.72	0.86	4.87
3	29.00	1.344	4.01	0.86	4.87
4	29.00	0.061	7.69	0.86	4.87
5	33.00	3.715	4.20	1.88	6.25
6	33.00	0.580	3.52	1.88	6.25
7	18.00	1.661	7.63	1.18	6.72
8	21.80	3.853	3.08	1.00	5.22
9	19.30	0.349	6.70	1.06	6.13
10	26.70	0.172	2.25	0.87	4.58
11	25.50	0.358	4.16	0.91	4.58
12	29.30	0.099	8.14	0.88	4.93
13	23.30	0.201	7.85	0.98	4.85
14	26.70	4.298	1.95	0.87	4.58
15	30.40	0.567	1.65	1.00	5.23
16	39.00	12.450	8.53	11.21	9.78
17	35.70	0.128	8.63	4.37	7.69
18	18.50	0.024	6.88	1.12	6.48
19	32.50	0.006	8.49	1.62	6.02
20	36.00	7.389	8.41	4.79	7.87
21	13.70	0.142	11.59	2.99	8.96
22	9.70	10.077	12.12	9.06	10.81
23	23.20	0.831	5.65	0.98	4.87
24	16.40	0.411	6.58	1.52	7.52
25	13.90	0.490	9.02	2.83	8.85
26	17.20	1.408	6.03	1.32	7.11
27	17.90	0.927	8.83	1.20	6.77
28	10.80	7.650	7.55	6.75	10.38
29	9.50	10.344	12.16	9.54	10.89
30	13.10	6.156	5.96	3.54	9.27
31	35.10	5.959	7.42	3.63	7.34
32	33.30	3.156	6.52	2.06	6.39
33	27.70	1.146	4.92	0.84	4.66
34	37.60	8.196	9.04	7.66	8.87
35	29.20	2.237	4.02	0.87	4.91
36	30.10	2.612	6.00	0.95	5.14
37	36.00	3.542	8.34	4.79	7.87
38	33.60	3.047	6.43	2.26	6.54
39	35.10	0.007	9.21	3.63	7.34

Appendix A-6 Erosion rate from JET test estimates

Table A-2 Erosion rate estimated from the field-derived critical shear stress, erodibility coefficients and boundary shear stress

SM (%)	τ_c (Pa)	K (Cm^3/N-s)	τ_0 (Pa)	ER (cm/min)
9.50	10.344	12.160	366.57	25.99
9.70	10.077	12.122	376.41	26.64
10.10	7.650	7.551	273.75	12.06
13.10	6.156	5.964	307.97	10.80
13.70	0.142	11.590	376.41	26.17
13.90	0.490	9.022	273.75	14.79
16.40	0.411	6.583	342.19	13.50
17.20	1.408	6.027	273.75	9.85
17.90	0.927	8.831	376.41	19.89
18.00	1.661	7.625	342.19	15.58
18.50	0.024	6.880	239.53	9.89
19.30	0.349	6.703	376.41	15.12
21.80	3.853	3.080	166.54	3.01
23.20	0.831	5.648	464.50	15.71
23.30	0.201	7.852	178.43	8.40
25.50	0.358	4.160	273.75	6.82
26.70	0.172	2.249	273.75	3.69
26.70	4.298	1.950	166.54	1.90
27.70	1.146	4.917	342.19	10.06
29.00	0.061	7.690	342.19	15.79
29.00	0.102	6.181	51.33	1.90
29.00	0.125	3.720	205.31	4.58
29.00	1.344	4.005	256.64	6.13
29.20	2.237	4.024	273.75	6.56
29.30	0.099	8.142	35.69	1.74
30.10	2.612	6.003	273.75	9.77
30.40	0.567	1.649	273.75	2.70
32.50	0.006	8.491	273.75	13.95
33.00	0.580	3.522	239.53	5.05
33.00	3.715	4.197	273.75	6.80
33.30	3.156	6.522	273.75	10.59
33.60	3.047	6.431	273.75	10.44
35.10	0.007	9.211	307.97	17.02
35.10	5.959	7.419	273.75	11.92
35.70	0.128	8.630	376.41	19.48
36.00	3.542	8.345	273.75	13.53
36.00	7.389	8.408	233.15	11.39
37.60	8.196	9.045	273.75	14.41
39.00	12.450	8.525	222.42	10.74

Appendix A-7 Sieve Test Analysis

Table A-3 Sieve test for site-1 streambank soil

Sieve No.	Sieve Mass	Sieve + Soil Mass	Mass Retained	Cumulative mass retained (g)	Cumulative Percent retained (%)	Cumulative Percent passing (%)
10	433.56	433.62	0.06	0.06	0.17	99.83
18	430.32	431.07	0.75	0.81	2.29	97.71
25	329.96	330.59	0.63	1.44	4.06	95.94
60	273.81	284.39	10.58	12.02	33.92	66.08
100	262.8	275.33	12.53	24.55	69.27	30.73
140	257.24	264.01	6.77	31.32	88.37	11.63
Pan	368.45	372.57	4.12	35.44	100.00	0.00
200			35.44			100.00

Appendix A-8 Hydrometer soil analysis parameters

Table A-4 Experimental Parameters for Organic Sediment (OS) Sample

Parameter	Value	Unit	Description
X_d	40	g/L	Desired concentration of dispersed solids
V_d	125	mL	Volume of dispersing solution
C_d	5	g/L	Concentration of dispersing agent
C_m	0.5	g/L	Concentration of modifier
G_s	2.7	–	Specific gravity of solids
a	0.99	–	Correction factor or absorptivity coefficient
Mass of OS	100.02	g	Initial dry mass of organic sediment
$W_{residue}$	35.44	g	Mass retained on sieve after washing
W_{200}	64.58	g	Mass passing through 200 sieve mesh
W_{200}/W_0	0.65	–	Fraction of soil finer than #200 sieve

Appendix A-9 Hydrometer soil lab test estimates

Table A-5 Hydrometer test for site-1 streambank soil texture

Time (min)	**T (°C)**	**Unit mass ρw (g/cm^3)**	**Hydro meter R (g/L)**	**Temp Adjust m**	**Actual H. R_{corr}**	**Depth L (cm)**	**K**	**Particle D (mm)**	**Particle Percent Finer**	**Total Percent Finer**
								0.074	0.646	64.58
0.5	19	0.99841	45	-0.155	40.345	9.7	0.01361	0.060	0.399	39.93
1	19	0.99841	44	-0.155	39.345	9.9	0.01361	0.043	0.389	38.94
2	19	0.99841	44	-0.155	39.345	9.9	0.01361	0.030	0.389	38.94
4	19	0.99841	44	-0.155	39.345	9.9	0.01361	0.021	0.389	38.94
8	19	0.99841	43	-0.155	38.345	10.1	0.01361	0.015	0.380	37.95
15	19	0.99841	43	-0.155	38.345	10.1	0.01361	0.011	0.380	37.95
30	19	0.99841	41	-0.155	36.345	10.4	0.01361	0.008	0.360	35.97
60	19	0.99841	39	-0.155	34.345	10.7	0.01361	0.006	0.340	33.99
90	19	0.99841	37	-0.155	32.345	11.1	0.01361	0.005	0.320	32.02
1440	19	0.99841	27	-0.155	22.345	12.7	0.01361	0.001	0.221	22.12

VITA

Probal Saha was born in Bangladesh. He began his academic journey in civil engineering with a focus on water resources at the Bangladesh University of Engineering and Technology (BUET), where he earned his Bachelor of Science degree in Water Resources Engineering in 2016.

Following graduation, Probal worked in both academic and applied research roles. He served as a Water Resources Engineer at the Center for Climate Change and Environmental Research (C3ER), BRAC University, and as a Research Assistant at the Institute of Water and Flood Management, where he contributed to hydrologic modeling, flood risk assessment, and sustainable water management planning. During this time, he was also involved in coastal hurricane surge modeling and taught as an adjunct lecturer in the Department of Architecture at BRAC University.

In 2019, he was admitted to the doctoral program in Civil and Environmental Engineering at the University of Tennessee, Knoxville, with a concentration in Water Resources Engineering. His Ph.D. research focused on soil moisture-driven streambank erosion modeling, integrating field observations with erosion models such as BSTEM and hydrologic models like SWMM. His work contributed to improving erosion prediction by linking soil moisture variability with erosion resistance parameters.

Probal is a certified Engineer-in-Training (EIT) and holds certifications in stormwater modeling and project management. He is passionate about applying advanced modeling tools to solve real-world water resource challenges and remains committed to integrating science with community-driven solutions.